AD_____
(Leave blank)

Award Number: **DAMD17-03-1-0363**

TITLE: **Therapeutic vascular targeting and irradiation: correlation of MRI tissue changes at cellular and molecular levels to optimizing outcome**

PRINCIPAL INVESTIGATOR: **Dawen Zhao, M.D., Ph.D.**

CONTRACTING ORGANIZATION: **University of Texas Southwestern Medical Center at Dallas Dallas, TX 75390-9058**

REPORT DATE: **June 2008**

TYPE OF REPORT: **Final**

PREPARED FOR: U.S. Army Medical Research and Materiel Command
Fort Detrick, Maryland 21702-5012

REPORT DOCUMENTATION PAGE

Form Approved
OMB No. 074-0188

1. Agency Use Only (Leave blank)	2. Report Date	3. Report Type and Period Covered (i.e., annual 1 Jun 00 - 31 May 01)
	30-06-2008	Final, 1 JUN 2003 - 31 MAY 2008

4. Title and Subtitle
Therapeutic vascular targeting and irradiation: correlation of MRI tissue changes at cellular and molecular levels to optimizing outcome

5. Award Number
DAMD17-03-1-0363

6. Author(s)
Dawen Zhao, M.D., Ph.D.

7. Performing Organization Name (Include Name, City, State, Zip Code and Email for Principal Investigator)
U.T. Southwestern Medical Center at Dallas
5323 Harry Hines Blvd.
Dallas, TX 75390-9058
E-mail: dawen.zhao@UTSouthwestern.edu

8. Performing Organization Report Number (Leave Blank)

9. Sponsoring/Monitoring Agency Name and Address
U.S. Army Medical Research and Materiel Command
Fort Detrick, Maryland 21702-5012

10. Sponsoring/Monitoring Agency Report Number (Leave Blank)

11. Supplementary Notes (i.e., report contains color photos, report contains appendix in non-print form, etc.)

12a. Distribution/Availability Statement (check one)
X Approved for public release; distribution unlimited
_ Distribution limited to U.S. Government agencies only - report contains proprietary information

12b. Distribution Code
(Leave Blank)

13. Abstract *(Maximum 200 Words)* *(abstract should contain no proprietary or confidential information)*

Vascular targeting agents (VTA) are new types of anticancer drugs that act on existing tumor vasculature, causing vascular disruption, which ultimately leads to extensive ischemic tumor cell death. Interesting findings showed that VTA killed cells predominantly in the more hypoxic tumor center, as a consequence of hemorrhagic necrosis after vascular collapse, whereas the better perfused peripheral rim was less affected. This apparently limits the effectiveness of such agents and rapid re-growth of tumor residues occurs. However, these findings suggest the possibility and promise of a combination of VTA with treatments specifically targeting the viable tumor rim. Radiation can certainly be expected to be most effective against the well-perfused and oxygenated cell populations at the peripheries of the tumors.

One major goal of this project is to fully understand and precisely assess the dynamic changes in blood perfusion and oxygenation after VTA, so that we may predict response and optimize the therapy. I propose to use *in vivo* MRI to measure and assess physiological changes, e.g. tumor blood perfusion and dynamic tissue oxygenation, in the tumors before and after treatment. I believe non-invasive MRI approaches may provide a valuable prognostic tool to predict the response of specific breast tumors to VTA.

14. Subject Terms (keywords previously assigned to proposal abstract or terms which apply to this award)
Vascular targeting, Magnetic resonance imaging (MRI), pO_2, Perfusion, irradiation

15. Number of Pages (count all pages including appendices) 94

16. Price Code

17. Security Classification of Report	18. Security Classification of this Page	19. Security Classification of Abstract	20. Limitation of Abstract
Unclassified	Unclassified	Unclassified	Unlimited

Table of Contents

Page

Introduction:

Targeting tumor vasculature promises effective cancer therapy (1, 2). It avoids issues of drug delivery and is potentiated by massive downstream effects where one blood vessel may supply the nutrients for thousands of tumor cells. Thus, disrupting the vascular supply should generate magnified tumor cell kill. Thus, inhibiting the growth of new blood vessels, i.e., antiangiogenesis, should prevent growth and metastasis of the primary tumor (1, 2). In addition to the focus on the antiangiogenic approaches, vascular targeting, directly attacking the existing neovasculature, is an alternative strategy against the tumor blood vessel network. Tubulin binding agents, *e.g.*, combretastatin A-4-phosphate (CA4P) represent one kind of vascular targeting agent (VTA) (3-5). Promising preclinical studies have shown that such agents selectively cause tumor vascular shutdown and subsequently trigger a cascade of tumor cell death in experimental tumors (4-6). However, survived tissues in a thin viable rim of tumor usually re-grow in spite of induction of massive necrosis. Thus, a combination of VTAs with additional conventional therapeutic approaches will be required (7, 8). To better understand the mode of action, and hence, optimize such combinations, we plan to apply *in vivo* MR imaging approaches to monitoring physiological changes in response to VTA administration. Dynamic contrast enhanced (DCE) MRI based on the transport properties of gadolinium-DTPA (Gd-DTPA) is the most commonly used imaging approach to study tumor vascular perfusion and permeability (9, 10). For combination with radiotherapy, measurement of tumor oxygen dynamics will be especially important since hypoxia affects radiation response. By applying ^{19}F *FREDOM* (Fluorocarbon Relaxometry using Echo planar imaging for Dynamic Oxygen Mapping) MRI (11), dynamic tumor oxygenation can be monitored following the treatment with CA4P. Based on pathophysiological changes monitored by MRI, optimum scheme of the combined radiation and CA4P will be designed and experimental treatment will be performed on the syngeneic rat breast tumors.

Successful completion of this project will confirm the potential of this new therapeutic approach to breast cancer. It will lay the foundation for future clinical application for treating breast cancer patients.

Body:

The Statement of Work in this project had two major tasks:

Task 1. To assess vascular and oxygen dynamics in response to VTA, Months 1-18.

a. *In vivo* MRI assessment of vascular and oxygen dynamics in response to VTA, Months 1-18

b. To study morphological and biological changes of tumor vasculature and hypoxia at cellular and molecular levels in response to VTA, Months 1-18.

Task 1 was completed during the Years 1 and 2.

In accordance with Statement of Work for Year 1 in this project, I have applied functional MRI approaches including DCE (dynamic contrast enhanced) MRI, BOLD (Blood oxygen level dependent) MR and ^{19}F *FREDOM* (Fluorocarbon Relaxometry using Echo planar imaging for Dynamic Oxygen Mapping) NMR oximetry to extensively studying tumor vasculature and oxygenation in subcutaneous model of 13762 rat breast tumors. For the untreated control tumors, I designed a novel MRI approach to study potential correlation between tumor vasculature evaluated by ^{1}H DCE, BOLD MRI and tumor oxygenation acquired by ^{19}F *FREDOM* oximetry. A significant correlation was found between changes in tissue pO_2 and BOLD response accompanying oxygen intervention in the total of nine 13762NF breast tumors ($R > 0.9$,Fig. 1)(11-14).

For the treated tumors, integrated functional MRI techniques including DCE, BOLD MRI and ^{19}F MRI oximetry were applied to detect early changes in tumor tissue, vasculature and oxygenation after a vascular targeting agent, Combretastatin A4 phosphate (CA4P; OXiGENE, Inc, Waltham, MA) injection. In terms of

CA4P dosage, I tried several doses ranging from 30mg/kg to 150mg/kg. Our results showed that even a lower dose at 30mg/kg produced significant effect on tumor vasculature. So the dose of 30mg/kg i.p. was used for the whole study. DCE MRI showed a ~70% decrease, averaged over a group of 13762NF rat breast tumors (n = 5), in perfusion/permeability (initial area under signal-intensity curve (IAUC)) at 2 h. The IAUC recovered fully after 24 h in a thin peripheral region, but not the tumor center (Fig. 2) (15, 16).

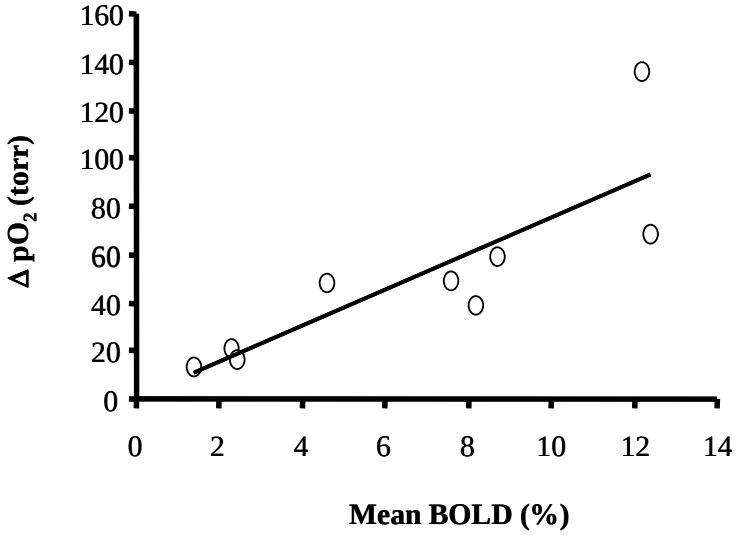

Figure 1 A significant linear correlation was found between mean increase in ^{19}F tissue pO_2 (ΔpO_2) and ^{1}H BOLD signal increase in the nine tumors with respect to oxygen intervention ($R > 0.9$; $p < 0.001$)(13).

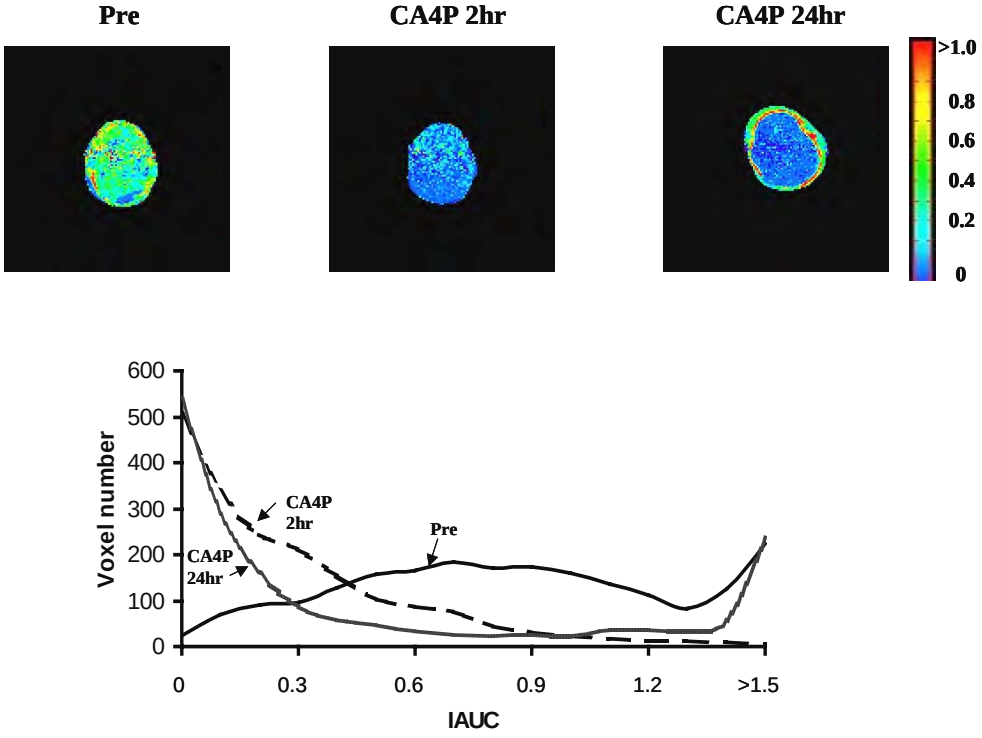

Figure 2. Dynamic contrast enhanced (DCE) MRI with respect to CA4P (30 mg/kg) treatment. A) Normalized T1-weighted contrast enhanced images were acquired 23 s after a bolus injection of contrast agent pre, and 2 h and 24 h after treatment. Significantly less signal enhancement was observed for the whole tumor region 2 h after treatment. A full recovery was apparent in the tumor rim 24 h post-treatment. B) IAUC frequency of DCE MRI on voxel by voxel basis obtained on the same tumor at pre, 2 h and 24 h after CA4P. Compared with pre, curves of 2 h and 24 h after showed a significant increase in the number of voxels with no signal enhancement (typically IAUC < 0.05). However, the frequency of highly enhancing voxels (IAUC > 1.5) at 24 h recovered to the pre-treatment level (15).

^{19}F *FREDOM* MRI further demonstrated that a significant decrease in the mean pO_2 for the group of 7 tumors was found at 90 min after CA4P (23 ± 5 vs. 9 ± 3 torr; $p < 0.05$) and a further decrease at 2 h (2 ± 2 torr). The mean pO_2 increased to 15 ± 4 torr at 24 h, which was still significantly lower than pretreated baseline ($p < 0.05$). More interestingly, the initial changes in pO_2 in central and peripheral regions were parallel, but by 24 h post treatment significant difference was apparent: pO_2 in the periphery improved significantly, while the center remained hypoxic (Figs. 3 and 4) (15).

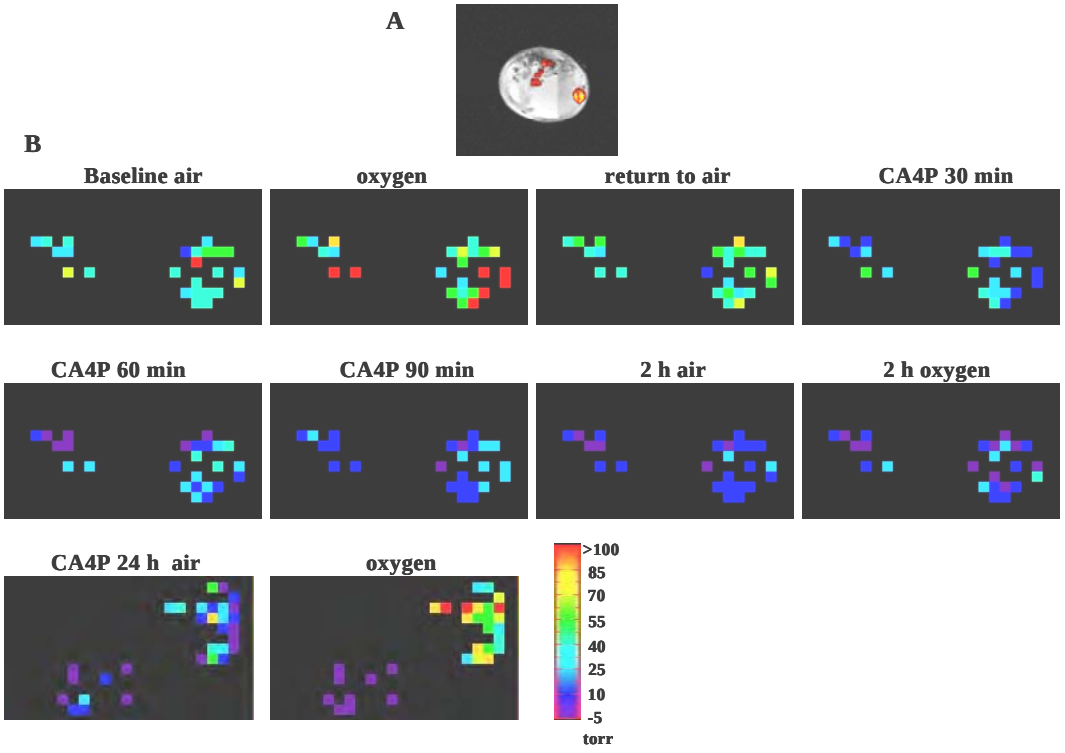

Figure 3 A) Distribution of hexafluorobenzene (HFB) in a representative tumor. An overlay of ^{19}F signal density on the anatomic image indicates HFB in both peripheral and central regions. B) pO_2 maps obtained from the same tumor comprise two separated groups of voxels, which correspond to the locations of HFB on the anatomic image. Twenty five individual voxels were traceable from the pretreated baseline to 2 h after CA4P with oxygen breathing. Thirty one voxels could be followed 24 h post-treatment. Significant decrease in pO_2 was evident for all the individual voxels after CA4P, and pO_2 did not respond to oxygen inhalation after 2 h. The 24 h maps showed improved pO_2 and significant response to oxygen breathing in the peripheral region (right), but not in the central region (left) (15).

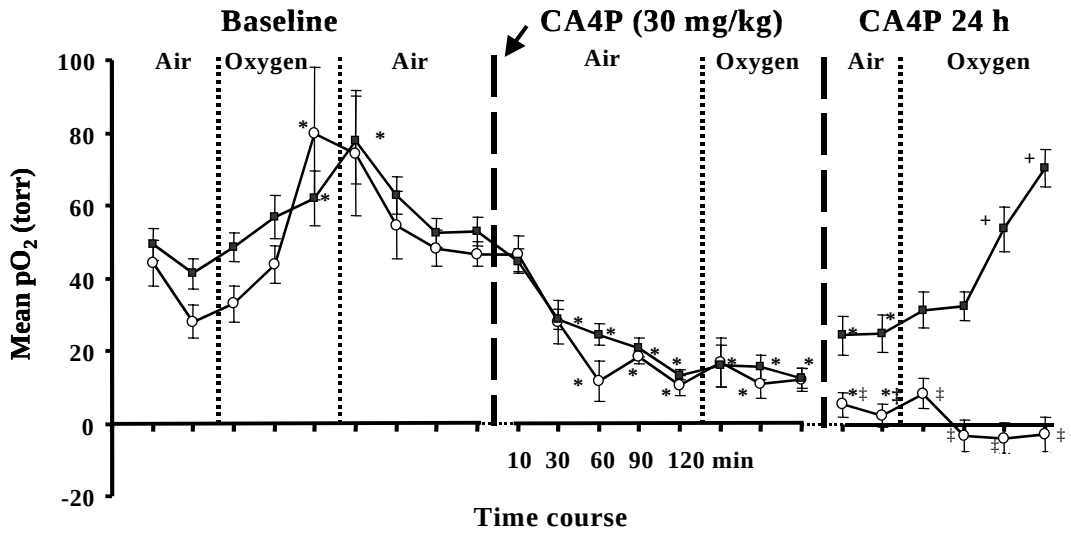

Figure 4 Mean pO_2 curves are shown for the peripheral (■) and central (○) voxels of the tumor shown in Fig. 3. Significant decrease in pO_2 was found as early as 30 min after CA4P (30 mg/kg) for both peripheral and central tumor. * $p < 0.05$ from baseline air, $^{+}$ $p < 0.05$ from 24 h air, ‡ $p < 0.05$ from periphery (15).

DCE MRI data of tumor vascular perfusion/permeability change in response to CA4P is summarized in Table 1, and ^{19}F MRI pO2 data is shown in Table 2 (15).

Table 1 Normalized IAUC by dynamic contrast enhanced MRI

Groups		Mean IAUC		
		baseline	2 h	24 h
CA4P (n = 6)	periphery	0.88 ± 0.06	0.31 ± 0.08*‡	0.86 ± 0.06
(30 mg/kg)	center	0.44 ± 0.11^{+}	0.13 ± 0.08*‡	0.12 ± 0.05$^{*+‡}$
Control (n = 3)	periphery	1.09 ± 0.04	0.93 ± 0.13	0.86 ± 0.05
(saline)	center	0.52 ± 0.19^{+}	0.46 ± 0.05^{+}	0.44 ± 0.03^{+}

IAUC: initial area under signal-intensity curve;

$^{*}p < 0.05$ from baseline; $^{+}p < 0.05$ from periphery; $^{‡}p < 0.05$ from control.

In addition to the rat breast tumor, I have also performed the MRI and bioluminescent imaging studies on human breast MDA-MB-231 tumors. Similar to the observations in the rat tumor, DCE MRI revealed significant reduction in tumor vascular perfusion/permeability in response to CA4P in the human tumors (Fig. 5)(17-19).

Table 2 Tumor oxygen dynamics assessed by ^{19}F MRI with respect to CA4P treatment

Groups	Case no.	Size cm^3	pO_2 (mean ± se torr)							
			baseline	Time course						
			Air	30 min	60 min	90 min	2 h	oxygen	24 h base	oxygen
CA4P (30 mg/kg) (n=7)	1	2.0	36 ± 1	NA	NA	NA	2 ± 3*	5 ± 2*	NA	NA
	2	0.9	12 ± 2	NA	NA	NA	-3 ± 2*	-3 ± 2*	NA	NA
	3	1.2	13 ± 0	35 ± 11	11 ± 3	9 ± 4	1 ± 2*	2 ± 2*	5 ± 0*	30 ± 6+
	4	0.7	43 ± 5	29 ± 3*	21 ± 3*	20 ± 2*	13 ± 1*	16 ± 5*	20 ± 2*	48 ± 7+
	5	0.4	12 ± 2	5 ± 3*	9 ± 3	4 ± 2*	2 ± 1*	7 ± 3*	NA	NA
	6	0.7	15 ± 1	19 ± 3	9 ± 2*	4 ± 2*	1 ± 2*	0 ± 3*	12 ± 1	73 ± 12+
	7	0.3	28 ± 6	29 ± 2	16 ± 4	6 ± 2*	1 ± 1*	7 ± 2*	23 ± 2*	79 ± 6+
	Mean	0.9 ± 0.2	23 ± 5	23 ± 13	13 ± 5	9 ± 3*	2 ± 2*	5 ± 3*	15 ± 4	58 ± 11+
Saline (n=3)	8	0.6	34 ± 2	47 ± 5	40 ± 5	36 ± 10	31 ± 8	88 ± 10*	37 ± 0	86 ± 5+
	9	0.2	47 ± 2	62 ± 8	65 ± 6	64 ± 5	61 ± 4	114 ± 8*	67 ± 1	159 ± 7+
	10	0.6	13 ± 1	16 ± 6	10 ± 4	9 ± 4	12 ± 6	35 ± 10*	14 ± 1	78 ± 15+
	Mean	0.5 ± 0.1	31 ± 10	42 ± 14	38 ± 16	36 ± 16	35 ± 14	79 ± 23*	39 ± 15	108 ± 26+

* $p < 0.05$ from baseline; + $p < 0.05$ from 24 h air (24 h after injection of CA4P); NA: no measurement.

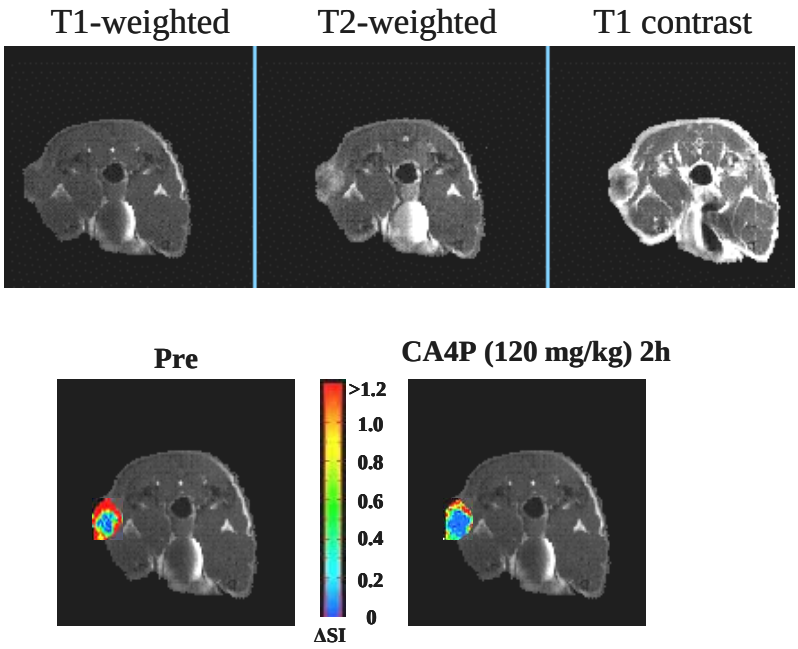

Figure 5. DCE MRI monitoring of tumor response to CA4P. **Top row**: Conventional T1- and T2-weighted, and T1- weighted contrast enhanced MR images of a nude mouse with MDA-MB-231-luc mammary tumor. **Bottom row**: Dynamic contrast enhance MRI was performed in the mouse before (left) and 2 h after (right) CA4P (120 mg/kg) i.p. injection. A normalized contrast enhanced image at 30 s after a bolus injection of Gd-DTPA-BMA acquired before and 2 h after treatment, respectively is superimposed on the T1-weighted image. Significantly decreased signal enhancement, compared to pretreatment, was observed 2 h after i.p. injection of CA4P (17).

I have also performed extensive histological studies on tumor blood vessels, perfusion, and hypoxia in breast tumors (Figs. 6 and 7). Immunohistochemical studies of tumor hypoxia and vasculature using hypoxic marker pimonidazole and endothelium marker CD31 showed that a higher microvascular density (MVD) and lower labeling index of pimonidazole in tumor periphery than the central regions.

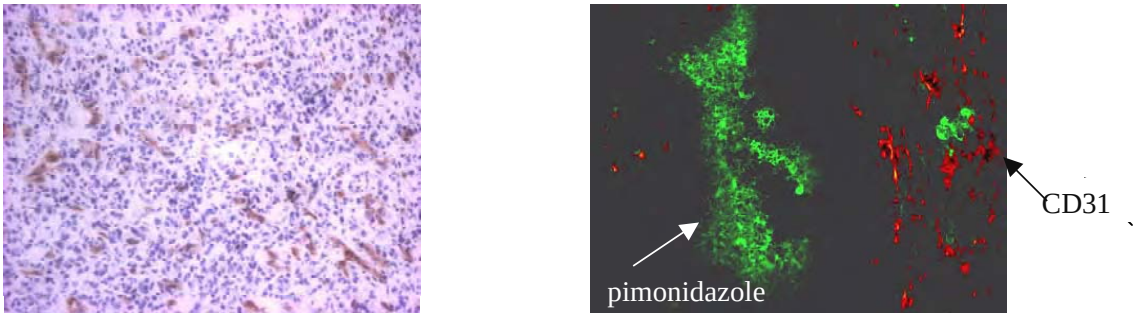

Figure 6 Comparison of pimonidazole and CD31 in a representative tumor. Light immunostaing for CD31 (left) indicated extensive vasculature. Fluorescent staining for hypoxia (pimonidazole, green) was observed at some distance from blood vessels stained for CD31 (red).

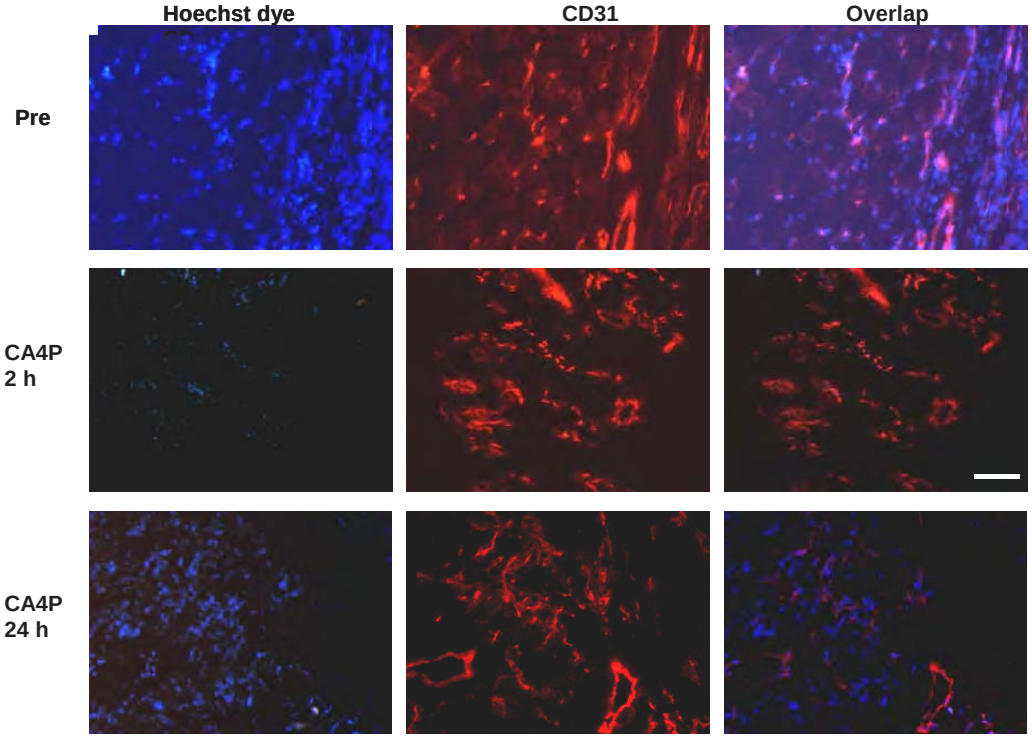

Figure 7 Perfusion marker Hoechst staining pre, 2 h, and 24 h post CA4P (left). Vascular endothelium of the same field was immunostained by anti-CD31 (red, middle). A good match (right) between Hoechst and anti-CD31 stained vascular endothelium was found in the pretreated tumor. Two hours after treatment, significant reduction in perfused vessels was detected, followed by a recovery at 24 h point. Bar = 100 μm (15).

Task 2. Experimental tumor therapy, Month 19-36

a. Learn and become proficient in operating state of the art irradiation system (AccuRay). **Completed.**

b. Design therapeutic protocol based on the MR and histological findings: compare the order and timing of the combined therapy (CA4-P 100mg/kg, i.p., irradiation 30 Gy single dose). **Completed.**

Doses for CA4P and Radiation:

CA4P dose: Based on the MRI studies, a dose of 30 mg/kg induced significant reduction in tumor vascular perfusion/permeability and tissue pO_2 (20). Therefore, we decided to use this dose instead of the proposed 100 mg/kg to investigate experimental treatment.

Radiation dose: While a 30 Gy single dose was proposed originally, we found this dose was well over the TCD_{50} for the proposed 13762NF breast tumor. A 10 Gy single dose was then investigated. Results showed that this dose also significantly inhibited tumor growth (Fig. 8). To study potential effects by adding CA4P, we decided to further lower the radiation dose to 5 Gy (21).

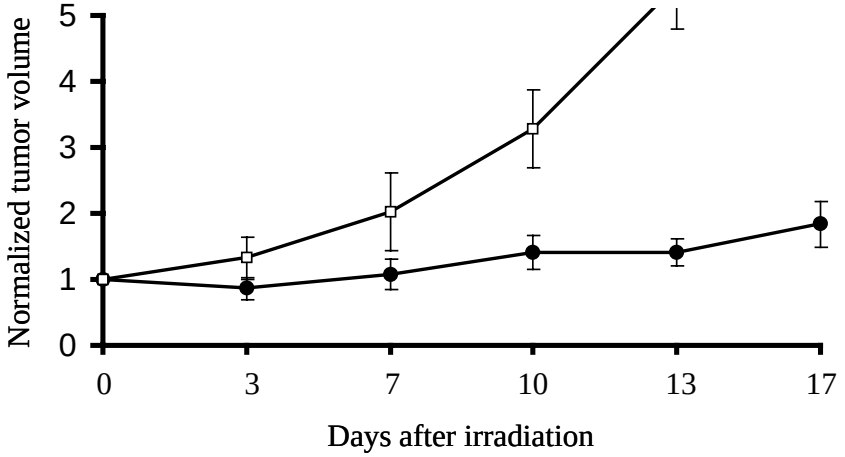

Figure 8. Tumor growth was significantly delayed by a single dose of 10 Gy radiation (●) compared to control tumors (□).

Order and timing of the combination: Our MRI results from Years 1 and 2 have shown that tumor blood perfusion/permeability decreased significantly to ~30% of baseline pretreatment level at 2 h after CA4P (30 mg/kg, i.p.) infusion, which recovered fully after 24 h in a thin peripheral region, but not the tumor center. More importantly, dynamic tumor regional pO_2, which is well recognized to correlate closely with radiation outcome, was evaluated by ^{19}F MRI. Tumor pO_2 was found to decline within 60 min, become significantly lower at 90 min, and decrease further at 2 h after CA4P infusion. Some regional recovery was seen 24 h later but the pO_2 was still significantly lower than the pretreatment level. However, oxygen breathing at this point modified tumor pO_2 significantly, which resulted in essential elimination of tumor hypoxia. All the MRI findings have been confirmed by histological and immunohistological studies. These results have recently been published (20).

c and **d**. Evaluate tumor growth delay after the vascular targeting treatment and/or irradiation.
Completed

Based on these observations, we proposed to administer CA4P (30 mg/kg) on Day 1, and 5 Gy radiation on Day 2, while having animals breathe 100% O_2 from 20 min before to the end of radiation. Previous studies by others have demonstrated that administration of VTA 1 h post radiation produced better improvements in tumor response than other combination schemes. Here, we plan to test and compare our combination approach with other possible combinations on the 13762NF tumors. The preliminary treatment data has been presented at national and international conferences (Fig. 9) (19, 21).

Animals bearing pedicle 13762NF tumors were grouped as:

1. Control without treatment (n = 6);
2. CA4P (30 mg/kg, i.p. single dose) alone (n = 6)
3. Radiation alone (5 Gy single dose, n = 6)
4. Radiation (5 Gy) + O_2 (n = 5), The animals started to breathe oxygen (100% O_2 + 1% isofluorane) 20 min before receiving a 5 Gy radiation delivered by Accuray system.
5. Radiation (5 Gy) + CA4P (1 h post Rx, 30 mg/kg, i.p. n = 6)
6. Radiation with O_2 (5 Gy) + CA4P (1 h post Rx, 30 mg/kg; n = 5); The animals started to breathe oxygen (100% O_2 + 1% isofluorane) 20 min before radiation
7. CA4P (30 mg/kg) + radiation (24 h later, 5 Gy; n = 6)
8. CA4P (30 mg/kg) + radiation with O_2 (24 h later, 5 Gy; n = 6). The animals started to breathe oxygen (100% O_2 + 1% isofluorane) 20 min before receiving a 5 Gy radiation delivered by Accuray system.

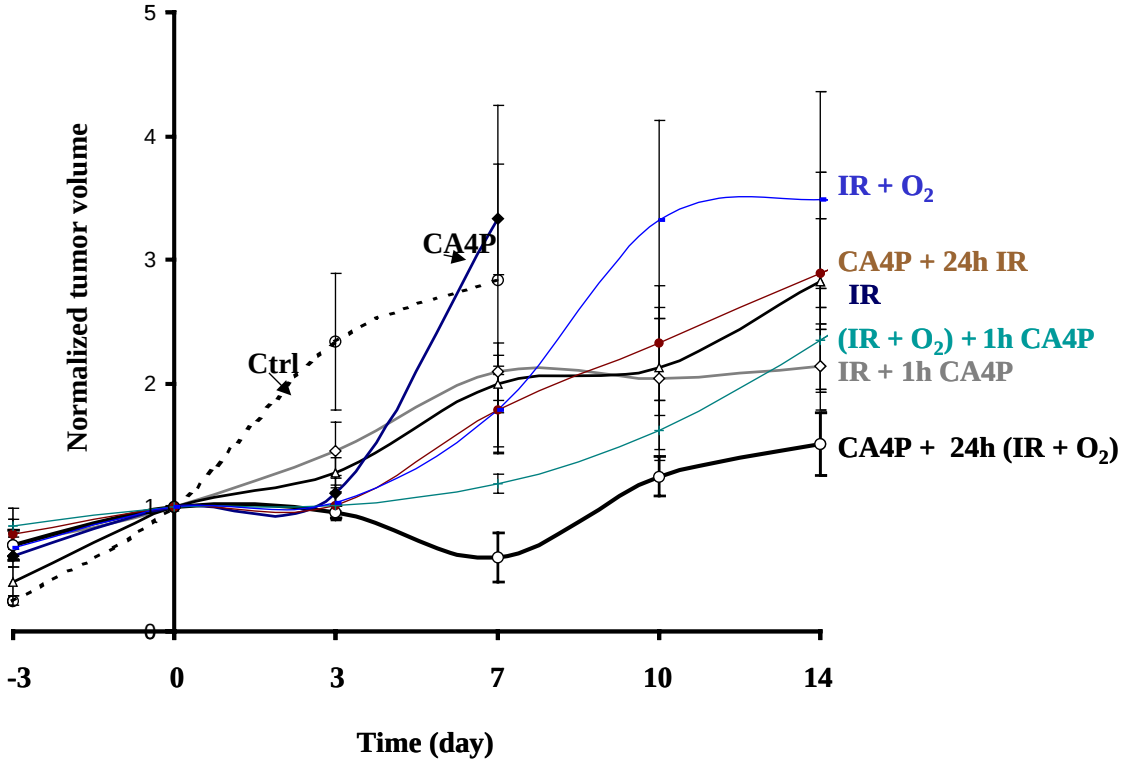

Figure 9. Growth delay versus time curve for the 13762NF tumors. Significant growth inhibition was observed in the CA4P + 24h (IR + O_2) treated group.

Tumor volume change (normalized mean ± s.e.) versus time curve was plotted, as shown in Fig. 9. Most tumors in radiation alone or the combination groups became severely ulcerated, which led to termination of this study on Day 17. The results showed that a single dose (5 Gy; **Group 3**) radiation alone inhibited tumor growth significantly ($p<0.05$). The relatively higher radiosensitivity of this tumor line is in a good agreement with the lower hypoxia fractions observed by MRI. While significant growth delay was achieved during the first 3 days after CA4P (30 mg/kg, i.p.; **Group 2**), tumors started to re-grow and caught up with the Control group rapidly on Day 7. This observation is in common with other studies (7, 8). Oxygen breathing didn't improve radiosensitivity in tumors of **Group 4**. This result again supported our MRI observation that this tumor line is relatively better oxygenated, which typically has a hypoxia fractions (< 5 torr) less than 20% (20). Similar observations has been reported in our previous studies in the Dunning prostate HI tumors that have a hypoxia range similar to the breast 13762NF tumors in this study (22). The approach with CA4P 1 h post radiation (IR + 1h CA4P; **Group 5**) showed no beneficial effects over the IR alone by Day 10. However, tumors in this group seemed to stop growing after Day 10 while the IR alone tumors started to grow rapidly on Day 10. Unfortunately, longer term of growth delay in these tumors could not be achieved because of tumor ulceration. Again, tumors in **Group 6** didn't benefit from addition of oxygen breathing. Our MRI data showed that significantly increased hypoxic fractions induced by CA4P was still observed 24 h later (20). Thus, delivery of radiation at this time point will not induced significant tumor growth delay. This has been proved in the tumors of **Group 7** when compared to tumors in **Group 5** or **6**. However, oxygen breathing 24 h after CA4P administration was found to essentially eliminate tumor hypoxia in the survived peripheral rim (20), which will improve radiosensitivity. Indeed, the tumors in **Group 8** showed significantly slower growth rate from Day 3 than any other group ($p < 0.05$).

Key Research Accomplishments:

- **Assessment of tumor perfusion and oxygenation in the untreated breast tumors by *in vivo* MR approaches**

  a. Heterogeneous vasculature and oxygenation within a tumor or between individual tumors has been evaluated in the 13762NF rat breast tumors using integrated proton and fluorine MR techniques.
  b. Results of ^{1}H BOLD and DCE MRI, providing information about qualitative vascular oxygenation and perfusion.
  c. Significant correlation has been found between changes in tissue pO_2 monitored by ^{19}F NMR oximetry and ^{1}H BOLD response accompanying oxygen intervention.

- **Assessment of dynamic perfusion and oxygenation in the breast tumors in response to a vascular targeting agent, Combretastatin A4 phosphate, by *in vivo* MR approaches**

  a. Significant reduction in tumor perfusion was found at early stage of treatment with CA4P (2hr) by ^{1}H DCE MRI and diffusion-weighted MRI.
  b. Tumor pO_2 started to drop significantly at 90 min and continued to decrease to a lowest value at 2hr after CA4P.
  c. Tumor pO_2 improved at 24hr later, but it was still lower than the pretreated baseline pO_2; pure oxygen inhalation at this time point significantly improved the pO_2, which can be useful in terms of timing for a combination with irradiation in my Task 2 study of this project.

- **Correlation of MR findings with biological studies**
    a. Immunohistochemical studies of tumor hypoxia and vasculature using hypoxic marker pimonidazole and endothelium marker CD31.
    b. Consistent with MRI findings, histological study of tumor perfusion using Hoechst dye 33342 showed a significant reduction in perfused vessels at 2hr after CA4P, which recovered 24 h later.

- **Experimental therapy**

    a. Based on *in vivo* study of tumor physiological dynamics evaluated by MRI, we designed a treatment scheme to administer CA4P 24 h before a single dose radiation plus oxygen inhalation.

    b. The results showed significantly slower tumor growth in this treatment group compared to those in other groups with different combination order or timing.

Reportable Outcomes

Abstracts (Published Conference Proceedings):
Oral presentation:

1. **Zhao, D**., Jiang, L., Constantinescu, A., Hahn, E.W., and Mason, R.P. Interrogation of tumor vasculature and oxygenation by integrated ^{1}H and ^{19}F MRI. *51st Radiat. Res. Soc*. St. Louis, MO, Apr 2004.
2. **Zhao, D**., Jiang, L., Constantinescu, A., Hahn, E.W., and Mason, R.P. Evaluation of breast tumor microcirculation and oxygenation using a combination of BOLD, DCE and ^{19}F MRI. *11th ISMRM*, #222, Kyoto, Japan, May 2004.
3. **Zhao, D**., Jiang, L., and Mason, R.P. MRI evaluation of tumor physiological response to combretastatin A4 phosphate: correlation with a combined radiation response. *Joint ISMRM-ESMRMB*, Berlin, Germany, May 2007.

Poster presentation:

4. **Zhao, D**., Jiang, L., Adam, A., Hahn, E.W., and Mason, R.P. Tumor physiological response to antivascular agent combretastatin A4 phosphate assessed by magnetic resonance imaging. *96th AACR*, #3799, Anaheim, CA, Apr 2005.
5. **Zhao, D**., Jiang, L., Adam, A., Hahn, E.W., and Mason, R.P. *In vivo* MRI monitoring of breast tumor response to the vascular targeting agent combretastatin A4 phosphate. Era of Hope Meeting, P67-24, Phaladephia, PA, June 2005.
6. **Zhao, D**., Richer, E., Liu, Li., Ya Ren, Slavine, N., Shay, J. W., Antich, P. P., Mason, R. P. *In vivo* monitoring of antivascular effects of combretastatin A4 phosphate in a breast cancer xenograft model. *97th AACR*, Washington, DC, Apr 2006.
7. **Zhao, D**., Chang, K, Richer, E., Antich, P, Mason, R.P. Dynamic *iIn vivo* imaging of breast tumors enhances therapeutic response to Combretastatin A4 phosphate. DoD Era of Hope, Baltimore, MD, Jun 2008.

Peer Reviewed Publications:

1. **Zhao, D**., Jiang, L., and Mason, R.P. Measuring changes in tumor oxygenation. *Methods Enzymol*. 386, 378-418, 2004.

2. **Zhao, D**., Jiang, L., Hahn, E.W., and Mason, R.P. Tumor physiological response to combretastatin A4 phosphate assessed by MRI. *Int. J. Radiat. Oncol. Biol. Phys*. 62, 872-80, 2005.
3. **Zhao, D.**, Richer, E., Antich, P. P., and Mason, R. P. Antivascular effects of combretastatin A4 phosphate in breast cancer xenograft assessed using dynamic bioluminescence imaging and confirmed by MRI. *FASEB J, 22:* 2445-2451, 2008.

Manuscript submitted:

1. **Zhao, D.**, Jiang, L., Hahn, E. W., and Mason, R. P. Evaluation of tumor oxygenation by integrated ^{1}H BOLD and ^{19}F MRI. *Magn. Reson. Med*. submitted 2008.

Manuscript in preparation:

1. **Zhao, D**., Chang, K., Jiang, L., Mason, R.P. *In vivo* monitoring of tumor physiological response to combretastatin A4 phosphate: correlation with a combined radiation response. *Radiat. Res.*

Conclusion:

Based on the data of *in vivo* tumor perfusion and oxygenation dynamics in response to the vascular targeting agent, combretastatin A-4-phosphate (CA4P) evaluated by MRI, we successfully designed a scheme to combine the radiation treatment and CA4P to treat breast tumors. This is the major goal of the proposed project. Moreover, the pathophysiological information will be especially useful for designing a complicated scheme, which usually involves combination of fractionated radiation and multiple dose of systemic chemotherapy at clinical settings. I am confident that the proposed project will be fulfilled by the next term.

References:

1. Folkman, J. Anti-angiogenesis: new concept for therapy of solid tumors. Ann Surg, *175:* 409-416, 1972.
2. Denekamp, J. Vascular attack as a therapeutic strategy for cancer. Cancer Metastasis Rev, *9:* 267-282, 1990.
3. Pettit, G. R., Temple, C., Jr., Narayanan, V. L., Varma, R., Simpson, M. J., Boyd, M. R., Rener, G. A., and Bansal, N. Antineoplastic agents 322. synthesis of combretastatin A-4 prodrugs. Anticancer Drug Des, *10:* 299-309, 1995.
4. Davis, P. D., Dougherty, G. J., Blakey, D. C., Galbraith, S. M., Tozer, G. M., Holder, A. L., Naylor, M. A., Nolan, J., Stratford, M. R., Chaplin, D. J., and Hill, S. A. ZD6126: a novel vascular-targeting agent that causes selective destruction of tumor vasculature. Cancer Res, *62:* 7247-7253, 2002.
5. Horsman, M. R. and Siemann, D. W. Pathophysiologic effects of vascular-targeting agents and the implications for combination with conventional therapies. Cancer Res, *66:* 11520-11539, 2006.
6. Dark, G. G., Hill, S. A., Prise, V. E., Tozer, G. M., Pettit, G. R., and Chaplin, D. J. Combretastatin A-4, an agent that displays potent and selective toxicity toward tumor vasculature. Cancer Res, *57:* 1829-1834, 1997.
7. Siemann, D. W., Warrington, K. H., and Horsman, M. R. Targeting tumor blood vessels: an adjuvant strategy for radiation therapy. Radiother Oncol, *57:* 5-12, 2000.
8. Thorpe, P. E., Chaplin, D. J., and Blakey, D. C. The first international conference on vascular targeting: meeting overview. Cancer Res, *63:* 1144-1147, 2003.
9. Rustin, G. J., Galbraith, S. M., Anderson, H., Stratford, M., Folkes, L. K., Sena, L., Gumbrell, L., and Price, P. M. Phase I clinical trial of weekly combretastatin A4 phosphate: clinical and pharmacokinetic results. J Clin Oncol, *21:* 2815-2822, 2003.
10. Galbraith, S. M., Maxwell, R. J., Lodge, M. A., Tozer, G. M., Wilson, J., Taylor, N. J., Stirling, J. J., Sena, L., Padhani, A. R., and Rustin, G. J. Combretastatin A4 phosphate has tumor antivascular activity in rat and man as demonstrated by dynamic magnetic resonance imaging. J Clin Oncol, *21:* 2831-2842, 2003.
11. Zhao, D., Jiang, L., and Mason, R. P. Measuring changes in tumor oxygenation. Methods Enzymol, *386:* 378-418, 2004.
12. Zhao, D., Jiang, L., Constantinescu, A., Hahn, E. W., and Mason, R. P. Evaluation of breast tumor microcirculation and oxygenation using a combination of BOLD, DCE and ^{19}F MRI. *In:* Proc Int Soc Magn Reson Med, Kyoto, Japan, 2004, pp. 222.
13. Zhao, D., Jiang, L., Hahn, E. W., and Mason, R. P. Evaluation of tumor oxygenation by integrated ^{1}H BOLD and ^{19}F MRI. Magn Reson Med, submitted 2008.
14. Zhao, D., Jiang, L., Constantinescu, A., Hahn, E. W., and Mason, R. P. Interrogation of tumor vasculature and oxygenation by integrated 1H and 19F MRI. *In:* 51st Radiat Res Soc, St. Louis, MO, 2004.
15. Zhao, D., Jiang, L., Hahn, E. W., and Mason, R. P. Tumor physiologic response to combretastatin A4 phosphate assessed by MRI. Int J Radiat Oncol Biol Phys, *62:* 872-880, 2005.
16. Zhao, D., Jiang, L., Adam, A., Hahn, E. W., and Mason, R. P. In vivo MRI monitoring of breast tumor response to the vascular targeting agent combretastatin A4 phosphate. *In:* Era of Hope, Phaladephia, PA, June 2005.
17. Zhao, D., Richer, E., Antich, P. P., and Mason, R. P. Antivascular effects of combretastatin A4 phosphate in breast cancer xenograft assessed using dynamic bioluminescence imaging and confirmed by MRI. Faseb J, *22:* 2445-2451, 2008.

18. Zhao, D., Richer, E., Liu, L., Ren, Y., Slavine, N., Shay, J. W., Antich, P. P., and Mason, R. P. In vivo monitoring of antivascular effects of combretastatin A4 phosphate in a breast cancer xenograft model. *In:* 97th AACR, Washington, DC, 2006.
19. Zhao, D., Chang, K., Richer, E., Antich, P. P., and Mason, R. P. Dynamic in vivo imaging of breast tumors enhances therapeutic response to Combretastatin A4 phosphate. *In:* DoD Era of Hope, Baltimore, MD, 2008.
20. Zhao, D., Jiang, L., Hahn, E. W., and Mason, R. P. Tumor physiological response to combretastatin A4 phosphate assessed by MRI. Int. J. Radiat. Oncol. Biol. Phys., *62:* 872-880, 2005.
21. Zhao, D., Jiang, L., and Mason, R. P. MRI evaluation of tumor physiological response to combretastatin A4 phosphate: correlation with a combined radiation response. *In:* ISMRM-ESMRMB, Berlin, Germany, 2007, pp. 467.
22. Zhao, D., Constantinescu, A., Chang, C. H., Hahn, E. W., and Mason, R. P. Correlation of tumor oxygen dynamics with radiation response of the dunning prostate R3327-HI tumor. Radiat Res, *159:* 621-631, 2003.

Appendices

Abstracts (Published Conference Proceedings):

Oral presentation:

1. **Zhao, D**., Jiang, L., Constantinescu, A., Hahn, E.W., and Mason, R.P. Interrogation of tumor vasculature and oxygenation by integrated ^{1}H and ^{19}F MRI. *51st Radiat. Res. Soc*. St. Louis, MO, Apr 2004.
2. **Zhao, D**., Jiang, L., Constantinescu, A., Hahn, E.W., and Mason, R.P. Evaluation of breast tumor microcirculation and oxygenation using a combination of BOLD, DCE and ^{19}F MRI. *11th ISMRM*, #222, Kyoto, Japan, May 2004.
3. **Zhao, D**., Jiang, L., and Mason, R.P. MRI evaluation of tumor physiological response to combretastatin A4 phosphate: correlation with a combined radiation response. *Joint ISMRM-ESMRMB*, Berlin, Germany, May 2007.
4. **Zhao, D**., Chang, K, Richer, E., Antich, P, Mason, R.P. *In vivo* multimodal imaging of antivascular effect of Combretastatin A4 phosphate enhances tumor response to radiation. *11th international symposium of The Tumor Microenvironment*, Miami, FL, May 2008.

Poster presentation:

5. **Zhao, D**., Jiang, L., Adam, A., Hahn, E.W., and Mason, R.P. Tumor physiological response to antivascular agent combretastatin A4 phosphate assessed by magnetic resonance imaging. *96th AACR*, #3799, Anaheim, CA, Apr 2005.
6. **Zhao, D**., Jiang, L., Adam, A., Hahn, E.W., and Mason, R.P. *In vivo* MRI monitoring of breast tumor response to the vascular targeting agent combretastatin A4 phosphate. Era of Hope Meeting, P67-24, Phaladephia, PA, June 2005.
7. **Zhao, D**., Richer, E., Liu, Li., Ya Ren, Slavine, N., Shay, J. W., Antich, P. P., Mason, R. P. *In vivo* monitoring of antivascular effects of combretastatin A4 phosphate in a breast cancer xenograft model. *97th AACR*, Washington, DC, Apr 2006.
8. **Zhao, D**., Chang, K, Richer, E., Antich, P, Mason, R.P. Dynamic *in vivo* imaging of breast tumors enhances therapeutic response to Combretastatin A4 phosphate. DoD Era of Hope, Baltimore, MD, Jun 2008.

Sections of Edited Books:

1. Kim, J. W., **Zhao, D**., Mason, R. P., Liu H. Chemotherapeutic (cyclophosphamide) effects on rat breast tumor hemodynamics monitored by multi-channel NIRS. *SPIE*, 5693, 282-92, 2005.

Peer Reviewed Publications:

1. **Zhao, D**., Jiang, L., and Mason, R.P. Measuring changes in tumor oxygenation. *Methods Enzymol*. 386, 378-418, 2004.
2. **Zhao, D**., Jiang, L., Hahn, E.W., and Mason, R.P. Tumor physiological response to combretastatin A4 phosphate assessed by MRI. *Int. J. Radiat. Oncol. Biol. Phys*. 62, 872-80, 2005.
3. **Zhao, D.**, Richer, E., Antich, P. P., and Mason, R. P. Antivascular effects of combretastatin A4 phosphate in breast cancer xenograft assessed using dynamic bioluminescence imaging and confirmed by MRI. *FASEB J, 22:* 2445-2451, 2008.

REFERENCE #: ZHA-1074-274136

Interrogation of tumor vasculature and oxygenation by integrated ^{1}H and ^{19}F MRI

AUTHORS:

Dawen Zhao [1]
Dallas, TX 75390 US[1]
Lan Jiang [1]
Dallas, TX 75390 US[1]
Anca Constantinescu [1]
Dallas, TX 75390 US[1]
Eric Hahn [1]
Dallas, TX 75390 US[1]
Ralph Mason [1]
Dallas, TX 75390 US[1]

ABSTRACT:

Tumor oxygenation has been widely recognized as a potent factor influencing tumor response to various therapies, especially radiotherapy. Recognizing the intimate interplay of tumor oxygenation and vascularization, we have initiated investigations to compare regional changes in tissue pO_2 with vascularity in syngeneic breast NF13762 carcinomas by integrated ^{1}H and ^{19}F MRI. Tissue pO_2 dynamics were assessed using FREDOM (Fluorocarbon Relaxometry using Echo planar imaging for Dynamic Oxygen Mapping) with hexafluorobenzene, as the reporter molecule. Dynamic Contrast Enhanced (DCE) ^{1}H MRI based on exogenous Gd-DTPA and Blood Oxygen Level Dependent (BOLD) ^{1}H MRI based on endogenous contrast deoxyhemoglobin were used to interrogate vascular characteristics. FREDOM revealed considerable intra tumoral heterogeneity in the distribution of pO_2 values. A mean pO_2 increased significantly from a baseline 18 ±4 (se) torr to a maximum value 78 ±16 torr and a mean HF<10 mmHg decreased from 23 % to 4 %, in response to oxygen breathing. The increase in tissue pO_2 (ΔpO_2) correlated closely with BOLD response to oxygen ($r > 0.9$, $p < 0.001$). However, DCE MRI data (IAUC) showed no correlation with ^{19}F pO_2 or BOLD data. The non-invasive BOLD and DCE MRI are capable of qualitatively measuring blood oxygenation and perfusion. Combination with information on quantitative tissue oxygenation by ^{19}F MR will provide better understanding of tumor physiology and response to intervention. *Supported by DOD Breast Cancer DAMD 170310363 and NCI RO1 EB2762 and P20 CA86354.*

KEYWORDS:

vasculature, Tumor hypoxia, ^{1}H MRI, ^{19}FMRI

Evaluation of breast tumor microcirculation and oxygenation using a combination of BOLD, DCE and 19F MRI

D. Zhao[1], L. Jiang[1], A. Constantinescu[1], E. W. Hahn[1], R. P. Mason[1]
[1]Radiology, UT Southwestern Medical Center, Dallas, TX, United States

Introduction: Tumor microcirculation and oxygenation play important roles in malignant progression and metastasis, as well as response to various therapies (1). Recognizing the intimate interplay of tumor oxygenation and blood flow, we have initiated investigations to compare regional changes in tissue pO_2 with vascularity. We have recently established a novel magnetic resonance approach to measuring regional tumor oxygen tension *FREDOM* (Fluorocarbon Relaxometry using Echo planar imaging for Dynamic Oxygen Mapping) with hexafluorobenzene, as the reporter molecule. This technique allows us to not only simultaneously examine multiple specific locations within a tumor, but also observe dynamic changes at individual locations with respect to intervention. Dynamic Contrast Enhanced (DCE) ^{1}H MRI based on exogenous Gd-DTPA and Blood Oxygen Level Dependent (BOLD) based on endogenous contrast deoxyhemoglobin are each sensitive to vascular characteristics. Here, we apply these MRI approaches to evaluate tumor oxygenation and vascularity and investigate the potential correlations among data set acquired by each technique.

Methods: Syngeneic breast NF13762 carcinomas were implanted in skin pedicles on the foreback of female Fisher rats. When the tumors reached ~ 1 cm diameter (Vol. ~ 0.6 cm^3), MR measurements were performed on a 4.7 T Varian system. Each rat was maintained under general anesthesia (air and 1% isoflurane). Hexafluorobenzene (50 µl) was injected into both central and peripheral regions in a single central plane of the tumor coronal to the rat's body. A tunable (^{1}H/^{19}F) single-turn solenoid coil (2 cm in diameter matched to the tumor size) was placed around the tumor-bearing pedicle. A single 2mm slice parallel to the rat body containing the strongest fluorine signal was chosen for the following ^{1}H DCE and BOLD and ^{19}F pO_2 studies. The transverse relaxation rate $R2^*$ was measured using multigradient echo sequence with 8 echoes (TR=195ms, TE=7ms and spacing =6ms) during air or oxygen breathing. After air equilibration, a series of spin echo planar images (constant recovery time τ = 500 ms (≡ TR) and TE=53 ms) obtained for BOLD response measurements during respiratory challenge. Following BOLD, the coil was retuned to ^{19}F. Tumor oxygenation was assessed on the same 2mm slice using ^{19}F PBSR-EPI of HFB with 6.5 minutes time resolution. A series of pO_2 maps was acquired over a period of 60 min with respiratory challenge, and corresponding regional pO_2 was estimated using the relationship: pO_2 (torr) = (R1-0.0836)/0.001876 (2). Finally, Dynamic Contrast Enhanced (DCE) MRI was performed on the 2mm slice using T1-weighted spin echo sequence (TR= 180ms, TE= 18ms) after a bolus injection of Gd-DTPA-BMA (0.1 mmol/kg, Omniscan) through a tail vein catheter. All data analysis was based on pixel by pixel basis.

Results: Each technique demonstrates intra-tumoral heterogeneity. As shown in Table 1, tumor pO_2 and BOLD SI increased and $R2^*$ decreased in response to respiratory challenge, and tumors with higher initial pO_2 and less hypoxic fraction (HF_{10}) had higher challenged pO_2 values ($r > 0.8$, $p < 0.01$). A significant correlation was found between ΔpO_2 and BOLD response ($r > 0.9$, $p < 0.001$, Fig. 1), while a lack of correlation between baseline pO_2 and the BOLD SI. There was no general correlation among pO_2, $R2^*$ and IAUC.

Table 1. Results of diverse MR approaches

Case	^{19}F pO_2 (torr)			BOLD	$R2^*$ (s^{-1})			DCE
no.	Air	HF_{10} (%)	Δ	(%)	Air	Oxygen	Δ	IAUC
1	36.3	0	136	14.1	46.1	42.6	-3.5	0.66
2	16.6	23	64.5	9.3	54.7	52.6	-2.1	1.00
3	12.5	31	49.6	7.5	69.4	63.8	-5.6	0.58
4	12.8	29	67.7	12.3	115.6	101.6	-14.0	0.49
5	11.5	33	21.5	2.9	64.1	66.7	2.6	0.40
6	12.3	21	19.8	2.3	49.9	47.6	-2.0	0.31
7	24.3	25	47.2	4.5	36.2	33.8	-2.4	0.61
8	NA	NA	NA	6.1	90.6	86.6	-4.0	0.87
Mean	18.0	23	58	7.4	65.8	61.9	-3.9	0.62

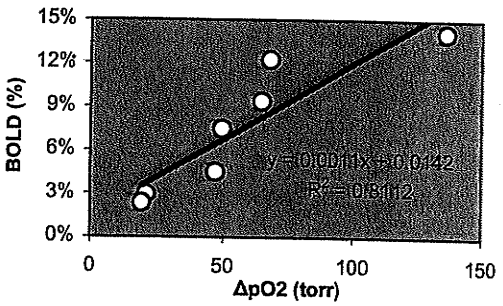

Fig.1. Correlation between ΔpO_2 and BOLD

Discussion: There is increasing evidence that tumor pO_2 has prognostic value in the clinic (1). Using the *FREDOM* approach we are able to detect intra-tumor differences in oxygenation. One might anticipate that non-invasive vascular dynamics could provide surrogate markers for tumor oxygenation. While we have found that BOLD and DCE provide a qualitative indication of tumor vascular dynamics, our results suggest a lack of correlation with tumor pO_2 itself. However, there was a strong correlation between BOLD response and ΔpO_2 accompanying oxygen challenge.

References:

1. Höckel, M., Vaupel, P., *J. Natl. Cancer Inst.*, 93, 266-276, 2001.
2. Hunjan, S., Zhao, D., Constantinescu, A., Hahn, E.W., Antich, P.P., Mason, R.P., *Int. J. Radiat. Oncol. Biol. Phys.*, 49, 1097-1108, 2001.

Acknowledgment: Supported by DOD Breast Cancer DAMD 170310363 and NCI RO1 EB2762 and P20 CA86354.

MRI evaluation of tumor physiological response to combretastatin A4 phosphate: correlation with a combined radiation response

D. Zhao[1], L. Jiang[1], and R. P. Mason[1]

[1]Radiology, University of Texas Southwestern Medical Center, Dallas, Texas, United States

Introduction: The vascular targeting agent, combretastatin A-4-phosphate (CA4P) causes tumor vascular shutdown inducing massive cell death. Although massive necrosis can be induced, tumors usually regrow from a thin viable rim. Thus, a combination of VTAs with additional conventional therapeutic approaches, *e.g.*, radiation, will be required (1). For combination with radiotherapy, measurement of tumor oxygen dynamics will be especially important, since reduced perfusion can induce hypoxia, potentially modulating radiation response. Thus, we have assessed dynamic changes in tumor oxygenation as compared with vascular perfusion/permeability after CA4P treatment by combining ^{1}H and ^{19}F MRI (2). Based on pathophysiological changes monitored by MRI, optimum scheme of the combined radiation and CA4P treatment was designed and experimental treatment was initiated on rat breast tumors.

Materials and Methods: Rat mammary carcinoma 13762NF was implanted syngeneically in a skin pedicle surgically created on the foreback of Fisher 344 adult female rats and allowed to grow to ~ 1 cm diameter.

MRI study: MRI studies were performed using a 4.7 T Varian Inova imaging system. Each rat was maintained under general anesthesia (air and 1% isoflurane). A tunable (^{1}H/^{19}F) volume RF coil was placed around the tumor-bearing pedicle. ^{1}H MRI R_2^* maps were obtained before and 2 h after CA4P (30 mg/kg, i.p., OXiGENE, Inc.) by gradient echo sequence (GEMS) with 8 echoes (TR = 195 ms, TE = 7 ms and spacing = 6 ms). Dynamic contrast enhanced (DCE) MRI using a T_1-weighted spin echo sequence (TR = 70 ms, TE = 12 ms) based on i.v. bolus injection of Gd-DTPA-BMA through a tail vein catheter was also acquired before, 2 h and 24 h after CA4P. For ^{19}F NMR oximetry, hexafluorobenzene (50 µl) was injected directly into the tumor along two or three tracks in a single central plane of the tumor using a fine sharp needle (32G), as described in detail previously (25). *FREDOM* (Fluorocarbon Relaxometry using Echo planar imaging for Dynamic Oxygen Mapping) MRI was performed to acquire a series of pO_2 maps under air or oxygen breathing before and at different time points after CA4P. Data analysis was carried out on a voxel-by-voxel basis with IDL based house made software.

Experimental treatment: Animals bearing 13762NF tumors (n = 30) were grouped as: 1) control without treatment; 2) CA4P (30 mg/kg, i.p.) alone; 3) Radiation (IR) alone (5 Gy single dose); 4) IR (5 Gy) + CA4P (1 h post IR, 30 mg/kg, i.p.); 5) CA4P (30 mg/kg) + IR plus O_2 (24 h post CA4P, 5 Gy). The animals started to breathe oxygen (100% O_2 + 1% isoflurane) 20 min before receiving a 5 Gy IR delivered by Accuray system.

Immunohistochemistry: Immunostaining for Hoechst 33342 (perfusion marker) and CD31 (vascular endothelium) was performed to correlate with imaging findings.

Results: ^{1}H MRI showed that tumor blood perfusion/permeability by DCE MRI decreased significantly to ~30% of baseline pretreatment level at 2 h after CA4P (30 mg/kg, i.p.) infusion, which recovered fully after 24 h in a thin peripheral region, but not the tumor center. Analysis of R_2* maps revealed significantly increased values after 2 h, compared to pretreatment (88.6 v.s. 85.1 s^{-1}, $p < 0.05$). Tumor pO_2 by ^{19}F MRI was found to decline within 60 min, become significantly lower at 90 min, and decrease further at 2 h after CA4P infusion. At this time there was no response to breathing O_2. Some regional recovery was seen 24 h later, but the pO_2 was still significantly lower than the pretreatment level. However, oxygen breathing at 24 h point modulated tumor pO_2 significantly, which resulted in essential elimination of tumor hypoxia (Fig. 1). Correlating well with MRI observations, the tumors of Group 5 with radiation plus oxygen 24 h post CA4P showed a significantly prolonged growth delay ($^{*}p < 0.05$, Fig. 2). Histological data using the perfusion marker, Hoechst 33342, confirmed a significant decrease in perfused vessels 2 h after CA4P, while there was recovery evident at 24 h.

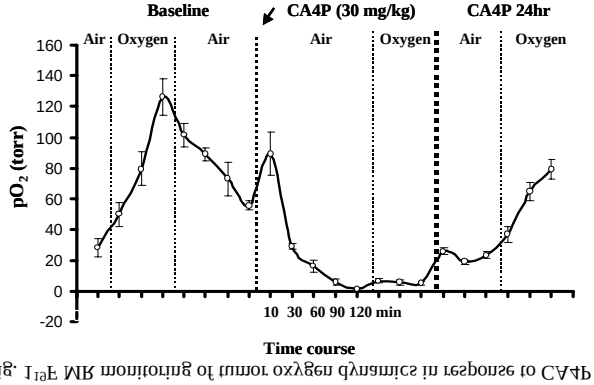

Fig. 1. ^{19}F MRI monitoring of tumor oxygen dynamics in response to CA4P.

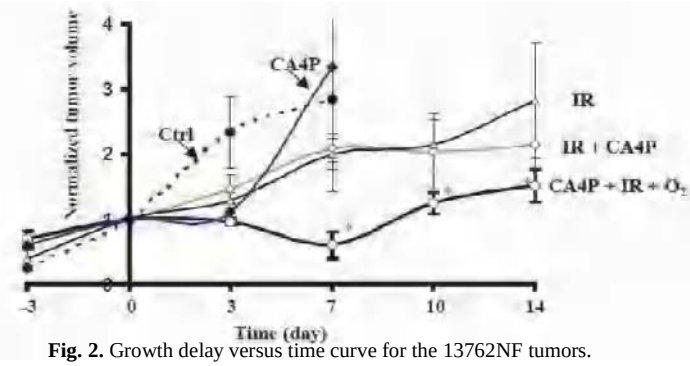

Fig. 2. Growth delay versus time curve for the 13762NF tumors.

Discussion: There is a distinct similarity between the results of the pO_2 measurements and the more traditional DCE, but the quantitative pO_2 values provide the potential for exploiting synergy with other oxygen dependent therapies. The observations further demonstrate the value of *FREDOM* in assessing dynamic changes in regional tumor pO_2 *in vivo* in response to intervention. We believe that dynamic measurements are particularly valuable for understanding the mode of action of therapeutic response to VTAs. Most significantly, these measurements lay a foundation to optimize the timing of combination therapy involving fractionated radiotherapy and multiple doses of VTAs.

References: 1. Stevenson, J. P., Rosen, M., Sun, W., Gallagher, M., et al. *J Clin Oncol, 21:* 4428-4438, 2003.
2. Zhao, D., Jiang, L., Hahn, E. W., and Mason, R. P. *Int J Radiat Oncol Biol Phys, 62:* 872-880, 2005.

Acknowledgment: Supported by DOD Breast Cancer DAMD 170310363 and P20 CA86354 and NIH BTRP facility #P41-RR02584.

IN VIVO MULTIMODAL IMAGING OF ANTIVASCULAR EFFECT OF COMBRETASTATIN A4 PHOSPHATE ENHANCES TUMOR RESPONSE TO RADIATION

Dawen Zhao, M.D., PhD., Karen Chang, PhD., Edmond Richer, PhD., Peter Antich, PhD., Ralph P. Mason, PhD.

Department of Radiology, University of Texas Southwestern Medical Center, Dallas, TX.

The vascular disrupting agent (VDA), Combretastatin A-4-phosphate (CA4P) causes tumor vascular shutdown inducing massive cell death. We have applied magnetic resonance imaging (MRI) and bioluminescent imaging (BLI) to evaluate pathophysiological response to CA4P in breast tumors. Although massive necrosis can be induced by CA4P, tumors usually regrow from a thin viable rim. Thus, a combination of VDAs with additional conventional therapeutic approaches, *e.g.,* radiation, will be required. Based on imaging data of temporal changes in tumor perfusion and especially hypoxiation, induced by CA4P, we have enhanced the combined treatment with radiation in a breast tumor model.

For BLI study of acute vascular perfusion change, MDA-MB 231 human breast tumors were infected to stably express firefly luciferase and highly expressing clones isolated and implanted subcutaneously in the thigh of a nude mouse. CA4P (120 mg/kg; OXiGENE, Inc. Waltham, MA) was injected i.p. immediately after baseline BLI and then 2 h and 24 h later the BLI time course was repeated. In the CA4P treated group, the detected light emission decreased between 50% and 90% and time to maximum was significantly delayed. Twenty-four hours later, there was some recovery of light emission. Comparable vascular changes were evidenced by dynamic contrast enhance (DCE) ^{1}H MRI, and further validated by histological study. Tumor hypoxiation induced by CA4P in syngeneic 13762NF rat breast tumors was evaluated by using the ^{19}F NMR oximetry approach, *FREDOM* (Fluorocarbon Relaxometry using Echo planar imaging for Dynamic Oxygen Mapping). Tumor pO_2 was found to decline within 60 min, become significantly lower at 90 min, and decrease further at 2 h after CA4P infusion. At this time there was no response to breathing O_2. Some regional recovery was seen 24 h later, but the pO_2 was still significantly lower than the pretreatment level. Oxygen breathing at the 24 h point modulated tumor pO_2 significantly, which essentially resulted in elimination of tumor hypoxia. Thus, a combination treatment with radiation plus oxygen 24 h post CA4P was tested and compared with alternatives. The results showed that the optimized combination scheme led to a significantly slower growth rate than any other group ($p < 0.05$).

Both BLI and MRI revealed tumor vascular shutdown after CA4P treatment. We believe that dynamic measurements are particularly valuable for understanding the mode of action of therapeutic response to VTAs. Most significantly, these measurements lay a foundation to optimize the timing of combination therapy involving fractionated radiotherapy and multiple doses of VTAs.

Acknowledgment: Supported by DOD Breast Cancer DAMD 170310363 and SAIRP U24 CA126608 and NIH BTRP facility #P41-RR02584.

3799 Tumor physiological response to antivascular agent combretastatin A4 phosphate assessed by magnetic resonance imaging

Dawen Zhao, Lan Jiang, Ammar Adam, Eric W. Hahn, Ralph P. Mason. *UT Southwestern Medical Ctr., Dallas, TX.*

Tumor oxygenation has been widely recognized as a potent factor, which influences tumor response to chemo- and radio-therapy. The vascular targeting agent, combretastatin A-4-phosphate (CA4P) causes tumor vascular shutdown and a combination of CA4P with radiotherapy has shown enhanced tumor response. We have recently established a novel magnetic resonance approach to measuring regional tumor oxygen tension *FREDOM* (Fluorocarbon Relaxometry using Echo planar imaging for Dynamic Oxygen Mapping) with hexafluorobenzene, as a reporter molecule. Here, the effect of CA4P on real-time tumor oxygenation and perfusion/permeability was monitored *in vivo* in NF13762 rat breast carcinomas by ^{19}F *FREDOM* and ^{1}H dynamic contrast enhanced (DCE) magnetic resonance imaging (MRI). Syngeneic NF13762 rat breast carcinomas were implanted in a skin pedicle on the foreback of Fisher 344 adult female rats. When tumors reached ~ 1 cm diameter (~ 0.6 cm^3) MRI was performed using a 4.7 T horizontal bore magnet with a Varian Unity Inova system. A series of pO_2 maps acquired at 10, 30, 60, 90, and 120 minutes after i.p. CA4P (30 mg/kg; OXiGENE, Inc. Waltham, MA) showed a significant decrease in pO_2 of some tumors as early as 30 min post injection. For all tumors there was a significant drop in tumor pO_2 within 90 min after treatment (mean baseline pO_2 = 23 torr to 9 torr, $p < 0.05$) and a further decrease was observed at 2 h (mean = 2 torr; $p < 0.01$). Intriguingly, the initial changes in pO_2 in central and peripheral regions were parallel, but by 24 h post treatment significant difference was apparent: the pO_2 in periphery improved significantly, while center remained hypoxic. These data are consistent with DCE MRI, which revealed a ~70% decrease in perfusion/permeability (initial area under signal-intensity curve (IAUC)) at 2 h after 30 mg/kg CA4P ($p < 0.001$). IAUC fully recovered in a thin peripheral region, but not the tumor center 24 h post-treatment. Vascular perfusion marker Hoechst 33342 staining confirmed that the number of perfused vessels decreased significantly at 2 h, and then recovered at 24 h. We conclude that magnetic resonance imaging can monitor *in vivo* dynamic changes in tumor vasculature and oxygenation following VTA administration. These results provide the first insight into regional tumor oxygen dynamics in response to CA4P in a syngeneic rat tumor. While dynamic contrast MRI indicates vascular shut down, the critical pO_2 measurements are potentially more important for optimizing therapeutic combination of VTAs with conventional therapy, in particular, irradiation. Supported by DOD Breast Cancer IDEA Award (DAMD 170310363), in conjunction with NCI RO1 CA79515/EB002762 and the Cancer Imaging Program, a P20 Pre-ICMIC CA86354.

Citation format: Proc Amer Assoc Cancer Res 2005;46:3799.

IN VIVO MRI MONITORING OF BREAST TUMOR RESPONSE TO THE VASCULAR TARGETING AGENT COMBRETASTATIN A4 PHOSPHATE

Dawen Zhao, Lan Jiang, Ammar Adam, Eric W. Hahn, Ralph P. Mason
Department of Radiology, UT Southwestern Medical Center at Dallas
primary author's e-mail address: dawen.zhao@utsouthwestern.edu

Hypoxic cells in tumors has long been recognized as a significant factor influencing tumor response to chemo- and radio-therapy. The vascular targeting agent, combretastatin A-4-phosphate (CA4P) causes tumor vascular shutdown and a combination of CA4P with radiotherapy has shown enhanced tumor response. For the potential combination with radiotherapy, measurement of tumor oxygen dynamics will be especially important. Here, we applied a novel magnetic resonance imaging (MRI) approach to measuring regional tumor oxygen tension: FREDOM (Fluorocarbon Relaxometry using Echo planar imaging for Dynamic Oxygen Mapping) with hexafluorobenzene, as a reporter molecule. FREDOM allowed us to quantitatively determine the in situ, in vivo dynamic action of CA4P on real-time tumor oxygenation.

Syngeneic NF13762 rat breast carcinomas were implanted in a skin pedicle on the foreback of Fisher 344 adult female rats. When tumors reached ~ 1 cm diameter (~ 0.6 cm3) MRI was performed using a 4.7 T horizontal bore magnet with a Varian Unity Inova system. A series of pO2 maps acquired at 10, 30, 60, 90, and 120 minutes after i.p. CA4P (30 mg/kg; OXiGENE, Inc. Waltham, MA) showed a significant decrease in pO2 of some tumors as early as 30 min post injection. For all tumors there was a significant drop in tumor pO2 within 90 min after treatment (mean baseline pO2 = 23 torr to 9 torr, $p < 0.05$) and a further decrease was observed at 2 h (mean = 2 torr; $p < 0.01$). Intriguingly, the initial changes in pO2 in central and peripheral regions were parallel, but by 24 h post treatment significant difference was apparent: the pO2 in periphery improved significantly, while center remained hypoxic. In contrast to tumor behavior, there was no significant change in pO2 of thigh muscles of rat at any time point after CA4P. These data are consistent with dynamic contrast enhanced (DCE) MRI, which revealed a ~70% decrease in perfusion/permeability (initial area under signal-intensity curve (IAUC)) at 2 h after 30 mg/kg CA4P ($p < 0.001$). IAUC fully recovered in a thin peripheral region, but not the tumor center 24 h post-treatment. Vascular perfusion marker Hoechst 33342 staining confirmed that the number of perfused vessels decreased significantly at 2 h, and then recovered at 24 h.

These results provide the first insight into regional tumor oxygen dynamics in response to CA4P in a syngeneic rat tumor. While dynamic contrast enhanced MRI will reveal vascular changes, dynamic pO2 measurements are potentially more important for optimizing combinations of VTAs with conventional anti-cancer therapies against breast cancers.

The U.S. Army Medical Research and Materiel Command under DAMD17-03-1-0363 supported this work.

1005 *In vivo* monitoring of antivascular effects of combretastatin A4 phosphate in a breast cancer xenograft model

Dawen Zhao, Edmond Richer, Li Liu, Ya Ren, Nikolai Slavine, Jerry W. Shay, Peter P. Antich, Ralph P. Mason.
UT Southwestern Medical Center, Dallas, TX.

The vascular targeting agent, combretastatin A-4-phosphate (CA4P) causes tumor vascular shutdown inducing massive cell death. We have recently shown acute hypoxiation within 90 mins following CA4P administration to rats bearing syngeneic breast 13762NF tumors using MRI. We have now applied MRI and bioluminescent imaging (BLI) to probe the acute effects of CA4P on human breast MDA-MB-231 tumors.
231 cells were infected with a lentivirus expressing a luciferase reporter and highly expressing clones isolated. 10^6 cells were implanted in the flank of nude mice and allowed to grow to ~ 6 mm diameter. For BLI studies, mice were anesthetized (isoflurane/O_2) and a solution of D-luciferin (450 mg/kg) was administered s.c. in the neck region and light images acquired immediately using one camera of our Light Emission Tomography System (LETS). Serial images (30 s each) were acquired over a period of 20 - 30 mins and the light intensity-time curves evaluated. Saline or CA4P in saline (120 mg/kg; OXiGENE, Inc. Waltham, MA) were injected i.p. immediately after baseline BLI and then 2 h and 24 h later the BLI time course was repeated. We also undertook 3D imaging by acquiring multiple images simultaneously using 3 cameras arranged in a circular gantry around the mouse. MRI studies were performed using a 4.7 T Varian Inova imaging system. The transverse relaxation rate R_2^* was measured using multigradient echo sequence before and 2 h after i.p. CA4P (120 mg/kg). Dynamic contrast enhanced (DCE) MRI based on i.v. bolus injection of Gd-DTPA-BMA through a tail vein catheter was also acquired before and 2 h after CA4P, respectively.
Control tumors showed intense light emission peaking within 8 mins and generally decreasing to about 50-70% after 20 mins. By contrast, CA4P led to a significantly lower light emission (peak ~ 2 to 10 times lower) and delayed peak emission when animals were imaged after 2 h. 24 h later signal remained considerably decreased. Traditional BLI provides a planar image only, but tumors are 3D and known to exhibit heterogeneity, particularly, after vascular targeting agents. LETS successfully provides a 3D representation of the tumors. In good agreement with the BLI data, DCE MRI revealed a ~70% decrease in perfusion/permeability of tumors 2 h after CA4P ($p < 0.001$), while little change was observed in perfusion of the femoral artery. R_2^* measurement showed a significant increase in R_2^* values 2 h after CA4P treatment (mean of 2 h = 131 s^{-1} vs pre = 113 s^{-1}, $p < 0.01$), which may suggest an elevated deoxyhemoglobin from hemorrhagic thrombosis.
Both BLI and MRI enabled accurate imaging of tumor vascular shutdown after CA4P treatment. However, BLI is much cheaper and offers a high throughput method for evaluating novel drugs and drug combinations and scheduling.

Supported by DOD Breast Cancer IDEA Awards (DAMD170310363 and BC031685), the NCI Cancer Imaging Program pre-ICMIC CA86354, and the UT Southwestern Simmons Cancer Center.

Citation format: Proc Amer Assoc Cancer Res 2006;47:1005.

CME: Disclosure of Financial Relationships

Dynamic in vivo imaging of breast tumors enhances therapeutic response to Combretastatin A4 phosphate

Dawen Zhao, Karen Chang, Edmond Richer, Nikolai Slavine, Peter Antich, Ralph P. Mason
University of Texas Southwestern Medical Center, Dallas, TX, United States

The vascular disrupting agent (VDA), Combretastatin A-4-phosphate (CA4P) causes tumor vascular shutdown inducing massive cell death. We have applied magnetic resonance imaging (MRI) and bioluminescent imaging (BLI) to evaluate pathophysiological response to CA4P in breast tumors. Although massive necrosis can be induced by CA4P, tumors usually regrow from a thin viable rim. Thus, a combination of VDAs with additional conventional therapeutic approaches, *e.g.*, radiation, will be required. Based on imaging data of temporal changes in tumor perfusion and especially hypoxiation, induced by CA4P, we have enhanced the combined treatment with radiation in a breast tumor model.

For BLI study of acute vascular perfusion change, MDA-MB 231 human breast tumors were infected to stably express firefly luciferase and highly expressing clones isolated and implanted subcutaneously in the thigh of a nude mouse. CA4P (120 mg/kg; OXiGENE, Inc. Waltham, MA) was injected i.p. immediately after baseline BLI and then 2 h and 24 h later the BLI time course was repeated. In the CA4P treated group, the detected light emission decreased between 50% and 90% and time to maximum was significantly delayed. Twenty-four hours later, there was some recovery of light emission. Comparable vascular changes were evidenced by dynamic contrast enhance (DCE) ^{1}H MRI, and further validated by histological study. Tumor hypoxiation induced by CA4P in syngeneic 13762NF rat breast tumors was evaluated by using the ^{19}F NMR oximetry approach, *FREDOM* (Fluorocarbon Relaxometry using Echo planar imaging for Dynamic Oxygen Mapping). Tumor pO_2 was found to decline within 60 min, become significantly lower at 90 min, and decrease further at 2 h after CA4P infusion. At this time there was no response to breathing O_2. Some regional recovery was seen 24 h later, but the pO_2 was still significantly lower than the pretreatment level. Oxygen breathing at the 24 h point modulated tumor pO_2 significantly, which essentially resulted in elimination of tumor hypoxia. Thus, a combination treatment with radiation plus oxygen 24 h post CA4P was tested and compared with alternatives. As shown in the figure, the optimized combination scheme led to a significantly slower growth rate than any other group ($p < 0.05$).

Both BLI and MRI revealed tumor vascular shutdown after CA4P treatment. The quantitative pO_2 values measured by *FREDOM* provide the potential for exploiting synergy with other oxygen dependent therapies.

Figure. Growth delay versus time curve for cohorts of 13762NF breast tumors.

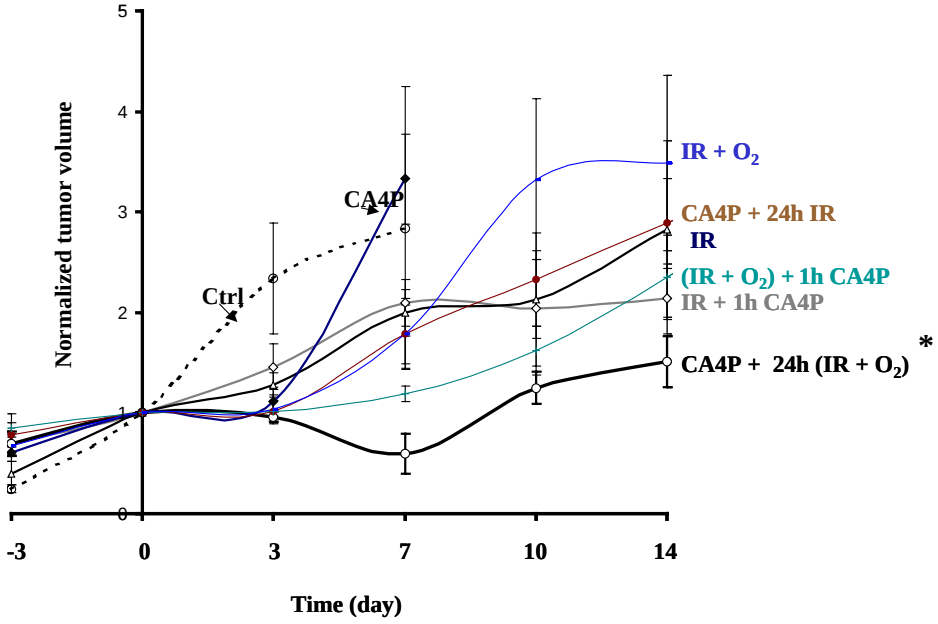

Acknowledgment: Supported by DOD Breast Cancer DAMD 170310363 and SAIRP U24 CA126608 and NIH BTRP facility #P41-RR02584.

Chemotherapeutic (Cyclophosphamide) Effects on Rat Breast Tumor Hemodynamics Monitored by Multi-Channel NIRS.

Jae G. Kim[a], Dawen Zhao[b], Ralph P. Mason[b], Hanli Liu*[a]

[a]Joint Graduate Program of Biomedical Engineering,
University of Texas Southwestern Medical Center at Dallas/ University of Texas at Arlington
Arlington, TX 76019

[b]Advanced Radiological Sciences, Department of Radiology
University of Texas Southwestern Medical Center at Dallas
Dallas, TX 75390

ABSTRACT

We previously suggested that the two time constants quantified from the increase of tumor oxyhemoglobin concentration, $\Delta[HbO_2]$, during hyperoxic gas intervention are associated with two blood flow/perfusion rates in well perfused and poorly perfused regions of tumors. In this study, our hypothesis is that when cancer therapy is applied to a tumor, changes in blood perfusion will occur and be detected by the NIRS. For experiments, systemic chemotherapy, cyclophosphamide (CTX), was applied to two groups of rats bearing syngeneic 13762NF mammary adenocarcinomas: one group received a single high dose i. p. (200 mg/kg CTX) and the other group continuous low doses (20 mg/kg CTX i. p. for 10 days). Time courses of changes in tumor $\Delta[HbO_2]$ were measured at four different locations on the breast tumors non-invasively with an inhaled gas sequence of air-oxygen-air before and after CTX administration. Both rat body weight and tumor volume decreased after administration of high dose CTX, but continuous low doses showed decrease of tumor volume only. Baselines (without any therapy) intra- and inter-tumor heterogeneity of vascular oxygenation during oxygen inhalation were similar to our previous observations. After CTX treatment, significant changes in vascular hemodynamic response to oxygen inhalation were observed from both groups. By fitting the increase of $\Delta[HbO_2]$ during oxygen inhalation, we have obtained changes of vascular structure ratio and also of perfusion rate ratio before and after chemotherapy. The preliminary results suggest that cyclophosphamide has greatest effect on the well perfused tumor vasculature. Overall, our study supports our earlier hypothesis, proving that the effects of chemotherapy in tumor may be monitored non-invasively by using NIRS to detect changes of hemodynamics induced with respiratory challenges.

Keywords: Breast Cancer, Cyclophosphamide, Hemodynamics, NIR Spectroscopy, Tumor vascular oxygenation

1. INTRODUCTION

In addition to surgical resection, many other types of cancer therapy are available for patients including radiotherapy, photodynamic therapy and chemotherapy. Chemotherapy plays an important role to treat cancers even though it has some side effects. Currently, the effect of chemotherapy is monitored by MRI or CT that can measure the tumor volume changes during cancer treatment. However, it can take up to 3 weeks to detect such changes, and this is considerably late for clinicians to decide whether initial therapeutic strategy should be continued or modified. This delay in detection of chemotherapy effect can reduce the quality of a patient's life and ineffective therapy is costly. Therefore, many researchers are trying to develop tools that can detect the early response to cancer treatment. For example, Li *et al.* have used ^{31}P nuclear magnetic resonance spectroscopy (NMRS) to measure the effectiveness of cyclophosphamide (CTX) treatment in radiation-induced fibrosarcoma (RIF).[1] They found that the ratio of inorganic phosphate to other phosphate metabolites in CTX treated group was significantly decreased during the tumor growth delay period compared to age-matched controls. Poptani *et al.* studied the effects of CTX treatment in RIF-1 tumors in terms of tumor oxygenation

and glycolytic rate changes by utilizing ^{13}C MRS, Eppendorf electrode, and Redox scanning.[2] They observed that CTX treatment caused reduction in glycolytic rate, a significant decrease in tumor tissue pO_2, and also an increase of NADH levels 24 hours after the treatment while tumor volume did not show any significant difference between the CTX-treated and control groups. Zhao *et al.* have reported significant changes in rat breast tumor perfusion following either single dose CTX or continuous low dose "metronomic" therapy.[3]

In the last decade, near infrared spectroscopy (NIRS) has been developed to examine tissue oxygenation and has been widely applied to investigate hemoglobin oxygenations of muscles,[4,5,6] the brain,[7,8,9] and animal tumors.[10,11,12,13,20] Since tumors have higher vascular density and also higher metabolism than normal tissues, total hemoglobin concentration ($[Hb_{total}]$), oxyhemoglobin concentration ($[HbO_2]$), and reduced scattering coefficient ($\mu s'$) were used as markers to identify tumors from the human breast by using NIRS.[14,15,16] In addition, an NIR spectrometer is a low-cost, portable, and real-time display instrument. Therefore, NIRS has a good potential to be used as a monitoring tool for tumor treatment planning and tumor prognosis.

We have previously studied breast tumor oxygenation under gas intervention using NIRS and found that oxyhemoglobin concentration changes ($\Delta[HbO_2]$) during gas intervention can be fitted by a two-exponential equation containing two time constants.[12] Based on the model, we formed a hypothesis that changes in oxygenated hemoglobin concentration result from well perfused and poorly perfused regions of an animal tumor to explain why there are two different time constants in the $\Delta[HbO_2]$ data. The model further allows us to associate the signal amplitudes and time constants to the ratio of vascular density and the ratio of the perfusion rates in the two different regions, respectively.

In this study, we applied the NIRS system to monitor the tumor oxygenation changes during oxygen intervention before and after CTX administration. The purpose for this study is to explore the NIRS as a possible tool for monitoring tumor responses to chemotherapy. This work is based on the following hypothesis: when tumor is treated with chemotherapy, changes in blood perfusion and vascular density in the tumor will occur and will be seen as changes of the two fitted parameters from the NIRS measurements. In addition, by developing a non-invasive tool for monitoring cancer therapy, we are not only monitoring the reduction of tumor size, but also detecting the changes of tumor physiological conditions, which are essential for tumor treatment planning and tumor prognosis.

2. MATERIALS AND METHODS

2.1 Tumor Model and Experimental Procedure

Rats were divided into three groups for this study. Two groups were treated with CTX at different doses, and the other group was administered saline instead of CTX as a control group. Cyclophosphamide was chosen as a chemotherapeutic agent for this study since our tumor line is highly responsive to alkylating agents and platinum chemotherapeutic agents.[17] CTX is an antineoplastic alkylating agent, and it has been used to treat lymphomas, cancers of the ovary, breast and bladder, and chronic lymphocytic leukaemia.[18,19] The tumor line was rat mammary adenocarcinomas 13762NF (cells originally provided by the Division of Cancer Therapeutics, NCI), and the tumors were implanted in the hind limb of adult female Fisher 344 rats (~200 g).

The rats were anesthetized with 0.2 ml ketamine HCl (100 mg/ml; Aveco, Fort Dodge, IA) when the tumors reached approximately 1 cm in diameter and maintained under general gaseous anesthesia using a small animal anesthesia unit with air (1 dm^3/min) and 1% isoflurane through a mask placed over the mouth and nose. During the experiments, the rat was placed on a warm blanket to maintain body temperature, which was monitored with a rectally inserted thermal probe connected to a digital thermometer (Digi-Sense, model 91100-50, Cole-Parmer Instrument Company, Vernon Hills, IL). Tumors were shaved before measurements to improve optical contact for transmitting light. A pulse oximeter (model: 8600V, Nonin, Inc.) was placed on the hind foot to monitor arterial oxygenation (S_aO_2) and heart rate. For the single high dose group (n=5), a light source and four detectors from a multi-channel, CW (continuous wave) NIRS (NIM, Inc, Philadelphia, PA) were attached to the tumor using posts and swivel post clamps (see Figure 1(a)). For the multi low dose (n=3) and control (n=3) groups, we have used four-channel, frequency domain (FD), NIRS (ISS, Champaign, IL). In the latter case, the four sets of light sources replaced four detectors shown in Figure 1(b), and one detector fiber was placed on the top center of the tumor to obtain signals from four different regions of tumor.

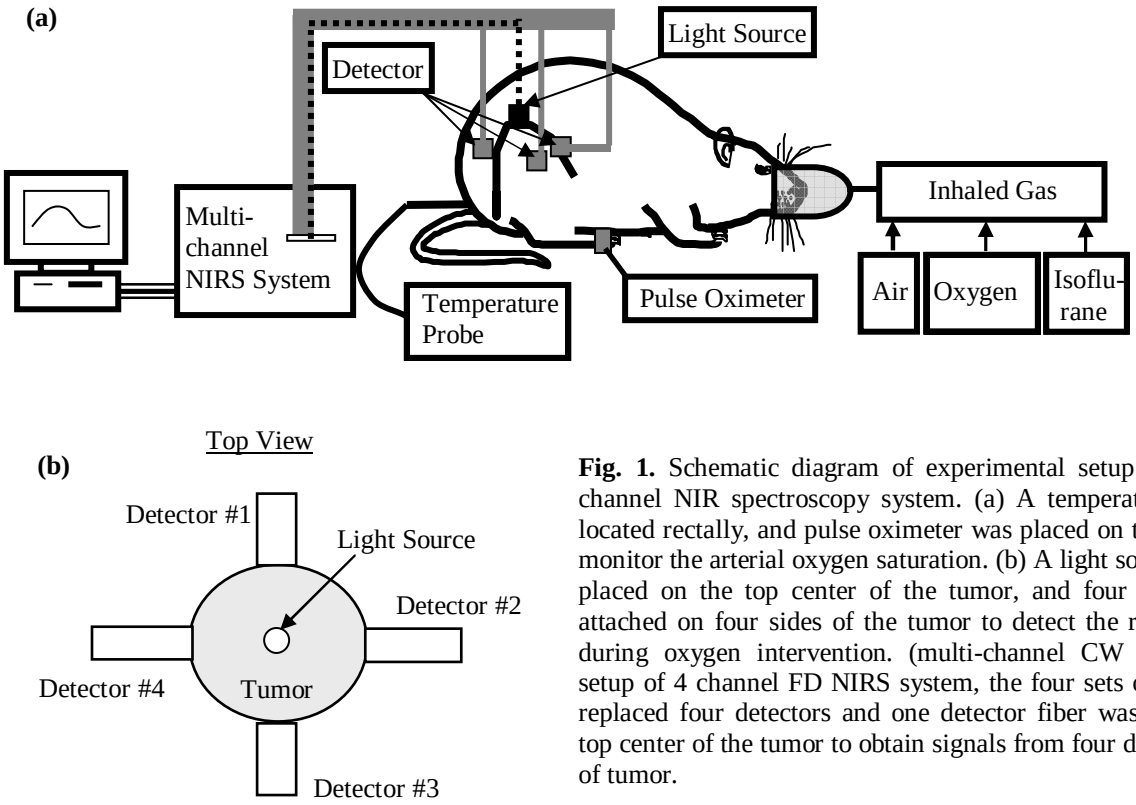

Fig. 1. Schematic diagram of experimental setup for the multi-channel NIR spectroscopy system. (a) A temperature probe was located rectally, and pulse oximeter was placed on the hind paw to monitor the arterial oxygen saturation. (b) A light source probe was placed on the top center of the tumor, and four detectors were attached on four sides of the tumor to detect the regional signals during oxygen intervention. (multi-channel CW NIRS). In the setup of 4 channel FD NIRS system, the four sets of light sources replaced four detectors and one detector fiber was placed on the top center of the tumor to obtain signals from four different regions of tumor.

All the measurements were performed in a dark room, and the measurements were initiated while the rats breathed air for 10 minutes to get a stable baseline. After 10 minutes of baseline measurement, the inhaled gas was switched to oxygen for 15 minutes, and then back to air for 15 minutes. This experimental procedure was repeated before and after the CTX treatment, and the four detectors were intended to be located at the same positions for each measurement on different days. Using an ellipsoidal approximation, tumor volume V (cm^3) was estimated as $V = (\pi/6)\cdot L\cdot W\cdot H$ where L, W, and H are the three respective orthogonal dimensions. Raw amplitude data from four locations were recorded simultaneously during the experiments and processed after the experiments to obtain the $\Delta[HbO_2]$ and $\Delta[Hb_{total}]$. The amplitude and time constant of $\Delta[HbO_2]$ were calculated by fitting the two-exponential model to the data using Kaleidagraph (Synergy Software, Reading, PA). The corresponding ratios of vasculature coefficients and perfusion rates, i.e., γ_1/γ_2 and f_1/f_2, were also calculated to show static and dynamic heterogeneities of the tumors at different locations.

2.2 Measurement System

As mentioned above, we have used two NIRS systems for this study: a multi-channel, CW, NIRS system was used in the single high dose study, while an ISS, 4-channel, frequency-domain, NIRS system was applied in the continuous low dose study. The original CW NIRS system has the ability to measure light signals from eight different locations, but due to the finite tumor size, we used only four detectors to monitor tumor vascular oxygenation dynamics during respiratory challenges. In common with our previous work[12,20], we assume that oxyhemoglobin and deoxyhemoglobin are the only significant absorbing materials in the blood-perfused tumor tissue in the NIR range. The absorption coefficients comprise the extinction coefficients for deoxyhemoglobin and oxyhemoglobin multiplied by their respective concentrations (Eqs. 1 and 2) at 730 nm and 850 nm, that have been employed in our multi-channel NIRS system.

$$\mu_a^{730} = \varepsilon_{Hb}^{730}[Hb] + \varepsilon_{HbO2}^{730}[HbO_2], \quad (1)$$

$$\mu_a^{850} = \varepsilon_{Hb}^{850}[Hb] + \varepsilon_{HbO2}^{850}[HbO_2]\ . \quad (2)$$

Based on modified Beer-Lambert's law, the data presented in this paper were analyzed using amplitude values to find the changes in absorption (Eq. 3). By manipulating Equations 1-3, changes in oxygenated hemoglobin, deoxygenated hemoglobin and total hemoglobin concentrations were calculated from the transmitted amplitude of the light through the tumor (Eqs. 4, 5 and 6).

$$\mu_{aB} - \mu_{aT} = \log (A_B/A_T) / L, \quad (3)$$

$$\Delta[HbO_2] = [-0.674*\log (A_B/A_T)^{730} + 1.117*\log (A_B/A_T)^{850}] / L, \quad (4)$$

$$\Delta[Hb] = [0.994*\log (A_B/A_T)^{730} - 0.376*\log (A_B/A_T)^{850}] / L, \quad (5)$$

$$\Delta[Hb_{total}] = \Delta[Hb] + \Delta[HbO_2]=[0.32*\log (A_B/A_T)^{730} + 0.741*\log (A_B/A_T)^{850}] / L, \quad (6)$$

where A_B = baseline amplitude; A_T = transition amplitude; L = optical pathlength between source/detector. The constants contained in these equations were computed with the extinction coefficients for oxy and deoxyhemoglobin at the two wavelengths used.[21] Notice that these coefficients have accounted for four hemes per hemoglobin molecule. In principle, L should be equal to the source–detector separation, d, multiplied by a differential pathlength factor (DPF), i.e., L=d*DPF. Little is known about DPF for tumors, although a DPF value of 2.5 has been used by others.[10] Since our focus is on dynamic changes and relative values of tumor [HbO_2] in response to oxygen intervention, we have taken the approach of including the DPF in the unit, and eq. (4) becomes as follows:

$$\Delta[HbO_2] = [-0.674*\log (A_B/A_T)^{730} + 1.117*\log (A_B/A_T)^{850}] / d, \quad (7)$$

where d is the direct source-detector separation in cm, and the unit of $\Delta[HbO_2]$ in Eq. (7) is mM/DPF.

Since the wavelengths of light sources from the ISS, frequency-domain system were 750 nm and 830 nm, the corresponding equations for $\Delta[HbO_2]$, $\Delta[Hb]$, and $\Delta[Hb_{total}]$ are modified as follows.

$$\Delta[HbO_2] = [-0.709*\log (A_B/A_T)^{750} + 1.404*\log (A_B/A_T)^{830}] / d, \quad (8)$$

$$\Delta[Hb] = [0.9546*\log (A_B/A_T)^{750} - 0.4992*\log (A_B/A_T)^{830}] / d, \quad (9)$$

$$\Delta[Hb_{total}] = \Delta[Hb] + \Delta[HbO_2]=[0.2456*\log (A_B/A_T)^{750} + 0.9048*\log (A_B/A_T)^{830}] / d. \quad (10)$$

2.3 Bi-exponential Model of Tumor Vascular Oxygenation

In our previous report,[12] we followed an approach used to measure regional cerebral blood flow (rCBF) with diffusible radiotracers, as originally developed by Kety[22] in the 1950's. By applying Fick's principle and defining γ as the ratio of HbO_2 concentration changes in the vascular bed to that in veins, we arrived at Eq. (11):

$$\Delta HbO_2^{vasculature}(t) = \gamma H_o[1-\exp(-ft/\gamma)] = A_1[1-\exp(-t/\tau)] \quad (11)$$

where γ is the vasculature coefficient of the tumor, H_o is the arterial oxygenation input and f is the blood perfusion rate.

If a tumor has two distinct perfusion regions, and the measured signal results from both of the regions (Figure 2), then it is reasonable to include two different blood perfusion rates, f_1 and f_2, and two different vasculature coefficients, γ_1 and γ_2, in the model. Therefore, Eq. (11) can be modified to count for the double exponential feature observed in the experiments:

$$\Delta HbO_2^{vasculature}(t) = \gamma_1 H_o[1-\exp(-f_1 t/\gamma_1)] + \gamma_2 H_o[1-\exp(-f_2 t/\gamma_2)]$$
$$= A_1[1-\exp(-t/\tau_1)] + A_2[1-\exp(-t/\tau_2)] \quad (12)$$

where f_1 and γ_1 are the blood perfusion rate and vasculature coefficient in region 1 for the well perfused region, respectively; f_2 and γ_2 have the same respective meanings in region 2 for the poorly perfused region, and $A_1 = \gamma_1 H_o$, A_2 =

$\gamma_2 H_o$, $\tau_1 = \gamma_1/f_1$, $\tau_2 = \gamma_2/f_2$. Then, if A_1, A_2, τ_1, and τ_2 are determined by fitting the measurements with the model, we can obtain the ratios of two vasculature coefficients and the two blood perfusion rates:

$$\frac{\gamma_1}{\gamma_2} = \frac{A_1}{A_2}, \qquad \frac{f_1}{f_2} = \frac{A_1/A_2}{\tau_1/\tau_2}. \tag{13}$$

With these two ratios, we are able to understand more about tumor physiology, such as tumor vasculature and blood perfusion.

3. RESULTS

3.1 Body weight and tumor volume changes during chemotherapy

Body weight and tumor volume were monitored before and after the CTX treatments to see the tumor responses and side effects from chemotherapy. In the single high dose treatment group, body weight decreased until 6 days after the treatment, but later increased for the rest of days of observation. Two rats among five in this group failed to survive at day 6 due to the toxicity from the high dose CTX treatment. Therefore, the data shown at day 8 and 10 represent the smaller group of rats which survived during the high dose treatment. Tumor volume did not further decreased after day 4. (Fig. 2(b)) In comparison, rats in the continuous low dose group initially lost weight after a low dose of CTX administration, but gradually gained the weight during the treatment, presenting low toxicity from the treatment. This group also showed a significant reduction in tumor volume during the treatment. For a control group, saline was injected into the rats instead of CTX, and a gradual decrease of body weight was observed, while their tumor volumes increased exponentially. Changes in rat body weight and tumor volume were normalized to day 0 (before CTX or saline administration). (Figures 2(a) and (b)) Solid circles represent the data from a control group, and open squares and open diamonds represent the continuous low dose group and single high dose group, respectively.

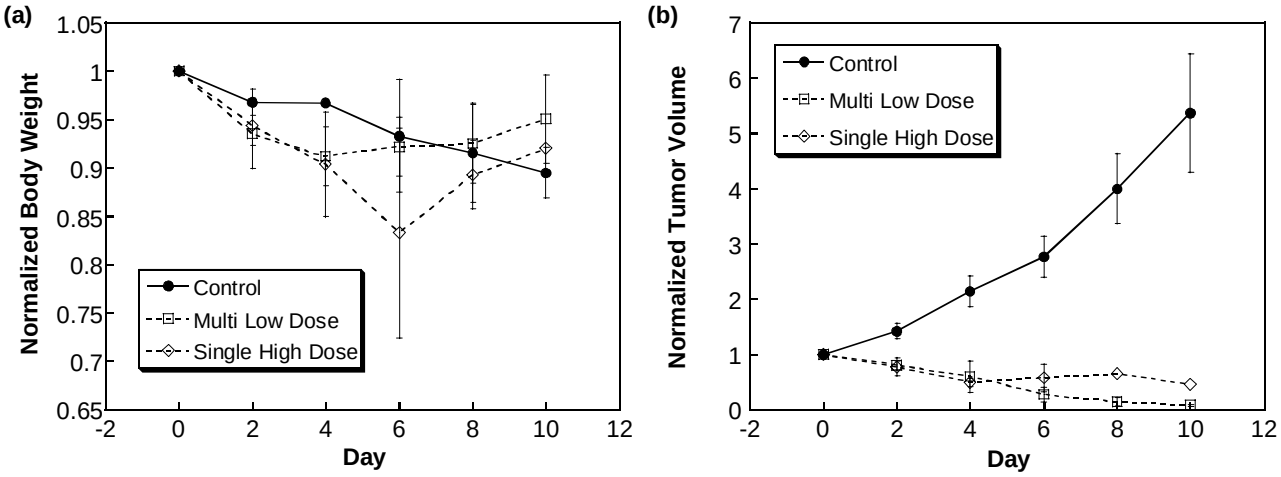

Fig. 2. Normalized changes in rat body weight (a) and tumor volume (b) during the saline and CTX treatments.

3.2 Intratumoral heterogeneity of vascular oxygenation observed by the multi-channel NIRS

In our experiment, we have utilized either one light source and four detectors and from the CW system (NIM, Inc) or four light sources and one detector from the FD system (ISS, Inc.) for the rat breast tumor measurements, and the setups (Fig. 1). After 10 minutes of baseline measurement with air breathing, gas was switched to pure oxygen, causing a rapid increase in tumor [HbO_2]. These changes were measured simultaneously from four locations of the tumor. Figure 3 shows a representative set of data before the CTX treatment, with the DC NIRS system. Open circles show the raw data

measured by multi-channel NIRS, and the solid black lines represent the fitted curves using our bi-exponential model for hemodynamics during oxygen intervention.[12] It is apparent that the data from each location differs though there are similar trends of $\Delta[HbO_2]$.

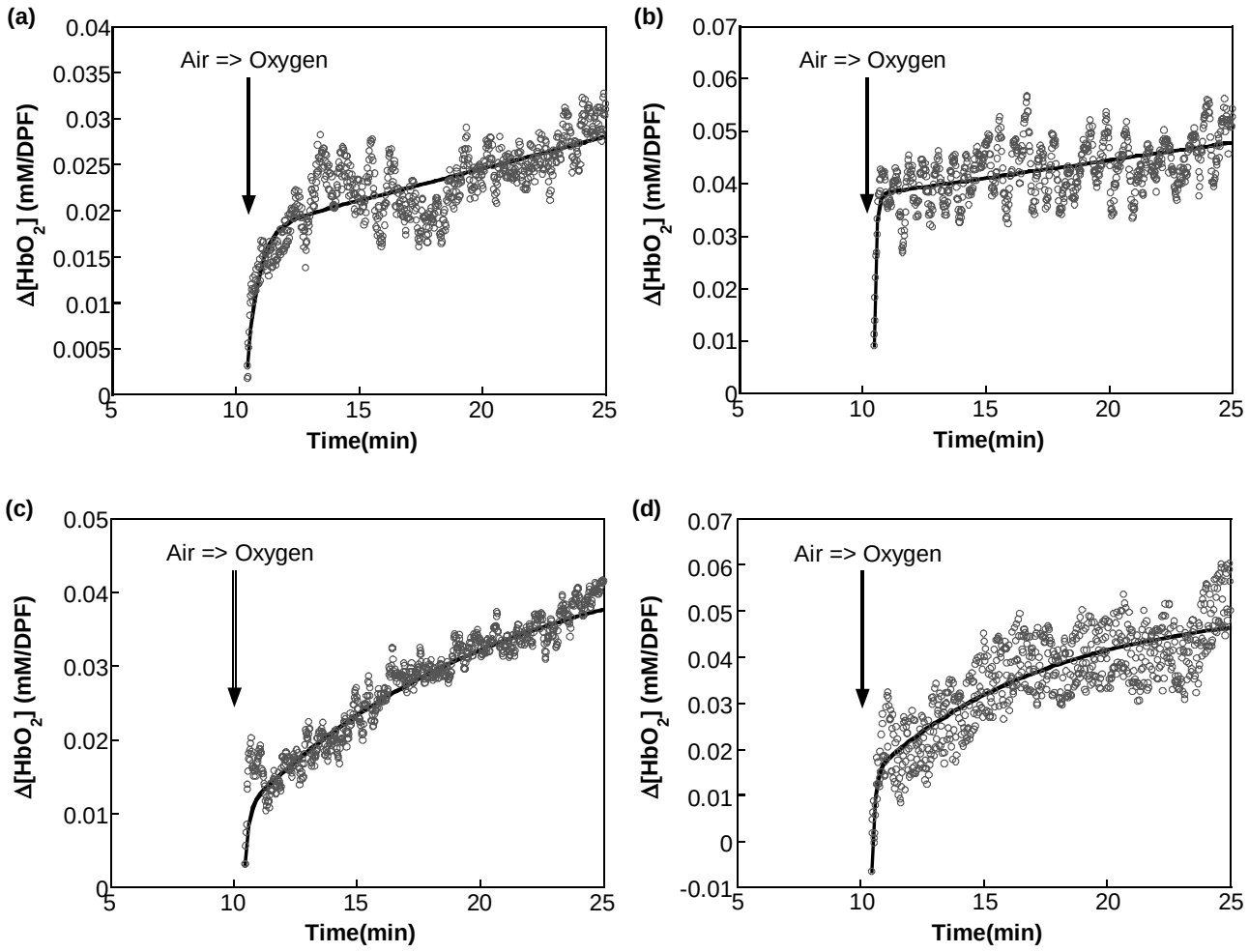

Fig. 3. Dynamic changes of tumor $[HbO_2]$ from four locations in a rat breast tumor. The rising parts of $\Delta[HbO_2]$ from the four locations were fitted using a double-exponential expression. Figures 3(a)-3(d) were taken from locations #1-#4, respectively. In this case, the tumor was not treated yet.

Table 1. Summary of vascular oxygen dynamics determined at the four detectors from tumor shown in the Fig. 3.

Location	A_1	A_2	τ_1	τ_2	A_1/A_2 (=γ_1/γ_2)	τ_1/τ_2	f_1/f_2
1 (Fig. 3a)	0.013	0.027	0.48	24.3	0.48	0.02	24
2 (Fig. 3b)	0.029	0.026	0.09	29.8	1.12	0.003	373
3 (Fig. 3c)	0.008	0.036	0.15	10.6	0.22	0.014	16
4 (Fig. 3d)	0.021	0.037	0.12	7.25	0.57	0.017	34

To compare the data taken from four locations of the tumor more clearly, the time constants and amplitudes from the four fitted curves are summarized in Table 1. The ratios of γ_1/γ_2 and f_1/f_2 characterize tumor vascular structure and blood

perfusion within the volume of tumor interrogated by light.[12] In principle, when γ_1/γ_2 is close to 1, it implies that the measured optical signal results equally from both regions 1 (*i.e.*, well perfused region) and 2 (i.e., poorly perfused region); if $\gamma_1/\gamma_2 < 1$, the measured signal results more from region 2 than region 1 [Figures 3(a), 3(c) and 3(d)]. As Table 1 demonstrates, only location #2 has a ratio of γ_1/γ_2 slightly higher than 1, and the readings from locations #1, #3 and #4 have the ratios of γ_1/γ_2 less than 1. This may suggest that the tumor volume that was optically interrogated from location #2 was dominated by well perfused regions, while most of other tumor volumes detected from locations #1, #3 and #4 are composed of more poorly perfused regions. Furthermore, all the ratios of f_1/f_2 from four locations of the tumor shown in Fig. 3 are much greater than 1, indicating that the blood perfusion rate in well perfused region is much greater than that in poorly perfused region. Especially, f_1/f_2 from location #2 is 10 to 20 times higher than those from locations #1, #3, and #4, showing a high level of intratumoral heterogeneity in dynamic vascular structure.

3.3 Monitoring vascular hemodynamics of breast tumors before and after chemotherapy

The tumor hemodynamics during oxygen intervention were measured before and after administration of CTX and saline. The representative data from the control group and continuous low dose group are shown in Figs. 4(a) and 4(b), respectively. Similar to Figure 3, open symbols are the raw data from measurements, and solid lines are the fitted curves using our double exponential model. As mentioned before, there were 4 light sources placed on the surface of tumor. Figure 4 shows the acute and then gradual changes of $[HbO_2]$ after switching the breathing gas from air to oxygen, and the data were observed at the same (or nearly the same) location of tumor from day 0 to day 6. From Figure 4(a), we can see different tumor hemodynamics at different days, but having similar trends and maximum $\Delta[HbO_2]$ for the control group. However, the data taken from the continuous low dose group show quite different hemodynamics throughout the treatment days (Fig. 4(b)). Especially, we notice that the fast increase part became much smaller at Days 2 and 6 compared to Day 0, implying a significant decrease in signal from the well perfused region.

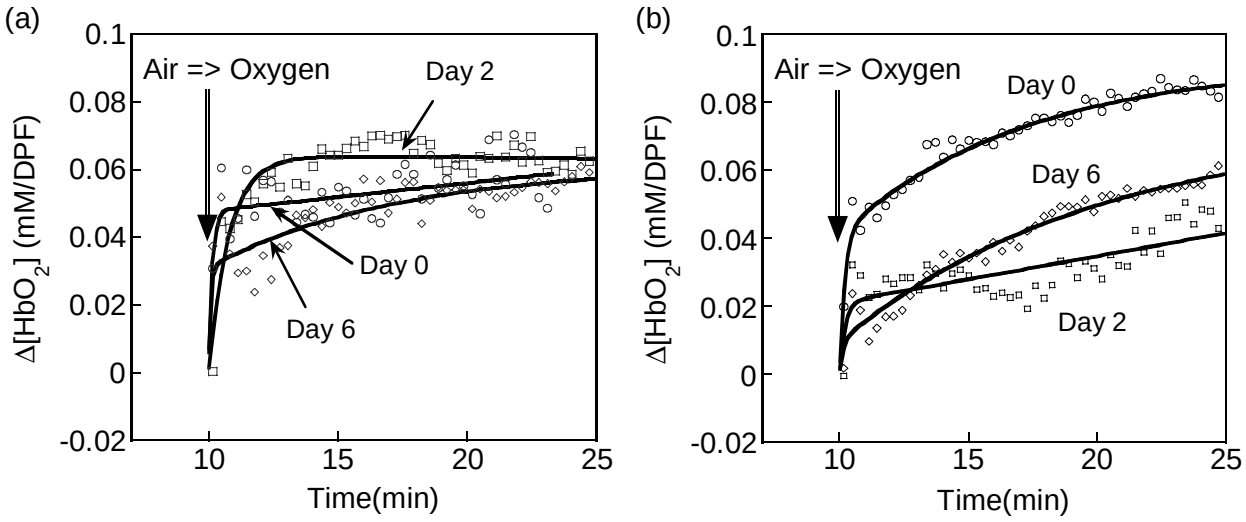

Fig. 4. Dynamic changes of Δ??$[HbO_2]$ taken at location #1 from a rat breast tumor before and after administration of (a) saline and (b) continuous low dose of CTX (20 mg/kg for 10 days). The rising part of $\Delta[HbO_2]$ from location #1 was fitted using the double-exponential expression.

Figure 5 also shows the changes of tumor hemodynamics during oxygen intervention, before and after a single high dose of CTX treatment, measured by the CW NIRS. This figure clearly demonstrates that we can observe significant changes in tumor hemodynamics after chemotherapy by using respiratory challenge as a mediator. The fitted parameters from our mathematical model are summarized in Table 2 to compare the changes in hemodynamic parameters before and after administration of CTX. The rising part of $\Delta[HbO_2]$ from location #1 was fitted using either a single- or double-exponential expression.

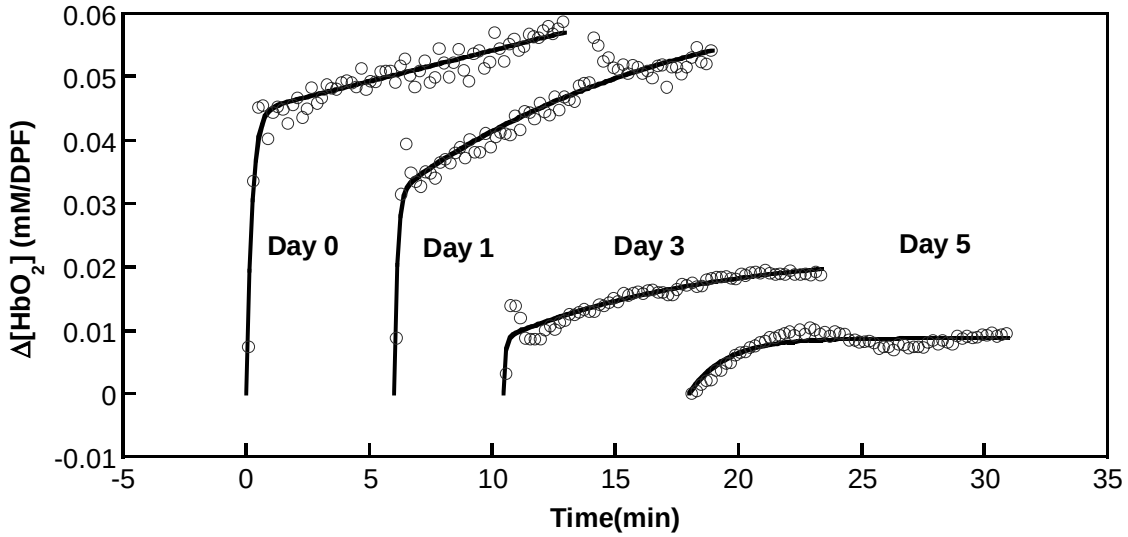

Fig. 5. Dynamic changes of [HbO_2] taken at location #1 from a rat breast tumor before and after a single high dose of CTX treatments (200mg/kg). The rising part of Δ[HbO_2] from location #1 was fitted using either a single- or double-exponential expression.

Table 2. Summary of vascular oxygen dynamics determined at location #1 from the tumor shown in Fig. 5 before and after CTX treatment.

Day	A_1	A_2	τ_1	τ_2	A_1/A_2 (=γ_1/γ_2)	τ_1/τ_2	f_1/f_2
0	0.044	0.031	0.23	25.21	1.42	0.0091	156
1	0.032	0.033	0.13	11.36	0.97	0.0114	85
3	0.0087	0.014	0.089	8.36	0.62	0.0106	58
5	0.0087		1.27				

4. DISCUSSION

Changes of rat body weight and tumor volume clearly show that CTX treatment is effective for the tumor type that we have used in this study. For the control group, the average rat body weight gradually decreased during the entire course of treatment, which implies the sickness of rats possibly due to the tumor growth (cachexia). (At Day 10, the tumor volume was ~5 times larger than that at Day 0.) It is clear that there is a different effectiveness of CTX treatment between the single high dose group (200mg/kg) and continuous low dose group (20mg/kg for 10 days). Both of the CTX treatments delayed the tumor growth and even further reduced the tumor volume. However, a single high dose of CTX treatment caused the death of two rats, and the tumor volume was not decreased further 4 days after the treatment, while the continuous low dose CTX treatment continued to provide tumor regression without causing severe sickness. From this observation, it is obvious that continuous low dose of CTX treatment is working much better than a single high dose of CTX treatment for a rat mammary adenocarcinomas 13762NF tumor.

NIRS is a portable, low cost, and real time measurement system that can monitor changes of vascular oxygen levels by using two wavelengths. We have previously used a single-channel NIRS system with one light source and one detector for global measurements of Δ[HbO_2] and Δ[Hb_{total}] in tumors during respiratory challenges.[12,20] Through those experiments, we have found that most tumors have a bi-phasic behavior in Δ[HbO_2] increase (i.e., a rapid increase followed by a slow and gradual increase) after switching the gas from air to carbogen/oxygen. To explain this bi-phasic behavior, we developed a mathematical model and formed a hypothesis that the bi-phasic behavior of Δ[HbO_2] during carbogen/oxygen inhalation results from two different vascular regions in tumor with two blood perfusion rates and vascular structures.[12]

By giving an oxygen intervention, tumor blood vessels are acutely subject to an increase of [HbO_2] due to higher supply of oxygenated blood from artery compared to that from air breathing. However, due to the irregular vascular structure in tumor, the well perfused regions in tumor may have an increase in [HbO_2] much faster than other parts of tumor that are poorly perfused. Therefore, two time constants obtained from tumor hemodynamic measurements during oxygen intervention are able to reveal two blood flow/perfusion rates in tumor, more precisely, two speeds of blood flow within the tumor blood vessels. More recently, we have shown that the bi-phasic increase in optical density changes occurs when there exist two different flow rates in tumor vascular phantom.[23] The bi-phasic model is a basis of our current study where we wish to detect any changes in vascular structures, hemodynamic features, or perfusion rate within a tumor after CTX treatment.

The amplitude and time constants obtained from Δ[HbO_2] increase (Fig. 5) are summarized in Table 2. At day 0, we can see that γ_1/γ_2 is higher than 1, indicating that the measured signal results more from the well perfused region than poorly perfused region. However, this ratio becomes less than 1 after injection of cyclophosphamide (Day 1 and 3). This may be explained by destruction of vascular structure in tumor after chemotherapy. We expect that after a single high dose administration of CTX, the drug circulates in the blood vessels and is delivered to the tumor cells more in the well perfused region than in the poorly perfused region. This will lead to death of tumor cells in the well perfused region more effectively than that in the poorly perfused region, eventually resulting in decreases in tumor volume in the well perfused region more than in the poorly perfused region. Then, the tumor volume containing the well perfused regions will consequently decrease, so will the contribution of detected NIR signals from the well perfused region. In other words, a decrease in γ_1/γ_2 may indicate deceases in well perfused regions in tumor volume, after the administration of CTX.

As shown in Table 2, moreover, the perfusion rate ratio, f_1/f_2, was also decreased after a single high dose of CTX administration. At Day 0, f_1/f_2 was very high, meaning that there was a big difference of perfusion rate between the well perfused and poorly perfused region in tumor. However, this ratio significantly decreased at Day 1 and 3 after CTX treatment, representing that the perfusion rate gap between the well perfused region and poorly perfused region became much smaller than that at day 0. At Day 5, changes in [HbO_2] during oxygen intervention do not show any bi-phasic behavior anymore, and it was fitted by a single-exponential model. This may indicate that most of tumor cells and/or tumor vasculature in the well perfused region are possibly destroyed by the effect of CTX, resulting in quite different hemodynamic behavior.

5. CONCLUSION

In conclusion, we have conducted this study to show the possibility of using NIRS to monitor tumor hemodynamics in response to chemotherapy by comparing the changes in tumor vascular oxygenation before and after CTX treatment. The heterogeneity of tumor vasculature was easily observed by quantifying the blood perfusion rate and vascular coefficients at four different locations of the tumor. Tumor hemodynamics has been significantly changed before and after CTX treatment compared to the saline-treated control group, showing high possibility of the NIRS system to be used as a monitoring tool for cancer treatments. Our future studies will include the development of NIR imaging systems to obtain a map of tumor hemodynamic changes from whole tumor, allowing us to predict the efficacy of tumor treatment.

ACKNOWLEDGEMENTS

This work was supported in part by the Department of Defense Breast Cancer Research grants DAMD 170310353(JGK), DAMD 170310363 (DZ), and DAMD 170010459 (HL) and by NIH/NCI P20 CA086354 (RPM). We are grateful to Ammar Adam for technical assistance and to Dr. Britton Chance at the University of Pennsylvania, Philadelphia for the support of the multi-channel NIRS system.

REFERENCES

1. S. Li, J. P. Wehrle, S. S. Rajan, R. G. Steen, J. D. Glickson, and J. Hilton, "Response of radiation-induced fibrosarcoma-1 in mice to cyclophosphamide monitored by in vivo ^{31}P nuclear magnetic resonance spectroscopy," *Cancer Research*, **48**, 4736-4742, 1988.

2. H. Poptani, N. Bansal, W. T. Jenkins, D. Blessington, A. Mancuso, D. S. Nelson, M. Feldman, E. J. Delikatny, B. Chance, and J. D. Glickson, "Cyclophosphamide treatment modifies tumor oxygenation and glycolytic rates of RIF-1 tumors: 13C magnetic resonance spectroscopy, Eppendorf electrode, and Redox scanning," *Cancer Research*, **63**, 8813-8820, 2003.

3. D. Zhao, A. Constantinescu, E. W. Hahn, and R. P. Mason, "*In vivo* evaluation of metronomic chemotherapy on prostate tumors by MRI," CaPCure, New York, NY, November 2003.

4. B. Chance, S. Nioka, J. Kent, K. McCully, M. Fountain, R. Greenfield, and G. Holtom, "Time resolved spectroscopy of hemoglobin and myoglobin in resting and ischemic muscle", *Anal. Biochem.*, **174**,698-707, 1988.

5. S. Homma, T. Fukunaga,, and A. Kagaya, "Influence of adipose tissue thickness on near infrared spectroscopic signals in the measurement of human muscle", *J. Biomed. Opt.*, **1**(4), 418-424, 1996.

6. M. Ferrari, Q. Wei, L. Carraresi, R. A. De Blasi, and G. Zaccanti, "Time-resolved spectroscopy of the human forearm", *J. Photochem. Photobiol. B: Biol.*, **16**,141-153, 1992.

7. B. Chance, E. Anday, S. Nioka, S. Zhou, L. Hong, K. Worden, C. Li, T. Murray, Y. Ovetsky, D. Pidikiti, and R. Thomas, "A novel method for fast imaging of brain function non-invasively with light", *Optics Express*, **2**(10), 411-423 1998.

8. R. Wenzel, H. Obrig, J. Ruben, K. Villringer, A. Thiel, J. Bernarding, U. Dirnagl, and A. Villringer, "Cerebral blood oxygenation changes induced by visual stimulation in humans", *J. Biomed. Opt.*, **1**(4),399-404, 1996.

9. M. Cope, and D. T. Delpy, "A system for long term measurement of cerebral blood and tissue oxygenation in newborn infants by near infrared transillumination", *Med. Biol. Eng. Comp.*, **26**, 289-294, 1988.

10. R. G. Steen, K. Kitagishi, and K. Morgan, "In vivo measurement of tumor blood oxygenation by near-infrared spectroscopy: immediate effects of pentobarbital overdose or carmustine treatment", *J. Neuro-Oncol.*, **22**, 209-220, 1994.

11. H. D. Sostman, S. Rockwell, A. L. Sylvia, D. Madwed, G. Cofer, H. C. Charles, R. Negro-Vilar, and D. Moore, "Evaluation of BA1112 rhabdomyosarcoma oxygenation with microelectrodes, optical spectrophotometry, radiosensitivity, and magnetic resonance spectroscopy", *Magn. Reson. Med.*, **20**, 253-267, 1991.

12. H. Liu, Y. Song, K. L. Worden, X. Jiang, A. Constantinescu, and R. P. Mason, "Noninvasive Investigation of Blood Oxygenation Dynamics of Tumors by Near-Infrared Spectroscopy", *Applied Optics*, **39**(28), 5231-5243, 2000.

13. H. Liu, Y. Gu, J.G. Kim, and R. P. Mason**,** "Near infrared spectroscopy and imaging of tumor vascular oxygenation", *Methods Enzymol.*, **386**, 349-378, 2004

14. S. Nioka, M. Miwa, S. Orel, M. Shnall, M. Haida, S. Zhao, B. Chance, "Optical imaging of human breast cancer," *Adv. Exp. Med. Biol.*, **361**, 171-179, 1994.

15. J. B. Fishkin, O. Coquoz, E. R. Anderson, M. Brenner, B. J. Tromberg, "Frequency-domain photon migration measurements of normal and malignant tissue optical properties in a human subject,"*Applied Optics*, **36**(1), 10-20, 1997.

16. B. Pogue, S. Jiang, S. Srinivasan, X. Song, H. Dehghani, K. Paulsen, T. Tosteson, C. Kogel, S. Soho, S. P. Poplack, "Near-infrared scattering spectrum differences between benign and malignant breast tumors measured in vivo with diffuse tomography," in Biomedical Topical Meetings on CD-ROM (The Optical Society of America, Washington, DC) 2004. ThB1.

17. D. B. S., Hoon, "Circlulating immune complexes in rats bearing 6-thioguanine-resistant variants of the 13762 mammary adenocarcinoma," *Cancer Res.*, **44**, 2406-2409 (1984).

18. A.R. Ahmed, S.M. Hombal, "Cyclophosphamide (Cytoxan). A review on relevant pharmacology and clinical uses," *J. Am. Acad. Dermatol.*, **11**(6), 1115-1126, 1984.

19. P. Calabresi, B. A. Chabner, "Antineoplastic agents", In: A.F. Gilman, T. W. Rall, A.S. Niss, and P. Taylor (Editors), The Pharmacological Basis of Therapeutics, 8th ed. MacGraw-Hill, Singapore. 1992.

20. J. G. Kim, D. Zhao, Y. Song, A. Constantinescu, R. P. Mason, and H. Liu, "Interplay of tumor vascular oxygenation and tumor pO_2 observed using near-infrared spectroscopy, an oxygen needle electrode, and ^{19}F MR pO_2 mapping", *J. Biomed. Opt.*, **8**(1), 53-62, 2003.

21. M. Cope, "The application of near infrared spectroscopy to non invasive monitoring of cerebral oxygenation in the newborn infant", PhD dissertation, Appendix A, University College London, 1991.

22. S. S. Kety, "The theory and applications of the exchange of inert gas at the lungs and tissue," *Pharmacol. Rev.*, **3**, 1-41, 1951.

23. J. G. Kim, and H. Liu, "Investigation of breast tumor hemodynamics using tumor vascular phantoms and FEM simulations", in Biomedical Topical Meetings on CD-ROM (The Optical Society of America, Washington, DC, 2004), WF16.

results exhibit a linear correlation between ΔHbO and ΔpO_2 of the tumors under hyperoxic gas intervention, suggesting that the NIRS approach could have a good potential value in the clinic. Finally, the newly developed tumor hemodynamic model allows us to reveal tumor heterogeneities at different tumor locations based on the multichannel NIRS results. Through this chapter, we lay a foundation for an NIR imaging technique to be further developed to facilitate investigations of tumor heterogeneity and vascular perfusion. Such a noninvasive imaging approach can enhance our understanding of the dynamics of tumor oxygenation and the mechanism of tumor physiology under baseline and perturbed conditions.

Acknowledgments

This work was supported in part by the Department of Defense Breast Cancer Research grants BC990287 (HL) and BC000833 (YG), and NIH R01 CA79515 (NCI)/EB002762 (NIBIB) (RPM). We are grateful to Vincent Bourke for his collaborative work on multichannel pO_2 measurements and Dr. Anca Constantinescu for her assistance with all the tumor investigations. We also gratefully acknowledge Dr. Britton Chance for his technical support on the multichannel NIR system.

[18] Measuring Changes in Tumor Oxygenation

By DAWEN ZHAO, LAN JIANG, and RALPH P. MASON

Introduction

Significance of pO_2 in Oncology

It has long been appreciated that hypoxic tumor cells are more resistant to radiotherapy.[1] Indeed, a 3-fold increase in radio resistance may occur when cells are irradiated under hypoxic conditions compared with oxygen pressure $pO_2 > 15$ torr for a given single radiation dose. However, recent modeling has indicated that the proportion of cells in the range 0–20 torr may be most significant in terms of surviving a course of fractionated radiotherapy.[2] Certain chemotherapeutic drugs also present differential efficacy, depending on hypoxia.[3,4] Increasingly, there is evidence that hypoxia also

[1] L. Gray, A. Conger *et al.*, *Br. J. Radiol.* **26,** 638 (1953).
[2] B. G. Wouters and J. M. Brown, *Radiat. Res.* **147,** 514 (1997).
[3] B. Teicher, J. Lazo *et al.*, *Cancer Res.* **41,** 73 (1981).
[4] A. C. Sartorelli, *Cancer Res.* **48,** 775 (1988).

0076-6879/04 $35.00

influences such critical characteristics as angiogenesis, tumor invasion, and metastasis.[5–8] Moreover, repeated bouts of intermittent hypoxic stress may be important in stimulating tumor progression.[9] Thus the ability to measure pO_2 noninvasively and repeatedly, with respect to acute or chronic interventions, becomes increasingly important.

Early work examined cells *in vitro*, where ambient oxygen concentrations are readily controlled. *In vivo*, hypoxia may be achieved by clamping the blood supply to a tumor,[10] but other levels of oxygenation reflect the interplay of supply and consumption.[11,12] Robust fine-needle polarographic electrodes opened the possibility of measuring pO_2 in tumors *in situ* and *in vivo* to define local pO_2 under baseline conditions or with respect to interventions. In early work, Cater and Silver[13] showed the ability to monitor pO_2 at individual locations in patients' tumors with respect to breathing oxygen. Later, Gatenby *et al.*[14] showed that pO_2 in a tumor was correlated with clinical outcome. Tumor oximetry received its greatest boost with the development of the Eppendorf Histograph polarographic needle electrode system.[15] This computer-controlled device equipped with a stepper motor can reveal distributions of tumor oxygenation and has been applied extensively to clinical trials. Many reports have now shown that tumors are highly heterogeneous and have extensive hypoxia; furthermore, strong correlations have been shown in cervix and head and neck tumors between median pO_2 or hypoxic fraction and survival or disease-free survival.[5,16–20] Extensive hypoxia also has been found in tumors of the prostate and breast.[21–23] Thus tumor oxygenation is now recognized as a strong

[5] E. K. Rofstad, K. Sundfor *et al.*, *Br. J. Cancer* **83,** 354 (2000).
[6] K. De Jaeger, M. C. Kavanagh *et al.*, *Br. J. Cancer* **84,** 1280 (2001).
[7] M. Höckel and P. Vaupel, *J. Natl. Cancer Inst.* **93,** 266 (2001).
[8] H. J. Knowles and A. L. Harris, *Breast Cancer Res.* **3,** 318 (2001).
[9] R. A. Cairns, T. Kalliomaki *et al.*, *Cancer Res.* **61,** 8903 (2001).
[10] J. Moulder and S. Rockwell, *Int. J. Radiat. Oncol. Biol. Phys.* **10,** 695 (1984).
[11] T. W. Secomb, R. Hsu *et al.*, *Adv. Exp. Med. Biol.* **454,** 629 (1998).
[12] M. W. Dewhirst, B. Klitzman *et al.*, *Int. J. Cancer* **90,** 237 (2000).
[13] D. Cater and I. Silver, *Acta Radiol.* **53,** 233 (1960).
[14] R. A. Gatenby, H. B. Kessler *et al.*, *Int. J. Radiat. Oncol. Biol. Phys.* **14,** 831 (1988).
[15] M. Nozue, I. Lee *et al.*, *J. Surg. Oncol.* **66,** 30 (1997).
[16] D. M. Brizel, S. P. Scully *et al.*, *Cancer Res.* **56,** 941 (1996).
[17] M. Höckel, K. Schlenger *et al.*, *Cancer Res.* **56,** 4509 (1996).
[18] M. Nordsmark, M. Overgaard *et al.*, *Radiother. Oncol.* **41,** 31 (1996).
[19] A. W. Fyles, M. Milosevic *et al.*, *Radiother. Oncol.* **48,** 149 (1998).
[20] T. H. Knocke, H. D. Weitmann *et al.*, *Radiother. Oncol.* **53,** 99 (1999).
[21] P. W. Vaupel, K. Schlenger *et al.*, *Cancer Res.* **51,** 3316 (1991).
[22] P. Hohenberger, C. Felger *et al.*, *Breast Cancer Res. Treat.* **48,** 97 (1998).
[23] B. Movsas, J. D. Chapman *et al.*, *Urology* **53,** 11 (1999).

prognostic indicator, and this device has laid a convincing foundation for the value of measuring pO_2 in patients. However, the Histograph is highly invasive, and it is not possible to make repeated measurements at individual locations, precluding dynamic studies to assess the influence of interventions on tumor pO_2.

Given that hypoxic tumors are more resistant to certain therapies, it becomes important to assess tumor oxygenation as part of therapeutic planning. Patients could be stratified according to baseline hypoxia to receive adjuvant interventions designed to modulate pO_2, or more intense therapy as facilitated by intensity modulated radiation therapy (IMRT). Tumors, which do not respond to interventions, may be ideal candidates for hypoxia-selective cytotoxins (e.g., tirapazamine[24]). Noting that any therapy and intervention may have side effects or simply add to clinical costs, it is vital that efficacy be established and therapy be optimized for an individual patient. Whether initially hypoxic regions of a tumor can be modified to become better oxygenated has long been considered a key to improving outcome of irradiation. However, many attempts to improve therapeutic outcome by manipulation of tumor oxygenation have shown only modest success in the clinic,[25] and it is thought that lack of success may have resulted from inability to identify those patients who would benefit from adjuvant interventions.

Although pO_2 determinations could be of great clinical value, they are also vital to many laboratory investigations of new drugs and studies of tumor development. Given the potential importance of measuring pO_2, many diverse techniques have been developed, as reviewed by others previously,[26–29] and here, in the next section.

Methods of Measuring Tumor Oxygenation

Table I lists various techniques that have been reported to provide quantitative estimates of pO_2. Historically, polarographic needle oxygen electrodes have been considered a ''gold standard,'' and they have been applied in the clinic since the 1950s. One or more electrodes may be placed in a tumor, facilitating measurement of baseline pO_2 and dynamic response to

[24] J. M. Brown, *Mol. Med. Today* **6,** 157 (2000).
[25] J. Overgaard and M. R. Horsman, *Semin. Radiat. Oncol.* **6,** 10 (1996).
[26] H. B. Stone, J. M. Brown *et al.*, *Radiat. Res.* **136,** 422 (1993).
[27] R. P. Mason, S. Ran *et al.*, *J. Cell. Biochem.* **87S,** (2002).
[28] H. M. Swartz, *Biochem. Soc. Trans.* **30,** 248 (2002).
[29] H. M. Swartz and J. F. Dunn, *in* ''Oxygen Transport to Tissue XXIV'' (J. F. Dunn and H. M. Swartz, eds.), Vol. 530, p. 1. Kluwer Academic, New York, 2003.

interventions.[13,30–32] Initially, the focus was on generating finer needles, which would be less invasive, and tips as fine as a few microns have been applied to animal tissues.[33] However, such needles are progressively brittle and generate such small current that stray electromagnetic fields can interfere. Stationary electrodes sample limited volumes, and recognizing tumor heterogeneity, the Eppendorf Histograph was developed to generate multiple measurements along tracks in tumors.[15,34,35] Following extensive studies in animals, the Histograph has found widespread application in the clinical setting and has unequivocally revealed hypoxia in many tumor types, for example, head and neck,[36,37] cervix,[19,38] breast,[21,22] and prostate.[23] Moreover, pO_2 distributions have been found to have prognostic value. Disease-free survival is significantly worse for patients with hypoxic tumors, though the optimal prognostic parameter has variously been median pO_2 or percent measurements <5 torr (HF_5).

Although the Eppendorf Histograph uses a large invasive needle (size = 26 G or about 0.35 mm), it has provided great impetus for further investigations. One aspect is the application of less invasive probes. Fiber-optic probes are typically finer and do not consume oxygen during measurement. Typically, only two or four locations are sampled simultaneously, but as with the earlier electrodes, these optical probes facilitate observation of dynamic changes in pO_2 in response to interventions.[39–43] Both the current commercial systems, the OxyLite (http://www.oxford-optronix.com/tissmon/oxylite/oxylite.htm) and FOXY (http://www.oceanoptics.com/Products/foxyfaqs.asp), exploit the fluorescent quenching by oxygen of a ruthenium complex coating. OxyLite measures fluorescent lifetime, whereas FOXY uses a simple intensity integration and is correspondingly much cheaper. Fibers are fragile, and coatings have a limited lifetime.

[30] N. Evans and P. Naylor, *Br. J. Radiol.* **36,** 418 (1963).
[31] C. Song, I. Lee *et al.*, *Cancer Res.* **47,** 442 (1987).
[32] D. Zhao, A. Constantinescu *et al.*, *Int. J. Radiat. Oncol. Biol. Phys.* **53,** 744 (2002).
[33] D. W. Crawford and M. A. Cole, *J. Appl. Physiol.* **58,** 1400 (1985).
[34] F. Kallinowski, R. Zander *et al.*, *Int. J. Radiat. Oncol. Biol. Phys.* **19,** 953 (1990).
[35] P. W. Vaupel, D. K. Kelleher, and M. Günderoth, "Tumor Oxygenation." Gustav Fischer Verlag, Stuttgart, Germany, 1995.
[36] D. M. Brizel, G. S. Sibly *et al.*, *Int. J. Radiat. Oncol. Biol. Phys.* **38,** 285 (1997).
[37] V. Rudat, B. Vanselow *et al.*, *Radiother. Oncol.* **57,** 31 (2000).
[38] C. Aquino-Parsons, A. Green *et al.*, *Radiother. Oncol.* **57,** 45 (2000).
[39] J. R. Griffiths, *Br. J. Radiol.* **72,** 627 (1999).
[40] J. Bussink, J. H. A. M. Kaanders *et al.*, *Radiat. Res.* **154,** 547 (2000).
[41] R. D. Braun, J. L. Lanzen *et al.*, *Am. J. Physiol. Heart Circ. Physiol.* **280,** H2533 (2001).
[42] D. Zhao, A. Constantinescu *et al.*, *Am. J. Clin. Oncol.* **24,** 462 (2001).
[43] Y. Gu, V. Bourke *et al.*, *Appl. Opt.* **42,** 1 (2003).

TABLE I
TUMOR OXIMETRY METHODS

Technique	Reporter	Parameter measured	Invasiveness	Characteristic resolution		References
				Spatial	Temporal	
FREDOM	HFB	R_1	Minimal 32-G needle	Map multiple locations each 8 mm^3	6.5 min	Hunjan, Zhao *et al.*[159]; Zhao, Constantinescu *et al.*[134]; Song, Constantinescu *et al.*[135]; Zhao, Constantinescu *et al.*[32]; Kim, Zhao *et al.*[106]; Zhao, Constantinescu *et al.*[136]; Zhao, Ran *et al.*[137]
^{19}F MRI	PFC	R_1	IV	Perfused regions	min	Hees and Sotak[153]; Dardzinski and Sotak[117]; Mclntyre, McCoy *et al.*[158]; Fan, River *et al.*[95]; Wang, Su *et al.*[88]
^{19}F MRS	PFC	R_1	IV	Perfused regions	s to min	Hees and Sotak[153]; Mason, Antich *et al.*[154]; Baldwin and Ng[156]; Mclntyre, McCoy *et al.*[158]; van der Sanden, Heerschap *et al.*[138]
DCE MRI	Gd-DTPA	Contrast kinetics	IV	Maps	min	Cooper, Carrington *et al.*[87]; Lyng, Vorren *et al.*[a]; Wang, Su *et al.*[88]
ESR/EPR	Charcoal, phthalocyanine	Linewidth	Needle	Single location 23 G IT	seconds	O'Hara, Goda *et al.*[b]; Goda, Bacic *et al.*[c]; O'Hara, Goda *et al.*[59]; Gallez, Jordan *et al.*[d];

						Jordan, Misson *et al.*[48]; He, Beghein *et al.*[49]; Jiang, Beghei *et al.*[50]; O'Hara, Blumenthal *et al.*[e]; Baudelet and Gallez[94]; Dunn, O'Hara *et al.*[f]; Jordan, Gregoire *et al.*[52]; Mahy, De Bast *et al.*[55]
ESR/EPR	Nitroxides	Linewidth	IV	Global or map	s to min	Elas, Williams *et al.*[53]
OMRI	Free radical	Overhauser enhancement	IV	mm^3 maps	10 min	Krishna, English *et al.*[60]
Needle electrode	Oxygen	Current	Needle 26 G IT	Single location	~1 s	Cater and Silver[13]; Evans and Naylor[30]; Hasegawa, Rhee *et al.*[g]; Gatenby, Kessler *et al.*[14]; Song, Shakil *et al.*[h]; Zhao, Constantinescu *et al.*[32]
(Histograph)	Oxygen	Current	Needle 26 G IT	Multiple tracks	1 s per location	Eble, Wenz *et al.*[i]; Falk, Laurence *et al.*[j]; Vaupel, Kelleher *et al.*[35]; Brizel, Scully *et al.*[16]; Höckel, Schlenger *et al.*[k]; Nozue, Lee *et al.*[15]; Fyles, Milosevic *et al*[19]; Siemann, Johansen *et al.*[l]; Mason, Constantinescu *et al.*[175]; Aquino-Parsons, Green *et al.*[38]; Jenkins, Evans *et al.*[75]; Höckel and Vaupel[7]

(continued)

TABLE I *(continued)*

Technique	Reporter	Parameter measured	Invasiveness	Characteristic resolution		References
				Spatial	Temporal	
Optical probe (OxyLite, FOXY)	Rh complex	Fluorescent lifetime	Needle (26 G)	2–4 locations	Real time	Griffiths[39]; Bussink, Kaanders *et al.*[40]; Braun, Lanzen *et al.*[41]; Zhao, Constantinescu *et al.*[134]; Gu, Bourke *et al.*[43]; Jordan, Beghein *et al.*[54]
Phosphorescence	PD complex	Lifetime	IV	Maps	<1 min	Wilson[m]; Vinogradov, Lo *et al.*[n]; Dewhirst, Ong *et al.*[o]; Wilson, Vinogradov *et al.*[63]; Erickson, Braun *et al.*[p]
Fluorescence	EF5	Fluorescent intensity	IV + biopsy	Maps microscopic	Once	Koch[79]
Mass spectrometry	Oxygen	Atoms	Needle	Single location		Potapov, Sirovskii *et al.*[q]

[a] H. Lyng, A. O. Vorren *et al.*, *J. Magn. Reson. Imaging* **14,** 750 (2001).
[b] J. A. O'Hara, F. Goda *et al.*, *Radiat. Res.* **144,** 222 (1995).
[c] F. Goda, G. Bacic *et al.*, *Cancer Res.* **56,** 3344 (1996).
[d] B. Gallez, B. F. Jordan *et al.*, *Magn. Reson. Med.* **42,** 627 (1999).
[e] J. A. O'Hara, R. D. Blumenthal *et al.*, *Radiat. Res.* **155,** 466 (2001).
[f] J. F. Dunn, J. A. O'Hara *et al.*, *J. Magn. Reson. Imaging* **16,** 511 (2002).
[g] T. Hasegawa, J. G. Rhee *et al.*, *Int. J. Radiat. Oncol. Biol. Phys.* **13,** 569 (1987).
[h] C. W. Song, A. Shakil *et al.*, *Int. J. Hyperthermia* **12,** 367 (1996).

[i] M. J. Eble, F. Wenz *et al*., *in* "Tumor Oxygenation" (P. W. Vaupel, D. K. Kelleher, and M. Günderoth, eds.), p. 95. Gustav Fischer, Stuttgart, Germany, 1995.
[j] S. Falk, V. Laurence *et al*., *in* "Tumor Oxygenation" (P. W. Vaupel, D. K. Kelleher, and M. Günderoth, eds.), p. 281. Gustav Fischer, Stuttgart, Germany, 1995.
[k] M. Höckel, K. Schlenger *et al*., *Semin. Radiat. Oncol*. **6,** 3 (1996).
[l] D. W. Siemann, I. M. Johansen *et al*., *Int. J. Radiat. Oncol. Biol. Phys*. **40,** 1171 (1998).
[m] D. F. Wilson, *in* "Oxygen Transport to Tissue XIV" (W. Erdmann and D. F. Bruley, eds.), p. 195. Plenum Press, New York, 1992.
[n] S. A. Vinogradov, L.-W. Lo *et al*., *Biophys. J*. **70,** 1609 (1996).
[o] M. W. Dewhirst, E. T. Ong *et al*., *Br. J. Cancer* **79,** 1717 (1999).
[p] K. Erickson, R. D. Braun *et al*., *Cancer Res*. **63,** 4705 (2003).
[q] A. A. Potapov, E. B. Sirovskii *et al*., *Vopre. Neirokhir*. **1,** 20 (1979).

Reporter molecules have been developed for use with electron spin resonance (ESR or EPR), where the line width is highly sensitive to oxygen.[28,44–55] Two primary approaches are used: (1) direct intratumoral (IT) injection of char crystals,[49,56] phthalocyanine,[57] or India ink[58] into a tissue or (2) intravenous (IV) infusion of water-soluble agents which disseminate throughout the tumor vasculature.[47,53] Direct IT injection is invasive and has generally been applied as a spectroscopic approach to report pO_2 at single locations only. Nonetheless, significant data have been achieved demonstrating hypoxiation and reoxygenation with respect to irradiation, and the importance of timing successive radiation doses to coincide with reoxygenation.[59] Char particles may be stable in tissue for weeks to years, allowing measurements of chronic changes in tissues (e.g., accompanying tumor growth).[28] The IV approach is noninvasive, but reporter molecules may predominately distribute in the well-perfused vasculature, potentially biasing measurements toward the well-oxygenated tumor regions. Progressive uptake and clearance of agents produces variable concentrations, and some agents degrade in tissue requiring appropriate correction factors.[47] Nonetheless, images of tumor oxygen distribution have been reported, including three-dimensional representations.[53] Spin radicals also may be applied to a combined ESR–NMR (nuclear magnetic resonance) approach, Overhauser-enhanced magnetic resonance imaging (OMRI), exploiting the Overhauser enhancement in the tissue water proton MRI signal that occurs by polarization transfer from free radicals upon electromagnetic irradiation.[60]

[44] H. M. Swartz, S. Boyer *et al.*, *Magn. Reson. Med.* **20,** 333 (1991).
[45] H. M. Swartz, S. Boyer *et al.*, *in* "Oxygen Transport to Tissue XIV" (W. Erdmann and D. F. Bruley, eds.), p. 221. Plenum Press, New York, 1992.
[46] H. M. Swartz, K. J. Liu *et al.*, *Magn. Reson. Med.* **31,** 229 (1994).
[47] P. Kuppusamy, R. Afeworki *et al.*, *Cancer Res.* **58,** 1562 (1998).
[48] B. F. Jordan, P. Misson *et al.*, *Int. J. Radiat. Oncol. Biol. Phys.* **48,** 565 (2000).
[49] J. He, N. Beghein *et al.*, *Magn. Reson. Med.* **46,** 610 (2001).
[50] H. Jiang, N. Beghei *et al.*, *Phys. Med. Biol.* **46,** 3323 (2001).
[51] P. E. James and H. M. Swartz, *Methods Enzymol.* **350,** 52 (2002).
[52] B. F. Jordan, V. Gregoire *et al.*, *Cancer Res.* **62,** 3555 (2002).
[53] M. Elas, B. B. Williams *et al.*, *Magn. Reson. Med.* **49,** 682 (2003).
[54] B. F. Jordan, N. Beghein *et al.*, *Int. J. Cancer* **103,** 138 (2003).
[55] P. Mahy, M. De Bast *et al.*, *Radiother. Oncol.* **67,** 53 (2003).
[56] N. Vahidi, R. B. Clarkson *et al.*, *Magn. Reson. Med.* **31,** 139 (1994).
[57] J. F. Glockner and H. M. Swartz, *in* "Oxygen Transport to Tissue XIV" (W. Erdmann and D. F. Bruley, eds.), p. 229. Plenum Press, New York, 1992.
[58] F. Goda, K. Jian Lu *et al.*, *Magn. Reson. Med.* **33,** 237 (1995).
[59] J. A. O'Hara, F. Goda *et al.*, *Radiat. Res.* **150,** 549 (1998).
[60] M. C. Krishna, S. English *et al.*, *Proc. Natl. Acad. Sci. USA* **99,** 2216 (2002).

Vascular oxygenation has been probed by fluorescence or phosphorescence imaging based on reporter complexes delivered IV.[61,62] Historically, the approach was limited to superficial tissues due to limited light penetration. The latest molecules are active in the near-infrared, permitting greater depth of signal penetration.[63]

NMR facilitates interrogation of deep tissues noninvasively, and ^{19}F NMR approaches will be reviewed in detail in the following section. The methods discussed earlier provide direct quantitative measurements of pO_2 based on various physiochemical parameters, such as electric current, fluorescent lifetime, magnetic resonance linewidth, or relaxation. Other approaches are less direct, but can reveal hypoxia or correlates of pO_2.

Specific classes of reporter molecules have been developed to reveal hypoxia[26,64] (e.g., pimonidazole,[65,66] EF5,[67,68] CCl-103F,[69] Cu-ATSM[70,71] galactopyranoside IAZA[72]). Following IV infusion, these agents become reduced in tissues and are trapped. However, in the presence of oxygen they are reoxidized and ultimately clear from the body. Histologic assessment of the distribution of these agents provides microscopic indications of local hypoxia. EF5, pimonidazole, and Cu-ATSM are currently being tested in clinical trials, and correlations have been reported with clinical outcome.[66,67,70] Many variants have been proposed over the past 20 years, and incorporation of radionuclides has facilitated noninvasive investigations using positron emission tomography (PET) or single photon emission computed tomography (SPECT), while ^{19}F labels permitted NMR spectroscopy.[72–74] Generally, only a single time point is investigated, but dynamic variations in hypoxia may be assessed, even in biopsy specimens, by applying pairs of hypoxia reporters in a pulse-chase fashion with respect to an intervention, as shown by Ljungkvist *et al.*[69]

[61] D. Wilson and G. Cerniglia, *Cancer Res.* **52,** 3988 (1992).
[62] G. Helminger, F. Yuan *et al.*, *Nature Med.* **3,** 177 (1997).
[63] D. F. Wilson, S. A. Vinogradov *et al.*, *Comp. Biochem. Physiol., Part A Mol. Integr. Physiol.* **132,** 153 (2002).
[64] J. R. Ballinger, *Semin. Nucl. Med.* **31,** 321 (2001).
[65] J. A. Raleigh, S. C. Chou *et al.*, *Radiat. Res.* **151,** 580 (1999).
[66] J. H. A. M. Kaanders, K. I. E. M. Wijffels *et al.*, *Cancer Res.* **62,** 7066 (2002).
[67] S. M. Evans, S. Hahn *et al.*, *Cancer Res.* **60,** 2018 (2000).
[68] W. R. Dolbier, Jr., A. R. Li *et al.*, *Appl. Radiat. Isotop.* **54,** 73 (2001).
[69] A. S. E. Ljungkvist, J. Bussink *et al.*, *Int. J. Radiat. Oncol. Biol. Phys.* **48,** 1529 (2000).
[70] F. Dehdashti, P. W. Grigsby *et al.*, *Int. J. Radiat. Oncol. Biol. Phys.* **55,** 1233 (2003).
[71] F. Dehdashti, M. A. Mintun *et al.*, *Eur. J. Nucl. Med. Molec. Imaging* **30,** 844 (2003).
[72] J. D. Chapman, E. L. Engelhardt *et al.*, *Radiother. Oncol.* **46,** 229 (1998).
[73] R. J. Maxwell, P. Workman *et al.*, *Int. J. Radiat. Oncol. Biol. Phys.* **16,** 925 (1989).
[74] R. J. Hodgkiss, *Anticancer Drug Des.* **13,** 687 (1998).

Several studies have shown a lack of correlation between hypoxic marker binding and pO_2 assessed using the Eppendorf Histograph, which may be related to chronic versus acute hypoxia, or the extent of necrosis.[75–77] The ultimate value of the techniques is evidenced by correlations between uptake and outcome.[66,70,71,78] Recent data also indicate that EF5 fluorescence may be correlated with pO_2.[79]

The techniques discussed so far all depend on exogenous reporter molecules or probes. Ideally, oxygenation could be related to endogenous characteristics. Because many biochemical pathways are under oxygen regulation, they can provide an elegant window on hypoxia, for example, induction of hypoxia-inducible factor 1 (HIF-1) and glucose transporter 1 (Glut-1) together with secondary responses, such as increased production of vascular endothelial growth factor (VEGF), NIP3 and tumor-associated macrophage activity.[8] Such molecules indicate hypoxia, though they may be induced by other factors. Intrinsic radiation sensitivity also may be assessed using the Comet assay.[80] These assays each require biopsy. Other markers potentially associated with hypoxia may be found in the plasma or urine and have been correlated with clinical outcome.[81] An attractive alternative is the introduction of transgenes with hypoxic response elements (HREs) as promoter sequences coupled to reporter genes such as GFP (green fluorescent protein)[82,83] or luciferase.[84,85] GFP synthesis is an energetic process, which could be hindered under hypoxia conditions. Likewise, bioluminescence accompanying action of luciferase on luciferin requires adenosine triphosphate (ATP) and O_2, but reports suggest that even under exceedingly low pO_2, sufficient oxygen remains to reveal hypoxia.

Many practical considerations govern clinical application of oximetry methods. Proton MRI is routinely applied for anatomic evaluation of tumors and would provide an ideal conduit for prognostic investigations. Application of contrast agents may reveal tumor boundaries to enhance detectability, and the dynamic contrast enhancement (DCE) changes provide insight into vascular perfusion and surface permeability area.[86]

[75] W. T. Jenkins, S. M. Evans *et al.*, *Int. J. Radiat. Oncol. Biol. Phys.* **46,** 1005 (2000).
[76] P. L. Olive, J. P. Banath *et al.*, *Acta Oncol.* **40,** 917 (2001).
[77] M. Nordsmark, J. Loncaster *et al.*, *Radiother. Oncol.* **67,** 35 (2003).
[78] C. J. Koch, S. M. Hahn *et al.*, *Cancer Chemother. Pharmacol.* **48,** 177 (2001).
[79] C. J. Koch, *Methods Enzymol.* **352,** 3 (2002).
[80] P. L. Olive, P. J. Johnston *et al.*, *Nature Med.* **4,** 103 (1998).
[81] Q. T. Le, P. D. Sutphin *et al.*, *Clin. Cancer Res.* **9,** 59 (2003).
[82] Y. Cao, C. Li *et al.*, "A Study of Hypoxia-Induced Gene Expression in Human Tumors." 48th Annual Meeting of Radiation Research, San Juan, Puerto Rico, 2001.
[83] D. Vordermark, T. Shibata *et al.*, *Neoplasia* **3,** 527 (2001).
[84] T. Shibata, A. J. Giaccia *et al.*, *Gene Ther.* **7,** 493 (2000).
[85] E. Payen, M. Bettan *et al.*, *J. Gene Med.* **3,** 498 (2001).
[86] A. R. Padhani, *J. Magn. Reson. Imaging* **16,** 407 (2002).

Specific studies have shown a correlation between DCE and pO_2,[87] and indeed, a theoretical underpinning has been provided based on the Krogh cylinder model.[88] However, the correlation is unlikely to be widely applicable, since DCE is sensitive to vascular flow, perfusion, and permeability, where pO_2 depends on oxygen consumption as well as delivery.

Blood oxygen level dependent (BOLD) contrast proton NMR facilitates rapid interrogation of vascular oxygenation and is particularly appropriate for examining dynamic responses to interventions.[48,89–91] Deoxyhemoglobin is paramagnetic and induces signal loss in T_2*-weighted images. However, BOLD does not provide absolute pO_2 values and is confounded by the influence of blood flow, as investigated extensively by Howe *et al.*,[92] who termed the expression *FLOOD* (flow and oxygen level dependent) contrast. In addition, variation in vascular volume can introduce signal perturbation.[93] Nonetheless, some studies have indicated a correlation with relative pO_2, but poor indication of absolute pO_2.[53,94,95]

Near-infrared spectroscopy (NIRS) offers an alternative approach based on the differential light absorption of the strong chromophores oxyhemoglobin and deoxyhemoglobin. NIRS provides a noninvasive means to monitor global tumor vascular oxygenation in real time based on endogenous molecules. Although many NIRS investigations have been conducted in the brain and breast in both laboratory and clinical settings over the past decade, there have been relatively few reports regarding solid tumors.[43,96–106] Most studies to date have used reflectance mode. By contrast, we have favored transmission mode, so as to interrogate deep tumor regions, and we have presented preliminary studies in rat breast

[87] R. A. Cooper, B. M. Carrington *et al.*, *Radiother. Oncol.* **57,** 53 (2000).
[88] Z. Wang, M.-Y. Su *et al.*, *Technol. Cancer Res. Treat.* **1,** 29 (2002).
[89] H. A. Al-Hallaq, J. N. River *et al.*, *Int. J. Radiat. Oncol. Biol. Phys.* **41,** 151 (1998).
[90] S. P. Robinson, F. A. Howe *et al.*, *Semin. Radiat. Oncol.* **8,** 198 (1998).
[91] R. Mazurchuk, R. Zhou *et al.*, *Magn. Reson. Imaging* **17,** 537 (1999).
[92] F. A. Howe, S. P. Robinson *et al.*, *Magn. Reson. Imaging* **17,** 1307 (1999).
[93] F. A. Howe, S. P. Robinson *et al.*, *NMR Biomed.* **14,** 497 (2001).
[94] C. Baudelet and G. Gallez, *Magn. Reson. Med.* **48,** 980 (2002).
[95] X. Fan, J. N. River *et al.*, *Int. J. Radiat. Oncol. Biol. Phys.* **54,** 1202 (2002).
[96] H. D. Sostman, S. Rockwell *et al.*, *Magn. Reson. Med.* **20,** 253 (1991).
[97] R. G. Steen, K. Kitagishi *et al.*, *J. Neurooncol.* **22,** 209 (1994).
[98] F. Steinberg, H. J. Rohrborn *et al.*, *Adv. Exp. Med. Biol.* **428,** 553 (1997).
[99] E. L. Hull, D. L. Conover *et al.*, *Br. J. Cancer* **79,** 1709 (1998).
[100] B. J. P. van der Sanden, A. Heerschap *et al.*, *Magn. Reson. Med.* **42,** 490 (1999).
[101] H. Liu, Y. Song *et al.*, *Appl. Op.* **39,** 5231 (2000).
[102] M. Kragh, B. Quistorff *et al.*, *Eur. J. Cancer* **37,** 924 (2001).
[103] G. Gulsen, H. Yu *et al.*, *Technol. Cancer Res. Treat.* **1,** 497 (2002).
[104] E. L. Heffer and S. Fantini, *Appl. Opt.* **41,** 3827 (2002).
[105] T. O. McBride, B. W. Pogue *et al.*, *J. Biomed. Opt.* **7,** 72 (2002).
[106] J. G. Kim, D. Zhao *et al.*, *J. Biomed. Optics* **8,** 53 (2003).

and prostate tumors with respect to various interventions.[43,101,106] NIR approaches are presented in detail in Chapter 17 of this volume.

Each technique has specific virtues and drawbacks, which must be considered for any given application, particularly the degree of invasiveness, the ability to generate maps of heterogeneity, and the ability to assess dynamic changes. In addition, the location of a measurement (e.g., vascular versus tissue compartments, the precision of measurements, and spatial and temporal resolution) must be considered. For further details of the techniques described earlier, the reader is referred to the references. In the next section, we present ^{19}F NMR approaches in greater detail.

^{19}F NMR Approaches to Measuring pO_2

Nuclear magnetic resonance (NMR) is attractive because it is inherently noninvasive. Liquid-state NMR is characterized by several parameters, including signal amplitude, chemical shift (δ), spin–spin relaxation (T_2), and spin–lattice relaxation (T_1). Oxygen could be quantified using ^{17}O NMR, but this is rather esoteric.[107] Alternatively, it has long been recognized that the oxygen molecule (O_2) is paramagnetic, causing increased spin–lattice relaxation rates ($R_1 = 1/T_1$). Indeed, physical and theoretical chemists must go to great lengths to rigorously remove oxygen from solutions (using freeze–thaw procedures) to achieve inherent relaxation rates for studying nuclear interactions.[108] Proton NMR studies have reported changes in the water relaxation rate as a result of tissue oxygenation,[109] but many other processes (metal ions, cellularity, pH, ionic strength) also cause relaxation, and thus it is not suitable for detecting pO_2, except under rare circumstances, such as with the eye.[110] There is also a substantial temperature response, whereas the relaxivity due to oxygen is only 0.0002 s^{-1}/torr.[110]

However, several investigators showed that the ^{19}F NMR spin–lattice relaxation rates for fluorocarbons are much more sensitive to pO_2.[111,112] Thomas *et al.*[113] pioneered the application of ^{19}F NMR relaxometry to measure pO_2 in tissues, *in vivo*, including lung, liver, and spleen; several other investigators demonstrated feasibility and applications,[114–120] as

[107] X. H. Zhu, H. Merkle *et al.*, *Magn. Reson. Med.* **45,** 543 (2001).
[108] M. A. Hamza, G. Serratice *et al.*, *J. Magn. Reson.* **42,** 227 (1981).
[109] E. Tadamura, H. Hatabu *et al.*, *J. Magn. Reson. Imaging* **7,** 220 (1997).
[110] B. A. Berkowitz, C. McDonald *et al.*, *Magn. Reson. Med.* **46,** 412 (2001).
[111] J.-J. Delpuech, M. A. Hamza *et al.*, *J. Chem. Phys.* **70,** 2680 (1979).
[112] M. A. Hamza, G. Serratice *et al.*, *J. Am. Chem. Soc.* **103,** 3733 (1981).
[113] S. R. Thomas, *in* "Magnetic Resonance Imaging" (C. L. Partain, R. R. Price, J. A. Patton, M. V. Kulkarni, and A. E. J. James, eds.), Vol. 2, p. 1536. W. B. Saunders, London, 1988.
[114] J. E. Fishman, P. M. Joseph *et al.*, *Magn. Reson. Imaging* **5,** 279 (1987).

reviewed some years ago by Mason.[121] The ^{19}F NMR R_1 of perfluorocarbons (PFCs) varies linearly with pO_2,[113,122] and each resonance is sensitive to pO_2, temperature, and magnetic field, but importantly, is essentially unresponsive to pH, CO_2, charged paramagnetic ions, mixing with blood, or emulsification.[123–127]

A particular PFC molecule may have multiple resonances, and each resonance has a characteristic R_1 response to pO_2. This is attributed to steric effects of O_2, as it approaches the molecule,[112] which implies that perfluorinated groups, which are both geometrically and magnetically comparable, should have similar R_1 responses to oxygen tension. At a fixed temperature and magnetic-field strength, the R_1 response to pO_2 of any single resonance obeys the simple formula

$$R_1 = R_{1a} + (R_{1p}X) \tag{1}$$

where X is the mole fraction of O_2 dissolved in the PFC, R_{1a} is the anoxic relaxation rate, and R_{1p} is the relaxation rate due to the paramagnetic contribution of oxygen. According to Henry's law, the dissolved mole fraction is related directly to the partial pressure of oxygen,

$$pO_2 = KX \tag{2}$$

where K represents Henry's constant for a given solution of gas at a specified temperature. By substitution,

$$R_1 = R_{1a} + (R_{1p}/K)pO_2 \tag{3}$$

The slope (R_{1p}/K) indicates the response of a particular resonance to pO_2.

PFCs essentially act as molecular amplifiers, since the solubility of oxygen is greater than in water, but thermodynamics require that the pO_2 in the PFC will rapidly equilibrate with the surrounding medium, and estimates of diffusion suggest the equilibration can occur within seconds.

[115] S. K. Holland, R. P. Kennan *et al.*, *Magn. Reson. Med.* **29,** 446 (1993).
[116] B. R. Barker, R. P. Mason *et al.*, *J. Magn. Reson. Imaging* **4,** 595 (1994).
[117] B. J. Dardzinski and C. H. Sotak, *Magn. Reson. Med.* **32,** 88 (1994).
[118] U. Noth, S. P. Morrissey *et al.*, *Magn. Reson. Med.* **34,** 738 (1995).
[119] H. T. Tran, Q. Guo *et al.*, *Acad. Radiol.* **2,** 756 (1995).
[120] S. Laukemper-Ostendorf, A. Scholz *et al.*, *Magn. Reson. Med.* **47,** 82 (2002).
[121] R. P. Mason, *Artif. Cells Blood Substit. Immobil. Biotechnol.* **22,** 1141 (1994).
[122] P. Parhami and B. N. Fung, *J. Phys. Chem.* **87,** 1928 (1983).
[123] L. C. Clark, Jr., J. Ackerman *et al.*, *in* "Oxygen Transport to Tissue VI" (D. Bruley, H. I. Bicher, and D. Reneau, eds.), p. 835. Plenum Press, New York,.
[124] C. F. Kong, G. M. Holloway *et al.*, *J. Phys. Chem.* **88,** 6308 (1984).
[125] C.-S. Lai, S. Stair *et al.*, *J. Magn. Reson.* **57,** 447 (1984).
[126] D. Eidelberg, G. Johnson *et al.*, *Magn. Reson. Med.* **6,** 344 (1988).
[127] S. R. Thomas, R. G. Pratt *et al.*, *Radiology* **18,** 159 (1991).

Because relaxation is proportional to oxygen concentration, the effect will be greater at a given pO_2 than for water. Importantly, ions do not enter the hydrophobic PFC phase, and thus do not affect the bulk relaxation. Indeed, PFCs are typically exceedingly hydrophobic and do not mix with the aqueous phases, but rather form droplets or emulsions. Based on these principles, PFCs have been applied to *in vivo* pO_2 measurements. Characteristics of many diverse PFCs are summarized in Table II.

At any given magnetic field (Bo) and temperature (T), sensitivity to changes in pO_2 is given by $R_1 = a + bpO_2$. Thus a greater slope is important, and the ratio $\eta = b/a$ has been proposed as a sensitivity index.[128] Generally, a small ''a'' value (intercept) represents greater sensitivity, but it also generates longer T_1 values under hypoxic conditions, potentially increasing data acquisition times. Indeed, the T_1 of hexafluorobenzene (HFB) at 4.7 T may reach 12 s, potentially creating long imaging cycles, but this is readily overcome by applying single-shot (echo planar) imaging techniques, as presented in a later section.

Many PFCs, such as perfluorotributylamine (PFTB), perflubron (formerly referred to as perfluorooctyl bromide; PFOB), and Therox (F44-E), have several ^{19}F NMR resonances, which can be exploited to provide additional information in spectroscopic studies, but seriously hamper effective imaging. Multiple resonances can lead to chemical shift artifacts in images, which compromise the integrity of relaxation time measurements, though they can be avoided by selective excitation, or detection, chemical shift imaging, deconvolution, or sophisticated tricks of NMR spin physics.[116,119,129–133] These approaches add to experimental complexity and are generally associated with lost signal to noise ratio (SNR). Thus we strongly favor PFCs with a single resonance, and we will describe the use of HFB,[27,32,42,106,134–137] though some research groups favor 5-crown-5-ether (15C5).[88,117,138,139]

[128] S. R. Thomas, R. G. Pratt *et al.*, *Magn. Reson. Imaging* **14,** 103 (1996).
[129] L. J. Busse, R. G. Pratt *et al.*, *J. Comp. Ast. Tomagr.* **12,** 824 (1988).
[130] R. P. Mason, N. Bansal *et al.*, *Magn. Reson. Imaging* **8,** 729 (1990).
[131] H. K. Lee and O. Nalcioglu, *J. Magn. Reson. Imaging* **2,** 53 (1992).
[132] U. Nöth, R. Deichmann *et al.*, *J. Magn. Reson. B* **105,** 233 (1994).
[133] R. G. Pratt, J. Zheng *et al.*, *Magn. Reson. Med.* **37,** 307 (1997).
[134] D. Zhao, A. Constantinescu *et al.*, *Radiat. Res.* **156,** 510 (2001).
[135] Y. Song, A. Constantinescu *et al.*, *Technol. Cancer Res. Treat.* **1,** 471 (2002).
[136] D. Zhao, A. Constantinescu *et al.*, *Radiat. Res.* **159,** 621 (2003).
[137] D. Zhao, S. Ran *et al.*, *Neoplasia* **5,** 308 (2003).
[138] B. P. J. van der Sanden, A. Heerschap *et al.*, *Int. J. Radiat. Oncol. Biol. Phys.* **44,** 649 (1999).
[139] T. Q. Duong, C. Ladecola *et al.*, *Magn. Reson. Med.* **45,** 61 (2001).

TABLE II
^{19}F NMR CHARACTERISTICS AND APPLICATIONS OF PFCs FOR TISSUE OXIMETRY

PFC	Sensitivity to pO_2 [a]	Temp. sensitivity (torr/°)	Magnetic field B_0(T)	Application/ comments	References
Hexafluorobenzene (HFB)	A = 0.0835 B = 0.001876	0.13	4.7	Rat breast tumor, prostate tumor, human lymphoma xenograft	Hunjan, Zhao *et al.*[159] Zhao, Constantinescu *et al.*[32,134,136]; Mason, Ran *et al.*[27]; Song, Constantinescu *et al.*[135]; Zhao, Ran *et al.*[137]
HFB	A = 0.074 B = 0.00158		4.7	Rat prostate tumor	Hunjan, Mason *et al.*[161]; Mason, Constantinescu *et al.*[175]
HFB	A = 0.093 B = 0.103	1.40	7	Phantom	Mason, Rodbumrung *et al.*[143]
Perfluoro-15-Crown-5-ether (15C5)	A = 0.345 B = 0.0034	2.94	2.0	Tumor cells	Helmer, Han *et al.*[157]
15C5	A = 0.333 B = 0.0033	3.98	2.0	Mouse tumor, spleen, liver	Dardzinski and Sotak[117]
15C5	A = 0.44 B = 0.0028		4.3	Human glioma tumor in mice	van der Sanden, Heerschap *et al.*[100]; van der Sanden, Heerschap *et al.*[138]
15C5	A = 0.375 B = 0.00198		4.7	Rat breast tumor	Fan, River *et al.*[95]
15C5	A = 0.362 B = 0.1239		4.7	Rat brain	Duong, Ladecola *et al.*[139]
Perfluorotributyl-amine (FC-43) PFTB	A = 1.09 B = 0.00623	4.43	0.14	Pig liver, spleen, lung	Thomas, Pratt *et al.*[128]
PFTB			0.14	Rat liver, spleen, lung	Pratt, Zheng *et al.*[133]; Thomas, Gradon *et al.*[163]

(continued)

TABLE II *(continued)*

PFC	Sensitivity to pO_2[a]	Temp. sensitivity (torr/°)	Magnetic field B_0(T)	Application/ comments	References
PFTB	A = 0.684 B = 0.00305		4.7	Rabbit eye	Berkowitz, Wilson *et al.*[166]; Wilson, Berkowitz *et al.*[b]
PFTB	A = 0.9072 B = 0.004486		1.5	Human eye	Wilson, Berkowitz *et al.*[167]
PFTB	A = 0.8848 B = 0.1307	8.17	7	Mouse Meth-A tumor and heart	Mason, Shukla *et al.*[141]
Perfluorotripropylamine (FTPA)	A = 0.314 B = 0.002760^{-3}		1.9	Rat subcutaneous tumor	Fishman, Joseph *et al.*[c]
FTPA	A = 0.301 B = 0.00312		1.4	Rat spleen, lung, liver	Fishman, Joseph *et al.*[114]
FTPA	A = 0.4052 B = 0.0023		2.0	Rat liver, spleen	Holland, Kennan *et al.*[115]
FTPA			4.4	Cells	Taylor and Deutsch[d]
Bis-perfluoro-butylethylene (F-44E)	A = 0.3421 B = 0.11172		7.05	Rat, alginate capsules	Noth, Grohn *et al.*[164]
F-44E	A = 0.342 B = 0.1201		7.05	Rat spleen, liver, abdominal aorta, vena cava	Noth, Morrissey *et al.*[118]
F-44E	A = 0.2525 B = 0.16527	0.59	2.0	Mouse tumor	Hees and Sotak[153]
Perfluoroctyl-bromide (perflubron) (PFOB)	A = 0.517 B = 0.0038		9.4	Rat heart	Shukla, Mason *et al.*[e]
PFOB	A = 0.2677 B = 0.12259	1.26	4.7	Prostate tumor in rat	Antich *et al.*[162]

PFOB	A = 0.328 B = 0.12137	2.85	7	Phantom	Mason, Shukla *et al.*[142]
PFOB			2.0	Rat tumor	Sostman, Rockwell *et al.*[96]
PFOB	A = 0.085 B = 0.0033		1.5	Rabbit liver	Tran, Guo *et al.*[119]
PFOB			8.5	Pig liver, lung, spleen	Millard and McGoron[f]
PFOB			1.45	Rat lung, Mouse lung	Thomas, Clark, Jr. *et al.*[g]
PFOB			1.5	Pig lung	Laukemper-Ostendorf, Scholz *et al.*[120]
Perfluoro-2,2,2′,2′-tetramethyl-4,4′-bis(1,3-fioxolane) (PTBD)	A = 0.50104 B = 0.1672		2.0	Phantom	Sotak, Hees *et al.*[h]

Some original papers presented calibration curves in other forms (e.g., including coefficients for temperature dependence). In those cases, equations have been derived assuming 37°. Where a PFC has more than one resonance, the equation presented is either for the most sensitive signal, or the equation used where the signal may have been unresolved.

[a] $R_1\ (s^{-1}) = A + B \times pO_2$ (torr).

[b] C. A. Wilson, B. A. Berkowitz *et al.*, *Exp. Eye Res.* **55,** 119 (1992).

[c] J. E. Fishman, P. M. Joseph *et al.*, *Invest. Radiol.* **24,** 65 (1989).

[d] J. Taylor and C. J. Deutsch, *Biophys. J.* **53,** 227 (1988).

[e] H. P. Shukla, R. P. Mason *et al.*, *Magn. Reson. Med.* **35,** 827 (1996).

[f] R. W. Millard and A. J. McGoron, *Artif. Cells Blood Subst. Immobil. Biotechnol.* **22,** 1251 (1994).

[g] S. R. Thomas, L. C. Clark, Jr. *et al.*, *J. Comput. Assist. Tomogr.* **10,** 1 (1986).

[h] C. H. Sotak, P. S. Hees *et al.*, *Magn. Reson. Med.* **29,** 188 (1993).

R_1 is sensitive to temperature, although the response varies greatly between PFCs and between individual resonances of each individual PFC. Over small temperature ranges, a linear correction to calibration curves is appropriate, but over larger temperature ranges, the response can be complex, as investigated extensively by Shukla *et al.*[140] for several PFCs. Differential sensitivity of pairs of resonances to pO_2 and temperature allowed Mason *et al.*[141] to simultaneously determine both parameters by solving simultaneous equations. However, generally it is preferable for a pO_2 sensor to exhibit minimal response to temperature, since this is not always known precisely *in vivo* and temperature gradients may occur across tumors. As shown in Table II, even a relatively small error in temperature estimate can introduce a sizable discrepancy into the apparent pO_2; for example, the relative error introduced into a pO_2 determination by a 1° error in temperature estimate ranges from 8 torr/° for PFTB[141] to 3 torr/° for PFOB (perflubron)[142] or 15C5[117] and 0.1 torr/° for HFB,[143] when pO_2 is actually 5 torr. It must be noted that error depends on actual pO_2 and the error varies with magnetic field and temperature. R_1 response does depend on magnetic field, necessitating calibration curves for each type of magnet system (e.g., 1.5, 4.7, or 7 T). Thus comparison of PFC utility for pO_2 measurements is complicated by the field used for specific published investigations, and in Table II, we consider sensitivity as presented.

Choice of PFC may be governed by practical considerations, such as cost and availability, since several products, particularly proprietary emulsions, may be difficult to obtain. HFB and 15C5 offer the immediate advantage of a high symmetry and a single ^{19}F NMR resonance. This offers maximum SNR and simplifies imaging, which may otherwise require frequency selective excitation, deconvolution, or other NMR tricks to avoid chemical shift artifacts.

Route of Administration. The most popular route for the delivery of PFCs is as emulsions injected intravenously. Given the extremely hydrophobic nature of PFCs, they do not dissolve in blood directly, but may be formulated as biocompatible emulsions. Much effort has been applied to formulate stable homogenous emulsions, as reviewed elsewhere.[144] Following IV infusion, the emulsion circulates in the vasculature with a

[140] H. P. Shukla, R. P. Mason *et al.*, *J. Magn. Reson. B* **106,** 131 (1995).
[141] R. P. Mason, H. P. Shukla *et al.*, *Magn. Reson. Med.* **29,** 296 (1993).
[142] R. P. Mason, H. P. Shukla *et al.*, *Biomater. Artif. Cells Immobilization Biotechnol.* **20,** 929 (1992).
[143] R. P. Mason, W. Rodbumrung *et al.*, *NMR Biomed.* **9,** 125 (1996).
[144] J. G. Riess, *Biomater. Artif. Cells Immobilization Biotechnol.* **20,** 183 (1992).

typical half-life of 12 h, (depending on the nature of the emulsion) providing substantial clearance within 2 days.[145,146] Primary clearance is by macrophage activity, leading to extensive accumulation in the liver, spleen, and bone marrow.[113,147] Indeed, this is a major shortcoming of IV delivery, since animals may exhibit extensive hepatomegaly or splenomegaly.[148] The emulsions are not toxic, and other than causing swelling, appear not to cause health problems. PFC clearance occurs from the liver with a typical half-life of 60 days for perfluorotripropylamine and 3 days for perflubron, with primary clearance by migration to the lungs and exhalation.[149]

Some investigators have examined pO_2 of tissues, while PFC remained in the blood, providing a vascular pO_2.[114,118,150] Flow can generate artifacts, and correction algorithms have been proposed.[151] Many investigators have measured pO_2 in liver, spleen, and tumors following clearance from the blood, thus providing measurement of tissue pO_2.[95,100,115,117–119,152–157]

Both spectroscopic and imaging approaches have been applied to tissue pO_2 measurements depending on the available SNR. It appears that uptake and distribution efficiency vary with tumor type, but in general, maximum signal is detected from the tumor periphery corresponding with regions of greater perfusion.[100,117,138,154,158,159] Several reports have examined changes in tumor pO_2 in response to acute interventions such as vasoactive drugs and hyperoxic gases.[32,95,100,135–137,153,160] Spectroscopic time resolution has ranged from seconds to minutes,[161,162] whereas imaging often takes longer.[160]

Long tissue retention facilitates chronic studies during tumor development, and progressive tumor hypoxiation has been observed over extended time periods of many days.[154,156] Correlated ^{19}F and proton MRI suggest

[145] M. C. Malet-Martino, D. Betbeder *et al.*, *J. Pharm. Pharmacol.* **36,** 556 (1984).
[146] T. F. Zuck and J. G. Riess, *Crit. Rev. Clin. Lab. Sci.* **31,** 295 (1994).
[147] R. P. Mason, P. P. Antich *et al.*, *Magn. Reson. Imaging* **7,** 475 (1989).
[148] W. I. Rosenblum, M. G. Hadfield *et al.*, *Arch. Pathol. Lab. Med.* **100,** 213 (1976).
[149] R. F. Mattrey and D. C. Long, *Invest. Radiol.* **23,** s298 (1988).
[150] D. Eidelberg, G. Johnson *et al.*, *J. Cereb. Blood Flow P. Metab.* **8,** 276 (1988).
[151] T. Higuchi, S. Naruse *et al.*, *in* "7th SMRM," p. 435, 1988.
[152] R. P. Mason, R. L. Nunnally *et al.*, *Magn. Reson. Med.* **18,** 71 (1991).
[153] P. S. Hees and C. H. Sotak, *Magn. Reson. Med.* **29,** 303 and erratum **29,** 716 (1993).
[154] R. P. Mason, P. P. Antich *et al.*, *Int. J. Radiat. Oncol. Biol. Phys.* **29,** 95 (1994).
[155] S. R. Thomas, R. W. Millard *et al.*, *Artif. Cells Blood Subst. Immobil. Biotechnol.* **22,** 1029 (1994).
[156] N. J. Baldwin and T. C. Ng, *Magn. Reson. Imaging* **14,** 541 (1996).
[157] K. G. Helmer, S. Han *et al.*, *NMR Biomed.* **11,** 120 (1998).
[158] P. P. Antich, R. P. Mason, A. Constantinescu *et al.*, *Proc. Soc. Nucl. Med.* **35,** 216P (1994).
[159] D. J. O. Mclntyre, C. L. McCoy *et al.*, *Curr. Sci.* **76,** 753 (1999).
[160] S. Hunjan, D. Zhao *et al.*, *Int. J. Radiat. Oncol. Biol. Phys.* **49,** 1097 (2001).
[161] R. P. Mason, F. M. H. Jeffrey *et al.*, *Magn. Reson. Med.* **27,** 310 (1992).
[162] S. Hunjan, R. P. Mason *et al.*, *Int. J. Radiat. Oncol. Biol. Phys.* **40,** 161 (1998).

that PFC does not redistribute, but remains associated with specific tissues, analogous to tree rings.[154,156] Thus in principle, a whole tumor can be investigated by administering successive doses of PFC emulsion during growth.

PFC emulsions may also be administered intraperitoneally (IP), resulting in similar distribution to IV administration (unpublished observations). Given the volatile nature of many PFCs, they could be inhaled, but although this is a popular route for delivery of anesthetics and blood flow tracers, it does not appear to have been widely exploited for oximetry. Nonetheless, aerosols have been delivered to the lungs by inhalation to facilitate pO_2 measurements.[163]

Two approaches have been applied to circumvent reticuloendothelial uptake. PFC has been incorporated in polyalginate beads for direct implantation at a site of interest.[164,165] We favor direct IT injection of neat PFC, allowing any region of interest in a tumor to be interrogated immediately. Use of a fine needle ensures minimal tissue damage, as described in detail in a later section. Others have used direct injection of emulsions into tumors, but this increases the volume considerably, making it more invasive.[88] Investigators have suggested that emulsification improves retention at the site of injection. Direct injection of neat PFC also has been used to investigate retinal oxygenation[166–168] and cerebral oxygenation in the interstitial and ventricular spaces.[139]

As described in the following section we favor direct intratumoral injection of neat HFB followed by echo planar imaging to generate pO_2 maps in tumors.

FREDOM (Fluorocarbon Relaxometry using Echo Planar Imaging for Dynamic Oxygen Mapping)

Recognizing that tumors are heterogeneous and that pO_2 may fluctuate, we developed a procedure, which allows repeated quantitative maps of regional pO_2 to be achieved with multiple individual locations simultaneously in 6.5 min with a precision of 1–3 torr, when pO_2 is in the

[163] S. R. Thomas, L. Gradon *et al.*, *Invest. Radiol.* **32,** 29 (1997).
[164] U. Nöth, P. Grohn *et al.*, *Magn. Reson. Med.* **42,** 1039 (1999).
[165] U. Zimmermann, U. Noth *et al.*, *Artif. Cells Blood Subst. Immobil. Biotechnol.* **28,** 129 (2000).
[166] B. A. Berkowitz, C. A. Wilson *et al.*, *Invest. Ophthalmol. Vis. Sci.* **32,** 2382 (1991).
[167] C. Wilson, B. Berkowitz *et al.*, *Arch. Ophthalmol.* **110,** 1098 (1992).
[168] W. Zhang, Y. Ito *et al.*, *Invest. Ophthalmol. Visual Sci.* **44,** 3119 (2003).

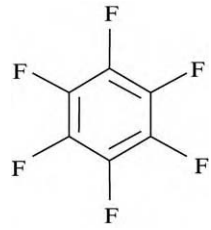

FIG. 1. Hexafluorobenzene (HFB) is a perfluorocarbon (PFC) exhibiting extensive symmetry.

range 0–10 torr.[160] We have applied FREDOM to diverse tumor types and interventions, as reviewed in a later section.

MRI is attractive because it is readily available at many institutions. For small animal work, ^{19}F NMR is widely available at 4.7, 7, and 9.4 T by minor adaptation of routine instrumentation, [e.g., retuning proton radio-frequency (RF) coils]. Within the recent past ^{19}F MRI is also becoming available on clinical systems, facilitating translation of these techniques to patients. ^{19}F NMR is particularly facile because there is essentially no background signal in tissues to interfere with measurements, yet the resonance frequency and sensitivity approach that of proton NMR. The pioneering work of Thomas[113] showed that tissue pO_2 could be imaged in various organs based on the ^{19}F NMR spin–lattice relaxation rate (R_1) of PFC reporter molecules following IV infusion. Prompted by these studies, we surveyed a number of PFCs and identified that HFB (Fig. 1) has many virtues as a pO_2 reporter.[143] Symmetry provides a single narrow ^{19}F NMR signal, and the spin–lattice relaxation rate is highly sensitive to changes in pO_2, yet minimally responsive to temperature (Fig. 2).[143] HFB also has a long spin–spin relaxation time (T_2), which is particularly important for imaging investigations. From a practical perspective, HFB is cheap (<$2/g) and readily available commercially in high purity (≥99%). We obtain supplies from Lancaster Synthesis (Windham, NH), though many other fine chemical supply houses also offer HFB. We do favor bottles over sealed ampoules, since they are easier to handle. HFB is well characterized in terms of lack of toxicity,[169,170] exhibiting no mutagenicity,[171] teratogenicity, or fetotoxicity,[172] and the manufacturer's material

[169] Y. S. Gorsman and T. A. Kapitonenko, *Izv. Estestvennonauchu. Inst. Pevinsk.* **15,** 155 (1973).
[170] I. M. C. M. Rietjens, A. Steensma *et al.*, *Eur. J. Pharmacol.* **293,** 292 (1995).
[171] K. E. Mortelmans and V. F. Simmon, *Gov. Rep. Announce. Index (US)* **81,** 2555 (1981).
[172] K. D. Courtney and J. E. Andrews, *J. Environ. Sci. Health B* **19,** 83 (1984).

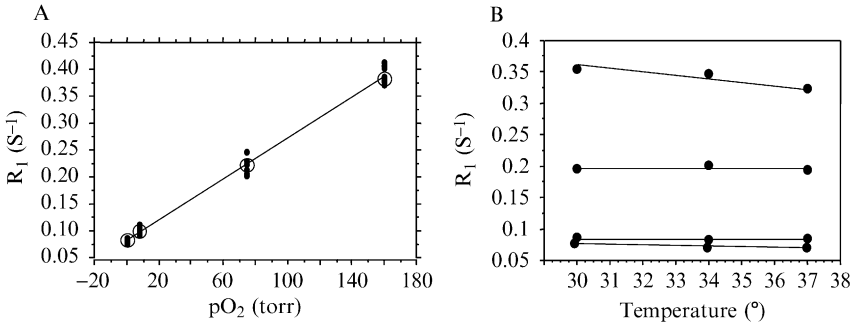

FIG. 2. (A) The ^{19}F NMR spin–lattice relaxation rate (R_1) of HFB shows a linear response to pO_2: at 37° and 4.7 T, $R_1 = 0.0835 + 0.001876 \times pO_2$. (B) The ^{19}F NMR R_1 of HFB shows minimal response to temperature in the physiologic range; separate curves are shown at four different pO_2s: 0, 1, 9.8, and 21% O_2.

data safety sheet indicates $LD_{50} > 25$ g/kg (oral—rat) and LC_{50} 95 g/m^3/2 h (inhalation—mouse).

HFB had been proposed as a veterinary anesthetic and has been used in many species, including ponies, sheep, cats, dogs, rats, and mice, but was abandoned because of its high volatility (boiling point 81°) and low flash point (10°).[173] This presented unacceptable dangers in veterinary suites for inhalation anesthetics. It is not a problem in our studies, where small quantities of liquid (typically, 50 μl) are injected directly into the tumor. HFB requires no special storage, other than a sealed bottle to prevent evaporation. Melting point is 4–6°, and density is 1.62 g/ml.

Methodology

Tumor Preparation. We have applied this technique to tumors in rats and mice, but our methodology will focus on our standard application to rats. As for electrode techniques, the tumor must be accessible (e.g., subcutaneous in flank of thigh), though we favor the pedicle model, which provides a tumor remote from the body, analogous to an additional limb.[174] This model is optimal for selective therapy such as local hyperthermia, irradiation, or excision. Noting the increasing interest in orthotopic tumors, the approach is also facile in breast tumors in the mammary fat pad and applicable in the prostate with a little practice.

[173] L. W. Hall, S. R. K. Jackson *et al.*, *in* "Recent Progress in Anaesthesiology and Resuscitation" (A. Arias, R. Llaurado, M. A. Nalda, and J. N. Lunn, eds.), p. 201. Excerpta Medica, Oxford, UK, 1975.

[174] E. W. Hahn, P. Peschke *et al.*, *Magn. Reson. Imaging* **11,** 1007 (1993).

Rats are preanesthetized with ketamine hydrochloride (100 mg/ml) as a relaxant and maintained under general gaseous anesthesia with air (1 dm^3/min) and 1.2% isoflurane [we do note that the appropriate concentration of anesthesia may depend on strain; for example, Copenhagen rats require (and tolerate) higher concentrations than Fisher rats]. In our latest refinement of the procedure, isoflurane may be stopped for a period of minutes during HFB administration, since rats occasionally exhibit respiratory distress, which may be caused by the anesthetic properties of HFB interacting with isoflurane. Within a few minutes, rats are stable and routine isoflurane anesthesia is maintained. In our earlier work we used 0.5% methoxyflurane in 33% oxygen with 66% N_2O,[160,175] but isoflurane appears to be a less stressful anesthetic.

HFB is deoxygenated by bubbling nitrogen for 5 min before use. We have previously shown in hypoxic tumor biopsies that use of aerated HFB may introduce a systematic apparent elevation in pO_2 (~2–3 torr). HFB is injected directly into tumors using a gas tight syringe with a custom-made fine sharp needle (32G #7803–04; Hamilton, Reno, NV). Generally, HFB is administered along three to five tracks in the form of a fan in a single central plane of the tumor coronal to the rat's body (Fig. 3A). The needle is inserted manually to penetrate across the whole tumor and withdrawn ~1 mm to reduce pressure, and 3 μl HFB is deposited. The needle is repeatedly withdrawn a further 2–3 mm, and additional HFB is deposited. Typically, HFB is deliberately deposited at about 16 individual locations per tumor, in both the central and peripheral regions of the tumors, to ensure that the interrogated regions are representative of the whole tumor.

The animal is placed on its side in a cradle with a thermal blanket to maintain body temperature. A fiber-optic probe is inserted rectally to monitor core temperature. Temperature measurement is optional, since the R_1 is essentially invariant with temperature and does not need correction for pO_2 estimates. Of course, temperature regulation and measurement is important to ensure stable tumor physiology. An MR-compatible pulse oximeter equipped with "rat" software (8600V; Nonin, Inc., Plymouth, MN) may be applied to a hind foot to monitor arterial oxygenation (S_aO_2) and heart rate (optional, but provides additional useful data regarding animal health and physiology).

Most of our MR experiments were performed using an Omega CSI 4.7 horizontal bore magnet system with actively shielded gradients (GE systems, acquired by Bruker Instrument, Inc., Fremont, CA). Recently, our MR system has been upgraded to a Varian Unity INOVA, providing

[175] R. P. Mason, A. Constantinescu *et al.*, *Radiat. Res.* **152,** 239 (1999).

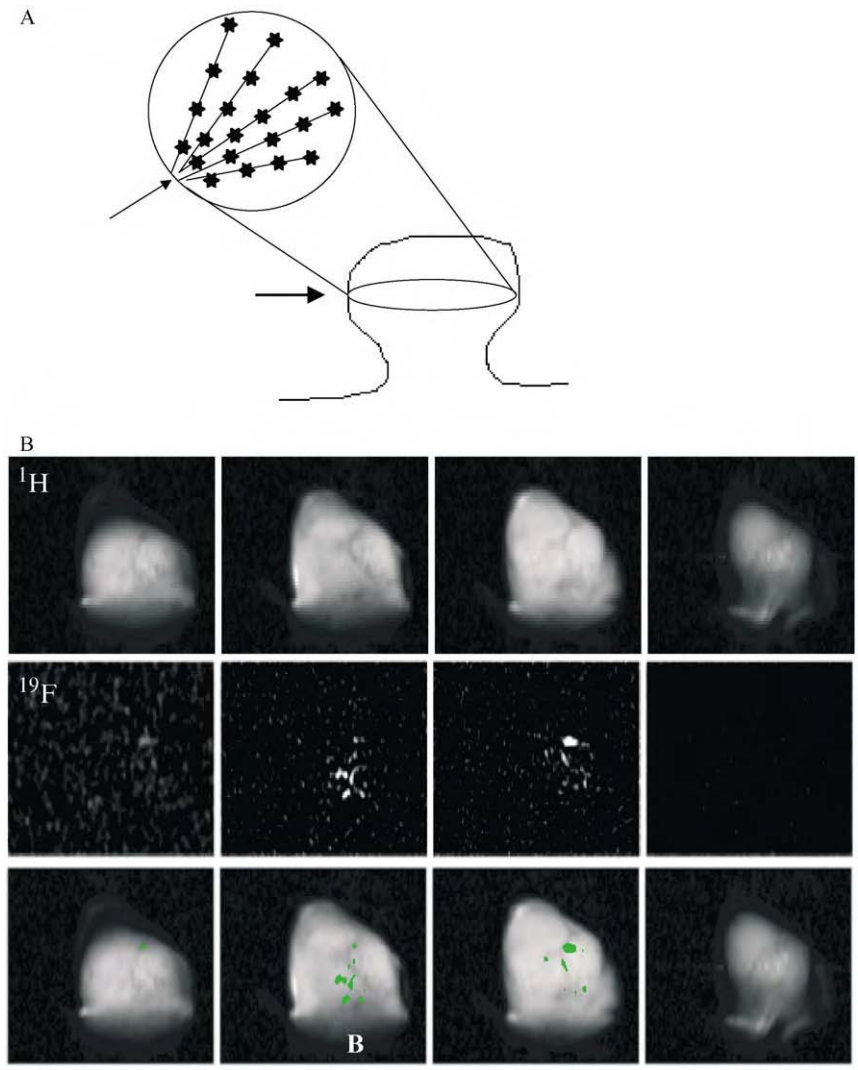

FIG. 3. (A) Recommended pattern of IT injection. Several tracks in the form of a fan in a single plane. (B) Four contiguous MR images (5 mm thick) of a representative Dunning prostate R3327-AT1 tumor (volume = 1.6 cm^3). *Top:* ^{1}H MRI; *middle:* corresponding ^{19}F; *bottom:* overlay to show interrogated regions. *B* marks point of attachment of the tumor to back of rat.

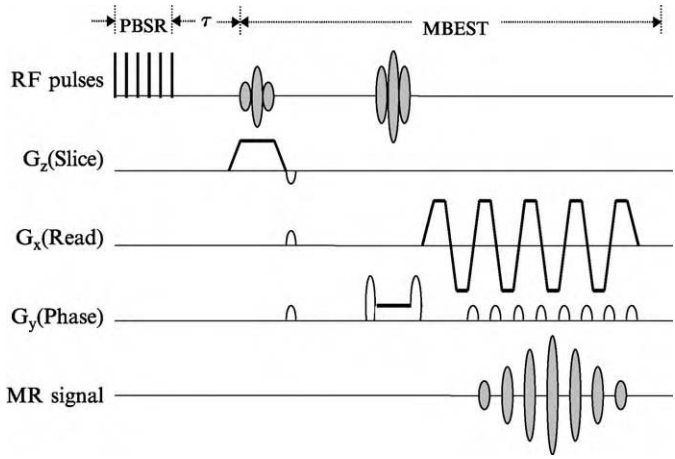

FIG. 4. MRI sequence used to achieve relaxation curves.

enhanced data acquisition and processing software and stronger imaging gradients. A tunable ($^1H/^{19}F$) MR coil, 2 or 3 cm in diameter matched to the tumor size (constructed from a cylindrical copper tube about 2 cm deep and acting as a single-turn solenoid), is placed around the tumor-bearing pedicle. Shimming is performed on the proton water signal to a typical linewidth of 60–100 Hz. Proton images are obtained for anatomic reference using a three-dimensional (3D) spin–echo sequence. The coil is then retuned in place to 188.27 MHz, and corresponding ^{19}F MR images are obtained. Overlaying the ^{19}F MR images on the corresponding proton images reveals the distribution of HFB (Fig. 3B). Typically, ^{19}F NMR signal is obtained from 6–10% of the total tumor voxels.[136,137,175]

pO_2 maps are obtained using our standard MR oximetry protocol.[116,160,176] This applies pulse burst saturation recovery (PBSR) echo planar imaging (EPI) relaxometry using the ARDVARC (*a*lternated *r*elaxation *d*elays with *v*ariable *a*cquisitions to *r*educe *c*learance effects) acquisition protocol to map the tumors (Fig. 4).[175,177] EPI uses a single spin–echo with ''blipped'' phase encoding (modulus-blipped echo-planar single-pulse technique [MBEST]), although other EPI sequences should be equally applicable. We chose the PBSR approach to T_1 relaxation measurements for historical reasons; our earliest work used ^{19}F NMR spectroscopy of tumors with excitation and detection based on surface coils.[152] The PBSR approach is suitable for use with the nonuniform excitation typical of surface

[176] B. R. Barker, R. P. Mason *et al.*, *Magn. Reson. Imaging* **11,** 1165 (1993).
[177] D. Le, R. P. Mason *et al.*, *Magn. Reson. Imaging* **15,** 971 (1997).

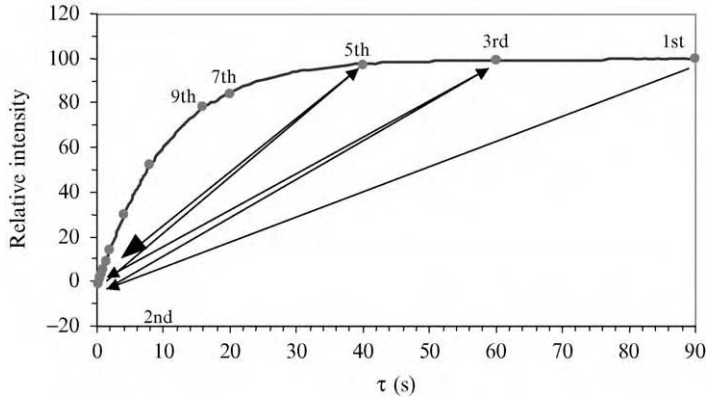

FIG. 5. Typical relaxation curve showing order of data acquisition. $y = A\,[1 - (1 + W)\exp(-R_1 \times \tau)]$ and $T_1 = 10.34 \pm 0.16$ s, $A = 99.5$, $W = 0.04$, and hence $pO_2 = 7.0 \pm 0.7$ torr.

coils as presented by Evelhoch and Ackerman.[178] For EPI, we do apply carefully calibrated $\pi/2$ pulses to ensure accurate refocusing of images, but we continue to favor the PBSR approach, since it provides particularly rapid estimation of T_1 by avoiding the need for extended relaxation recovery times between acquisitions. Saturation is achieved by a series of 20 nonspatially selective $\pi/2$ pulses with 50-ms spacing, which is sometimes called a ''Comb'' format.

Typical FREDOM parameters use 32×32 data points across a field of view of 40×40 mm, providing 1.25 mm in-plane resolution. Recently, we have applied a slice selection gradient, providing 5-mm-thick slices, and hence, 8-μl voxels. However, the deposition of HFB is designed to occur in a plane, and thus the discrete distribution of the reporter molecule itself can be used to define the slice. We apply a PBSR preparation sequence because it is ideally suited for measuring diverse, long T_1 values. Unlike more traditional inversion recovery sequences, there is no need to wait >5 T_1 between successive images. As shown in Fig. 5, we use 14 delays in the order 90 s, 200 ms, 60 s, 400 ms, 40 s, 600 ms, 20 s, 800 ms, 16 s, 1 s, 8 s, 1.5 s, 4 s, and 2 s, selected to cover the whole range of T_1s (viz pO_2 values). Many papers have been published on optimizing relaxation curves and choosing parameters to enhance precision.[179–181] Our experience suggests that our

[178] J. L. Evelhoch and J. J. H. Ackerman, *J. Magn. Reson.* **53,** 52 (1983).
[179] A. P. Crawley and R. M. Henkelman, *Magn. Reson. Med.* **7,** 23 (1988).
[180] S. J. Doran, J. J. Attard *et al.*, *J. Magn. Reson.* **100,** 101 (1992).
[181] F. Franconi, F. Seguin *et al.*, *Medical Phys.* **22,** 1763 (1995).

parameters are appropriate for interrogating a broad range of pO_2 values, though they have not been rigorously or theoretically optimized. More delays could improve curve fitting, but would increase experiment time. We believe fewer delays would degrade quality of the curve fitting.

Traditional T_1 measurement sequences acquire data with delays in monotonic order, whereas we alternate longer and shorter delays to minimize any systematic errors, which would be introduced if the signal amplitude varies during the measurement. We have found that HFB clears from tissue with a typical half-life of 600 min,[162] which would introduce errors into the amplitude. Although the total acquisition time for a T_1 map is 6.5 min, we reduce the time between first and last acquisitions further by applying the longest delay first. Our experience shows that it is important to measure at least two data points on the plateau of the curve (i.e., $>5 \times T_1$, and we choose 60 and 90 s, respectively. The data points with longer recovery times have greater SNR, and we find that a minimum SNR = 10 is required to produce satisfactory T_1 curves and pO_2 estimates. The variation in amplitude between longest and shortest delays approaches 100-fold. The poorest SNR data points (short delay; τ) could compromise the quality of the T_1 curves, and thus we obtain multiple acquisitions at these times to provide enhanced SNR by signal averaging. Because the τ values are short, it adds little to the overall experimental time. We use NA = 12 for $\tau < 1$ s; NA = 8 for $\tau = 1$ s; NA = 4 for $\tau = 1.5$, 2, and 4 s; NA = 2 for $\tau = 8$ s; and 16 s and NA = 1 for the longer delays. Signal amplitudes are corrected for the additional acquisitions, and a 2-d Fourier transform (FT) is applied to each image. Curve fitting is then applied on a voxel-by-voxel basis to each image set. Data quality could probably be enhanced by application of apodization and filtering functions, such as Fermi and Hanning filters, though we have not yet implemented these approaches. The acquisition protocol is not part of the standard software supplied by the manufacturer, but we can assist interested investigators.

Data are transferred to a personal computer (PC) for further analysis using a program created in our laboratory (T_1map [Fig. 6], PASCAL by Dennis Le). T_1map recognizes issues in data analysis and provides filters, clustering algorithms, and temporospatial correlation to assist in effective data reduction. At top right of Fig. 6 is a map, which may be toggled to display signal amplitude, T_1, T_1 error ($T_{1\ err}$), or pO_2 (Fig. 7). Blank pixels indicate that no curve fit could be achieved. Gray pixels indicate a successful curve fit and potential pO_2 value, but with errors beyond the specified range. In this example, thresholds were set as $T_{1\ err} < 2.5$ s and the ratio $T_{1\ err}/T_1 < 50\%$. Tightening these thresholds can produce higher-quality data, but eliminates more data. Colored pixels report measurements satisfying the threshold criteria, and these are tabulated in the form of a

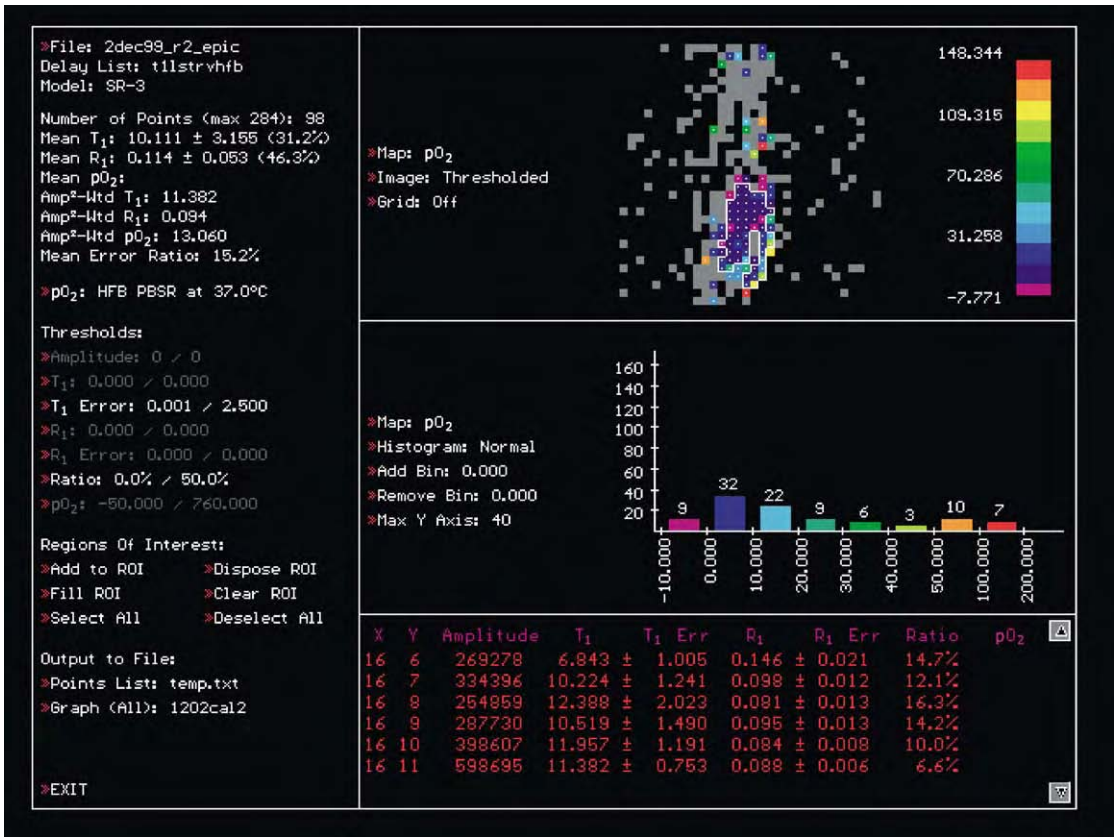

FIG. 6. Example T_1map used for data filtering, clustering, and analysis.

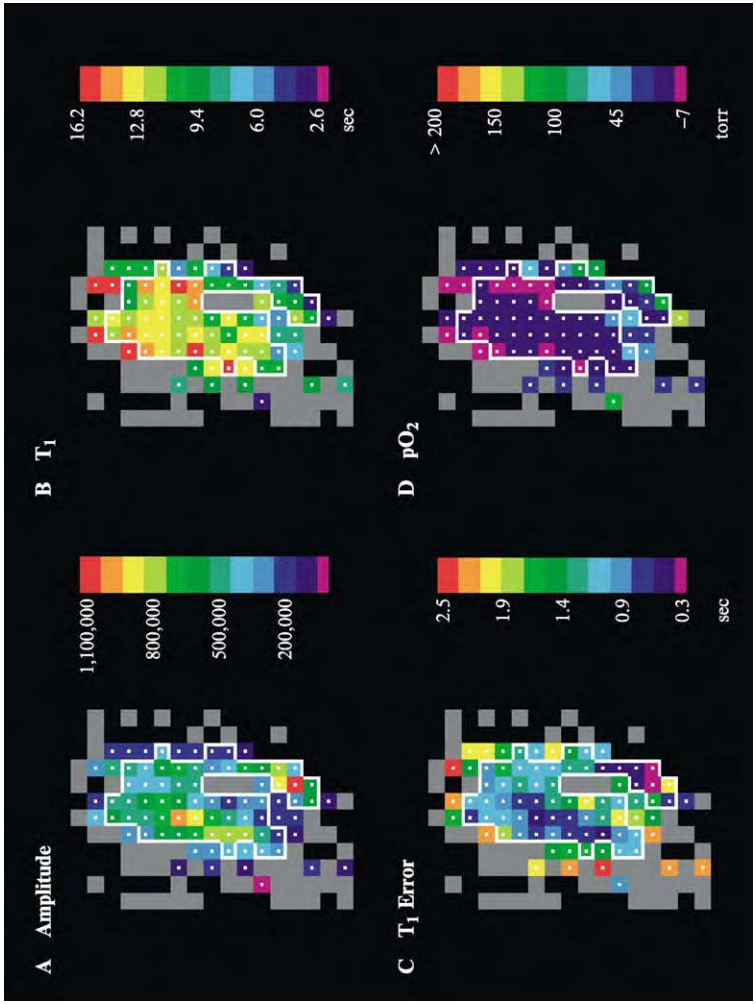

FIG. 7. *(continued)*

histogram (center), which can be plotted with selected data bins and ranges of interest. At bottom right of Fig. 6 are data for each pixel, including coordinate and fitted parameters. In the box on the left are shown the number of fitted data points, number of accepted data points, and statistics such as mean T_1, pO_2, and corresponding amplitude-weighted values.

pO_2 is calculated on the basis of a curve fit to exponential data. Any curve fitting is associated with uncertainty, and indeed our procedure determines $T_{1\ err}$ values. Although the concept of negative pO_2 values may appear impossible, it is perfectly reasonable, provided that error bars and uncertainties are considered. Thus a value of -2 torr $\pm$ 3 torr legitimately indicates an actual pO_2 very close to zero. Some oximetry approaches ignore negative values or bin them all as zero. We accept any value providing that the error estimated for T_1 is within a specified range.

The most powerful aspect of FREDOM is the ability to follow the fate of individual voxels, and thus we usually acquire at least three baseline pO_2 maps, followed by further maps accompanying interventions, such as hyperoxic gas breathing. Even under baseline conditions, fluctuations in T_1 are apparent. These may arise from uncertainty in T_1, which may be reflected in $T_{1\ err}$ or transient fluctuations in pO_2.

T_1 map allows us to investigate sequential maps and select only those pixels that consistently show small $T_{1\ err}$s, for example, white regions of interest (ROI). In subsequent maps we may include only these regions, which satisfy the inclusion criteria for every map. This allows us to follow population dynamics based on specific tumor regions, avoiding potential anomalies due to varying numbers of ''good quality'' pixels in sequential images. Typically, 50–150 pixels provide high-quality data in any given map, but generally 20–80 pixels may be followed for a series of 23 maps associated with interventions.

The ROI tool also facilitates clustering, for example, selection of only those tumor regions, which consistently have $pO_2 < 10$ torr throughout the baseline period (these may be considered as chronically hypoxic, as opposed to regions, which fluctuate and may only be <10 torr in some

FIG. 7. Maps showing (A) ^{19}F NMR signal intensity, (B) spin–lattice relaxation times (T_1), (C) estimated errors in T_1, and (D) pO_2 values. Black squares show regions where signal to noise or data quality was so poor as to not provide a T_1 curve fit. Gray voxels show regions that provided a curve fit, but where the uncertainty in the data exceeded the threshold criteria (i.e., $T_{1\ err} > 2.5$ s or $T_{1\ err}/T_1 > 50\%$). All colored voxels ($n = 100$) provided a curve fit within the acceptance criteria in this map, but only those 56 voxels within the white regions of interest (ROI) provided consistently high-quality data throughout the sequence of eight maps acquired during baseline and with oxygen breathing. Data were obtained using the FREDOM approach from a representative Dunning prostate R3327-AT1 tumor (2 cm^3).

baseline maps). The ability to follow groups of pixels with particular baseline characteristics has revealed heterogeneity in response to many interventions—often those regions initially well oxygenated show rapid and large response to hyperoxic gas breathing, whereas those that are initially poorly oxygenated show little and sluggish response (e.g., Fig. 8). This approach can also reveal phenomena such as the ''steal'' effect, whereby initially well-oxygenated regions decrease in pO_2, while others increase, which might appear as ''no change,'' when histogram-based population statistics are used.

Figure 9 shows that the data quality is strongly related to signal amplitude. Although these data represent 56 voxels from a single tumor, we have previously shown similar data for the alternate PFC perflubron.[116] Given the high solubility of O_2 in PFCs, there could be a concern that PFCs act as reservoirs, perturbing local pO_2. Fig. 9B shows that there is no correlation ($r^2 < 0.05$) between signal amplitude (viz. HFB concentration) and pO_2.

As with any measurement, sampling is a critical issue. FREDOM is analogous to the Eppendorf Histograph in that it samples multiple locations, which appear to reflect interstitial pO_2. Histograph data suggest that a minimum of 100–140 data points[182] along five tracks[183] are required to accurately represent the pO_2 distribution of a tumor, though such criteria do depend on tumor size and heterogeneity. We applied Monte Carlo simulation to assess the data requirements for FREDOM. A data set was selected, which provided 120 high-quality data points, and these data points were accessed in random order with continuous calculation of mean pO_2 to assess the asymptotic trend lines toward the actual mean pO_2 (Fig. 10). It appears that about 50 data points are required to well represent the pO_2 distribution of the tumor, which is generally achievable in any individual pO_2 map. However, the unique ability to observe dynamic changes in pO_2 at multiple locations simultaneously is the greatest strength of FREDOM. Detection of heterogeneous responses is useful even if fewer data points are examined, since each location serves as its own control.

Validation of Measurements. The spin–lattice relaxation rate (R_1) is determined for each voxel using a three-parameter fit of signal intensities to

$$y_i = A[1 - (1 + W)\exp(-R_1 \times \tau)] \quad (4)$$

using the Levenberg–Marquardt least squares fitting protocol.[116] Typically, ~100–300 voxels provide an R_1 fit and potential pO_2 value. Because noise

[182] K. A. Yeh, S. Biade *et al.*, *Int. J. Radiat. Oncol. Biol. Phys.* **33,** 111 (1995).
[183] O. Thews, D. K. Kelleher *et al.*, *in* ''Tumor Oxygenation'' (P. W. Vaupel, D. K. Kelleher, and Günderoth, eds.), Vol. 24, p. 39. Gustav Fischer Verlag, Stuttgart, Germany, 1995.

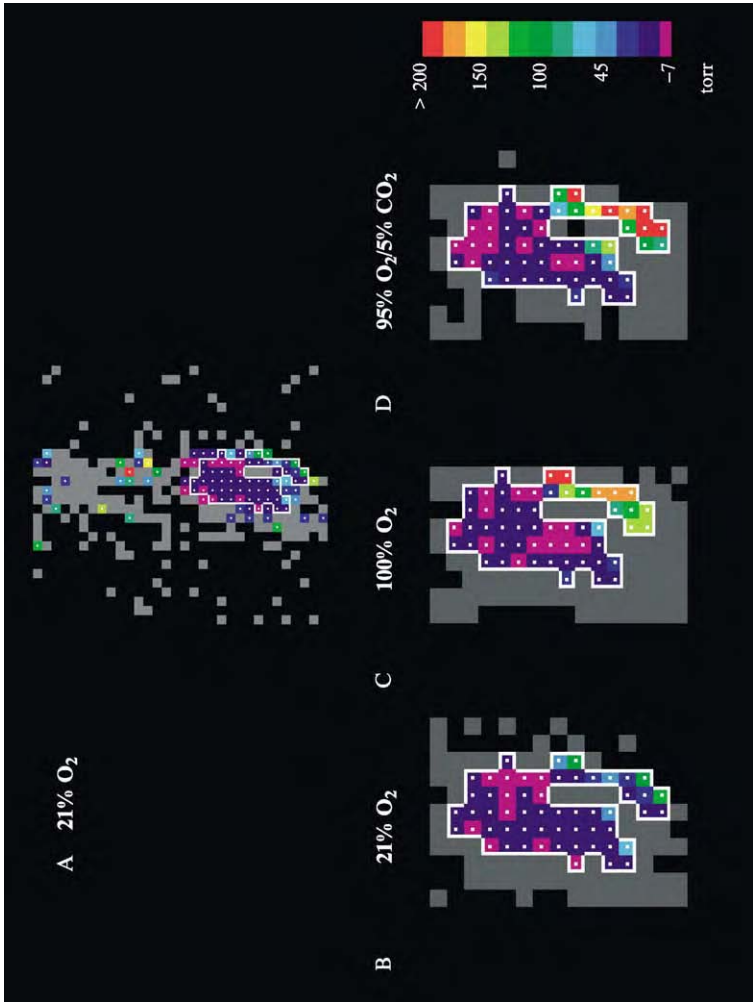
A 21% O2
B 21% O2
C 100% O2
D 95% O2/5% CO2
> 200
150
100
45
~7
torr

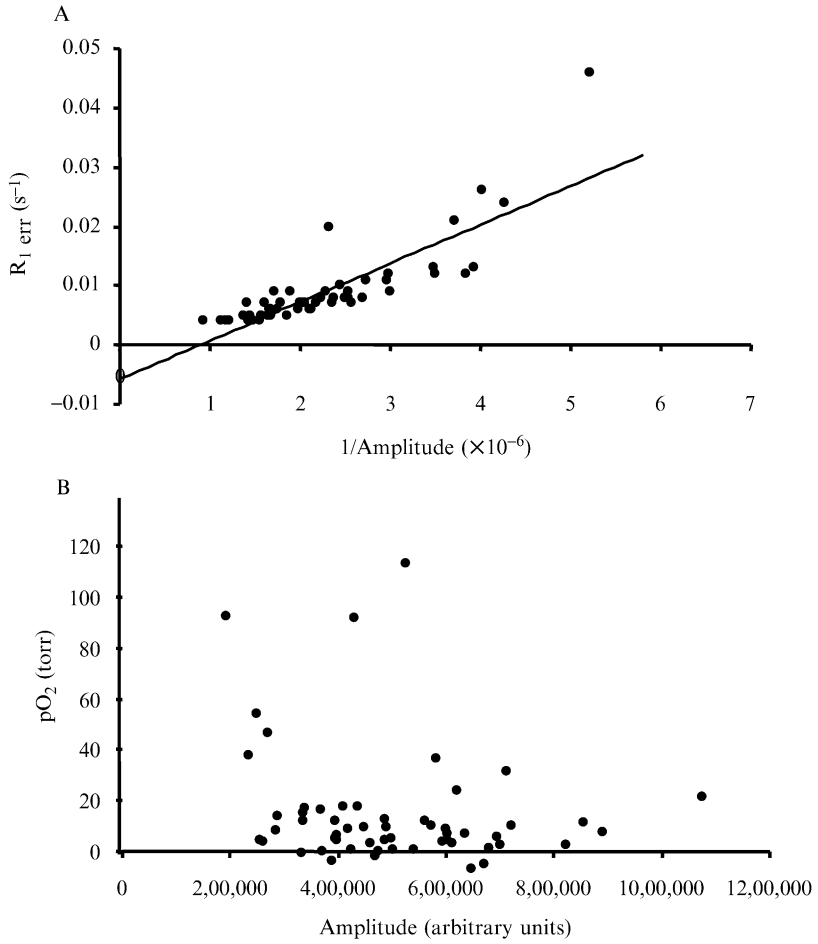

FIG. 9. (A) Relationship of $R_{1\ err}$ with signal amplitude showing strong correlation ($r^2 > 0.69$). (B) Relationship of pO_2 and signal amplitude showing lack of correlation ($r^2 < 0.05$).

FIG. 8. PO_2 maps obtained using the FREDOM approach from the tumor shown in Fig. 3. (A) Under baseline conditions, those voxels ($n = 56$) within the white region provided consistently reliable data during repeated measurements. (B) Baseline map (breathing air: $FO_2 = 21\%$): mean $pO_2 = 7.2 \pm 2.6$ (SE) torr, median $pO_2 = 1.3$ torr (range −7–88 torr). (C) Breathing oxygen ($FO_2 = 100\%$): fourth map obtained 24–32 min after switching from air: mean $pO_2 = 47.2 \pm 10.7$ torr ($p < 0.0001$ compared with baseline), median $pO_2 = 8.3$ torr (range −3–204 torr). (D) Breathing carbogen ($FO_2 = 95\%$): fifth map after switching to carbogen: mean $pO_2 = 43.1 \pm 9.2$ torr ($p < 0.0001$ compared with baseline), median $pO_2 = 5.6$ torr (range −10–216 torr).

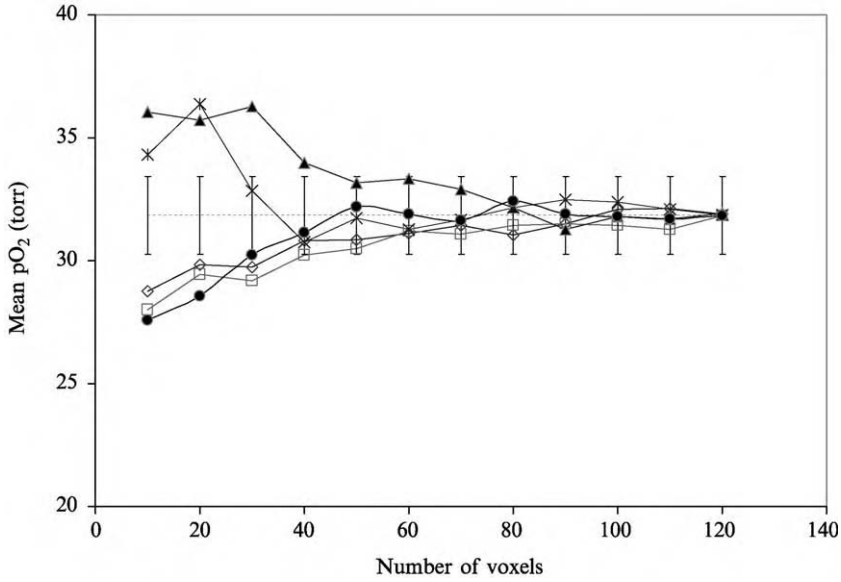

FIG. 10. Monte Carlo simulation of tumor oxygenation. Asymptotic behavior shows that tumor may be characterized by about 50 data points. For this large AT1 tumor in a rat breathing oxygen, all estimates converge on the mean $pO_2 = 31.7 + 1.0$ (SE) torr.

itself may give an apparent relaxation curve (R_1) fit, data are selected within a region of interest, having $T_{1\ err} < 2.5$ s and the ratio $T_{1\ err}/T_1 < 50\%$. With respect to respiratory interventions, only those voxels that provided consistently reliable data throughout the measurements are included for further analysis. At 37° and 4.7 T

$$pO_2(\text{torr}) = [R_1(s^{-1}) - 0.0835]/0.001876 \quad (5)$$

Equation (5) provides pO_2 in units of torr. The literature can be complicated by use of various units, and it may be instructive to provide conversion factors. We favor torr (1 torr = 1 mmHg), since radiobiologic hypoxia develops in the range 0–15 torr and this is the traditional unit favored by radiation biologists and oncologists. Further, 760 torr = 1 standard atmosphere (atm.), and gases are often quoted in %atm. For SI units, 101, 325 Pa (or N/m^2) = 1.01325×10^6 dynes/cm^2 = 1 atm. Some investigators quote oxygen concentrations in μM, often assuming that the solubility of oxygen in water at 37° is 1.35 μM/torr.[29] Quoting concentrations can be confusing because the solubility of oxygen is highly variable in solutions. FREDOM calibration is based on pO_2 values, and as shown by Eqs. 1–3,

these are directly related to the solubility of oxygen in HFB. However, partitioning of oxygen between the aqueous and PFC phases depends on pO_2, not concentrations. Thus the pO_2 determined by FREDOM will accurately reflect the ambient tissue pO_2 and if the solubility of oxygen can be estimated in the particular milieu, then $[O_2]$ could be calculated.

Both systematic and random errors may interfere. Random errors may be diminished by performing multiple repeat measurements (provided that the biologic system is stable). Systematic errors are more complex and could arise *inter alia* from erroneous calibrations, inappropriate curve fitting, and temperature changes. Appropriate curve fitting may be the greatest problem in relaxation analysis. Provided signal/noise > 10 for the most intense signals, we generally obtain excellent curve fits. Each voxel (or ROI) will comprise HFB at a range of pO_2 values, creating a multiexponential curve. However, modeling shows that the fit provides an ''average'' value. For population data, we sometimes determine error-weighted means $[\Sigma(x/\sigma^2)]/[\Sigma(1/\sigma^2)]$ in order to exploit as much available data as possible.

In terms of absolute pO_2 values, the most critical aspect is effective calibration curves. Over the years we have achieved pO_2-dependent ^{19}F NMR relaxation curves for many PFCs[116,141–143,160] and encountered potential pitfalls. The calibration curve we recommend at 4.7 T and 37° is given by Eq. (5) which was originally presented by Hunjan *et al.*[160] Briefly, 125 μl HFB was added to each of four gas-tight NMR tubes together with 0.5 ml water and saturated at 37° by bubbling with carbon dioxide, 1% O_2 (balance N_2), 9.8% O_2 (balance N_2), or air, respectively. Tubes were sealed, and the phantom was maintained at 37° in a water bath within a coil in the magnet. FREDOM was applied using the parameters described earlier, and the spin–lattice relaxation rates were estimated on a voxel-by-voxel basis using three-parameter fit. Equation (5) was established using linear regression analysis of amplitude squared weighted mean values for each gas.[159]

Although the relationship $R_1 = f(pO_2)$ is theoretically expected to be linear and empirically found to be so, we believe that it is important to use calibration gases in the range of physiologic pO_2. We recommend purchase of rigorously calibrated gases. We bubble gases for 30 min and use gas-tight Wilmad NMR tubes, which may be sealed with ground glass joints. Samples are used within hours of saturation. As desired, multiple tubes may be prepared at given pO_2, but since a linear relationship is expected, it may be equally appropriate to use additional gases. T_1 may be determined multiple times for each sample, and we recommend using the pulse sequence to be applied for *in vivo* investigations. In 1997, we published a calibration curve

$$R_1(s^{-1}) = 0.074(\pm 0.003) + 0.012(\pm 0.0002)pO_2(\%atm.) \quad (6)$$

for HFB at 37° and 4.7 T.[177] Considering temperature sensitivity gave

$$R_1(s^{-1}) = 0.77(\pm 0.03) - (0.00009 \pm 0.001)T(°C) + (0.018 \pm 0.003)P(\%atm.) - (0.00017 \pm 0.00008)TP(°C\%\ atm.) \quad (7)$$

More recently, we achieved Eq. (5) as a new calibration curve at 37° and 4.7 T using the ARDVARC approach.[160] This calibration curve is based on higher-quality data and provides superior pO_2 estimates. In particular, when tissue is expected to be hypoxic (excised tissue), we find fewer apparently negative pO_2 values.

A major strength of the FREDOM approach is that calibration curves remain valid between samples and across experimental platforms. Calibration curves obtained *in vitro* are valid *in vivo*. Thus we believe other investigators can apply Eq. (5) without the need to establish their own calibrations, provided that studies are undertaken at about 4.7 T and in the range 30–45°. As discussed in an earlier section and Table II, a 1° error in temperature estimates will only introduce a 0.13-torr error in pO_2 estimate, when pO_2 is about 5 torr. We also note that the calibration curves for HFB are relatively insensitive to magnetic field.[111,143]

We have previously investigated microbiodistribution of HFB based on Oil Red O stain, which indicated that HFB occurs as microscopic droplets (1–20 μm) widely distributed across tumor tissue.[175] Significantly, there was no evidence for formation of films, which could act as conduction conduits, causing oxygen equilibration. Occasionally, an animal (viz. tumor) will move slightly during a long time series of measurements. In this case the requirement of consistently high-quality curve fits throughout the data set for individual voxels fails because the tissues have moved relative to the voxel grid. Such motion is immediately apparent when examining the images. There is a choice of eliminating such a data set or relaxing the acceptance criteria and examining pO_2 population distribution without spatial continuity. It is important to recognize that all methods include a degree of sampling. In some approaches, this involves the selective placement and tracking of electrodes; in others, the choice of locations for biopsy and the number of microscopic fields of view. Sampling can be avoided by obtaining global measurements, as commonly acquired using near-infrared approaches, but this may itself mask the fundamental tumor heterogeneity[101] (see Chapter 17 in this volume).

We have previously shown that HFB shows little macroscopic redistribution over a period of hours.[177] It does clear from the tumors with a

typical half-life of HFB of about 600 min, though some tumors show essentially no detectable clearance over a period of 6 h.[143,162] Clearance of HFB precludes long-term studies of chronic oxygenation, unless further doses of HFB are administered.

Comparison of pO_2 distributions using FREDOM or the Eppendorf Histograph has shown close similarity in both small and large tumors.[175] Dynamic studies in several tumor types have shown equivalent behavior when assessed using polarographic oxygen electrodes or OxyLite or FOXY optical probes.[32,43,134] Relative hypoxia has been compared with the histologic reporter pimonidazole, revealing similar trends across tumor types.[137]

Applications of FREDOM

FREDOM has been applied to investigations of diverse tumor types (syngeneic rat prostate and breast tumors and xenograft human lymphomas) with respect to growth and acute interventions.[27,32,134–137,160] Perhaps the greatest strength is the ability to investigate regional dynamic changes in pO_2 accompanying acute interventions. Figure 8 shows changes in regional pO_2 in an AT1 tumor accompanying hyperoxic gas breathing. As published previously,[137,160,162] the areas that were initially better oxygenated responded with elevated pO_2, whereas those relatively hypoxic regions showed little response. Data also may be presented as histograms (Fig. 11), revealing significant differences between mean and median pO_2 and hypoxic fractions between small and large tumors, and between the slow- and fast-growing sublines H and AT1 of the Dunning prostate R3327. Figure 12 shows variation in global mean pO_2 accompanying respiratory challenge with oxygen or carbogen and return to baseline following the intervention. Because individual tumor regions may be observed, local response may be compared at identical locations, efficiently comparing the efficacy of interventions (Fig. 13). Figure 14 shows the differential behavior of regions in undifferentiated Dunning prostate R3327-AT1 tumors versus highly differentiated H tumors. In each tumor type there are both well and poorly oxygenated regions under baseline conditions (see Fig. 11). In response to hyperoxic gas breathing, well-oxygenated regions in both tumor types show a rapid and significant elevation in pO_2, which is reversible when inhaled gas is returned to air (Fig. 14). Poorly oxygenated regions in H tumors respond slowly, but ultimately rise above the range of radiobiologic hypoxia, whereas corresponding regions in AT1 tumors do not. We also have investigated vasoactive drugs[42] and vascular targeting agents,[27] and the short-term changes in pO_2 following irradiation also have been examined.[184] Perhaps the most significant results to date

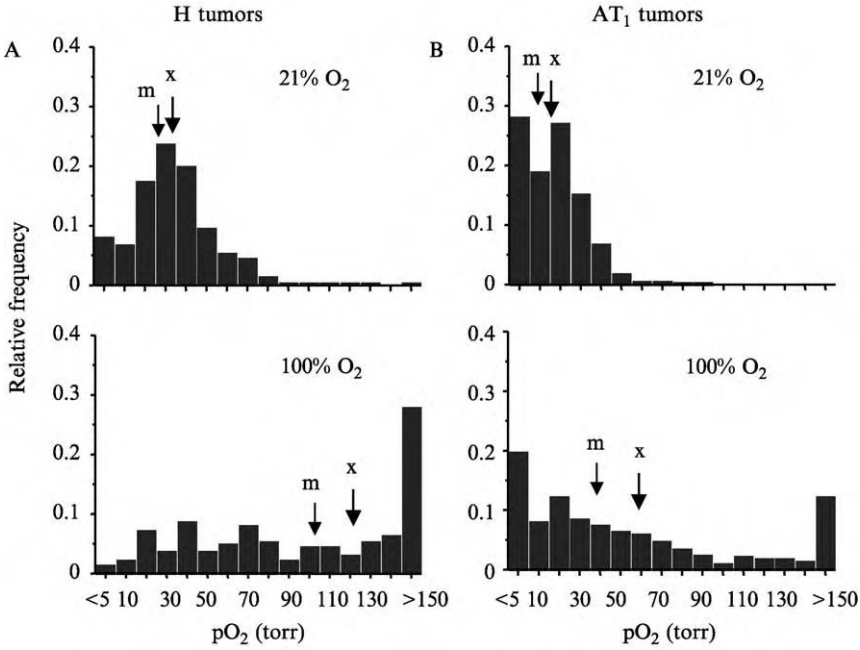

FIG. 11. Histograms of tumor oxygenation pooled for six H (A) and seven AT1 (B) small Dunning prostate R3327 rat tumors. The H tumors (219 voxels) showed significantly higher baseline pO_2 (mean = 31 ± 2 torr, median = 27 torr) than the size-matched AT1 tumors (338 voxels; mean = 14 ± 1 torr, median = 11 torr; $p < 0.0001$). With respect to oxygen challenge *(bottom)*, mean pO_2 in both groups increased significantly (mean = 122 ± 7 in the H versus, mean = 58 ± 4 in the AT1; $p < 0.0001$). Arrows indicate mean (x) and median (m) pO_2, respectively.

show that pO_2 measurements and detection of changes in pO_2 accompanying interventions correlate with the efficacy of tumor irradiation.[136]

Future

Ultimately, the value of a technique depends on its robustness, ease of use, and widespread implementation. To date, few laboratories had adopted the FREDOM approach because efficient investigation of HFB requires an unusual NMR pulse sequence. With the recent upgrade of our own instrumentation to the Varian Unity INOVA, the software is

[184] R. P. Mason, S. Hunjan *et al.*, *Int. J. Radiat. Oncol. Biol. Phys.* **42,** 747 (1998).

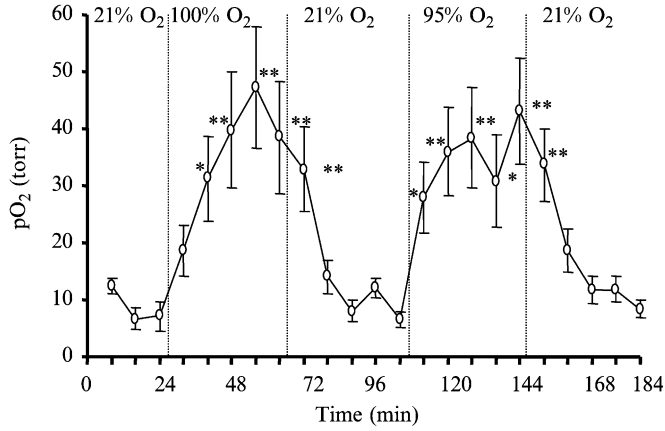

FIG. 12. Dynamic pO_2 (mean ± SE) obtained from sequential maps of the AT1 tumor shown in Fig. 8 with respect to respiratory challenge. *, $p < 0.001$; **, $p < 0.0001$ versus baseline.

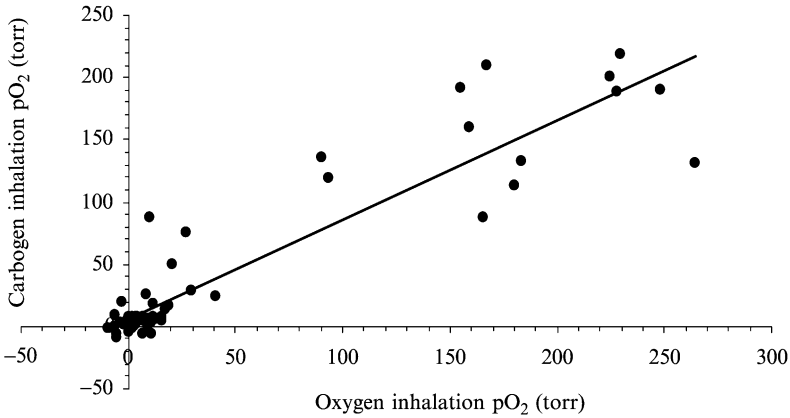

FIG. 13. Correlation between maximum pO_2 detected in each of 56 voxels from the AT1 tumor shown in Fig. 8, when the rat breathed oxygen versus carbogen ($r^2 > 0.85$).

now available on this popular platform, facilitating ready implementation elsewhere. In terms of research applications, it is known that tumor tissue pO_2 varies rapidly in response to many acute interventions, ranging from irradiation to photodynamic therapy, and various chemotherapies. We foresee FREDOM as a valuable tool for assessing the dynamic time course

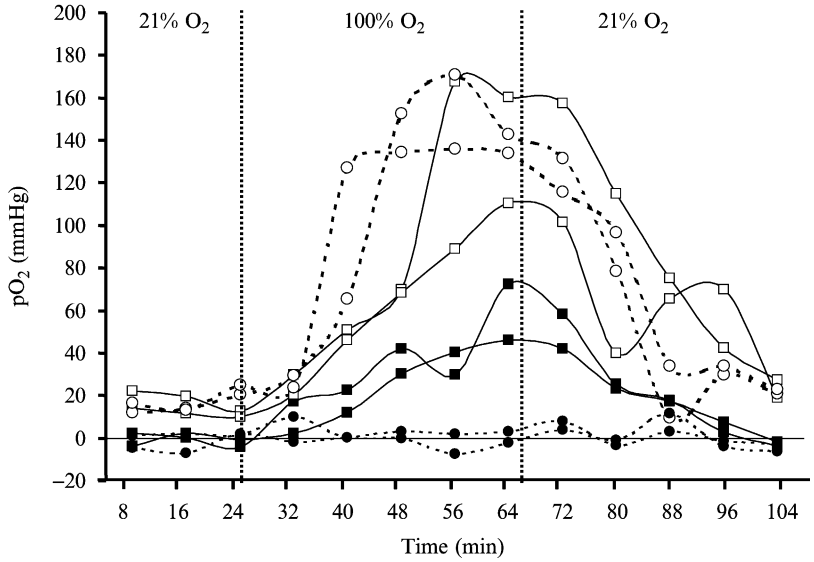

FIG. 14. Variation in pO_2 with respiratory challenge for individual regions chosen as initially well oxygenated ($pO_2 > 10$ torr) or hypoxic ($pO_2 < 5$ torr) from an AT1 (dotted lines) and H (solid lines) tumor, respectively. All the well-oxygenated regions in the two sublines increased significantly in pO_2 in response to oxygen breathing ($p < 0.01$). The hypoxic regions from the H tumor increased, whereas those in the AT1 tumor did not.

of such interventions to provide clear insight into the mode of action of therapeutic approaches and aid in the high-throughput screening of new drugs, such as vascular targeting and antiangiogenic agents.

Acknowledgments

This work was supported in part by NIH R01 CA79515 (NCl)/EB002762 (NIBIB), DOD Breast Cancer Initiative IDEA Award (DAMD 17–03–1–0363) (DZ) and predoctoral scholarship (DAMD 17–02–1–0592) (LJ) in conjunction with Cancer Imaging Program P20 CA 86354 and NIH BRTP Facility P41-RR02584. We are grateful to Dr. Anca Constantinescu for facilitating all the tumor investigations, Ms. Soon-Hee Sul for undertaking the Monte Carlo simulations, and Professor Eric Hahn for mentoring us in tumor biology.

Int. J. Radiation Oncology Biol. Phys., Vol. 62, No. 3, pp. 872–880, 2005

0360-3016/05/$–see front matter

ELSEVIER

doi:10.1016/j.ijrobp.2005.03.009

BIOLOGY CONTRIBUTION

TUMOR PHYSIOLOGIC RESPONSE TO COMBRETASTATIN A4 PHOSPHATE ASSESSED BY MRI

DAWEN ZHAO, M.D., PH.D., LAN JIANG, M.S., ERIC W. HAHN, PH.D., AND RALPH P. MASON, PH.D.

Department of Radiology, University of Texas Southwestern Medical Center, Dallas, TX

Purpose: To evaluate the effect of the vascular targeting agent, combretastatin A4 phosphate, on tumor oxygenation compared with vascular perfusion/permeability.
Methods and Materials: ^{19}F MRI oximetry and dynamic contrast-enhanced (DCE)-MRI were used to monitor tumor oxygenation and perfusion/permeability in syngeneic 13762NF rat breast carcinoma.
Results: A significant drop was found in the mean tumor pO_2 (23 to 9 mm Hg, $p < 0.05$) within 90 min after treatment (30 mg/kg of combretastatin A4 phosphate) and a further decrease was observed at 2 h (mean 2 mm Hg; $p < 0.01$). The initial changes in pO_2 in the central and peripheral regions were parallel, but by 24 h after treatment, a significant difference was apparent: the pO_2 in the periphery had improved significantly, and the center remained hypoxic. These data are consistent with DCE-MRI, which revealed an ~70% decrease in perfusion/permeability (initial area under signal-intensity curve) at 2 h ($p < 0.001$). The initial area under signal-intensity curve recovered fully after 24 h in a thin peripheral region, but not in the tumor center.
Conclusion: The response observed by DCE-MRI, indicating vascular shutdown, paralleled the pO_2 measurements as expected, but quantitative pO_2 measurements are potentially important for optimizing the therapeutic combination of vascular targeting agents with radiotherapy.

MRI, Vascular targeting agent, Vasculature, Oxygenation, Breast tumor.

INTRODUCTION

Tumor growth, survival, and metastasis depend critically on the development of new blood vessels (1). Therefore, extensive research has focused on developing strategies to attack the tumor vasculature (1, 2). Tubulin-binding agents (e.g., combretastatin A4 phosphate [CA4P] and ZD6126) represent one kind of vascular targeting agent (VTA) (3, 4). Promising preclinical studies have shown that such agents selectively cause tumor vascular shutdown and subsequently trigger a cascade of tumor cell death in experimental tumors (4, 5). Although massive necrosis can be induced, tumors usually regrow from a thin viable rim. Thus, a combination of VTAs with additional conventional therapeutic approaches will be required (6, 7). Several studies involving the combination of VTAs with radiotherapy (8–11) or chemotherapeutic agents (12) have shown enhanced tumor response.

To better understand the mode of action, and hence, optimize such combinations, *in vivo* imaging approaches have been initiated to monitor the physiologic changes resulting from VTA administration (13–15). Dynamic contrast-enhanced (DCE)-MRI based on the transport properties of gadolinium-diethylenetriamine pentaacetic acid (Gd-DTPA) is the most commonly used imaging approach to study tumor vascular perfusion and permeability. DCE-MRI was included as part of the Phase I clinical trials of CA4P (16, 17). The results of preclinical and clinical DCE-MRI studies have shown a reversible change in vascular perfusion in the tumor periphery after a single dose of VTA (18–21). For combination with radiotherapy, measurement of tumor oxygen dynamics will be especially important, because reduced perfusion can induce hypoxia, potentially modulating the radiation response. A number of studies have reported an improved response when administering VTAs after radiotherapy, with the enhancement reduced or lost, if VTAs were administered before radiotherapy, implying increased hypoxia induced by VTAs (8, 10). Direct measurements of tissue pO_2 using the Eppendorf electrode, conducted by Horsman *et al.* (22, 23), found increased hypoxia 3 h after CA4P or ZD6126 administration. We have

Reprint requests to: Ralph P. Mason, Ph.D., C.Sci., C.Chem., Department of Radiology, University of Texas Southwestern Medical Center, 5323 Harry Hines Blvd., Dallas, TX 75390-9058. Tel: (214) 648-8926; Fax: (214) 648-2991; E-mail: Ralph.Mason@UTSouthwestern.edu

Supported by DOD Breast Cancer IDEA Award (DAMD 170310363) (D.Z.), in conjunction with NCI RO1 CA79515/EB002762 and the Cancer Imaging Program, a P20 Pre-ICMIC CA86354; MRI experiments were performed at the Mary Nell & Ralph B. Rogers MR Center—an NIH BTRP No. P41-RR02584.
Acknowledgments—We are grateful to Ammar Adam, and Drs. Philip Thorpe and Matthew Merritt for technical and collegial support.

Received Oct 14, 2004, and in revised form Feb 28, 2005. Accepted for publication Mar 7, 2005.

developed a method for measuring tumor oxygenation and dynamics based on ^{19}F nuclear magnetic resonance echo planar imaging after direct intratumoral injection of the reporter molecule hexafluorobenzene (HFB) called "fluorocarbon relaxometry using echo planar imaging for dynamic oxygen mapping" (FREDOM) (24, 25). This technique provides pO_2 measurements at multiple specific locations simultaneously within a tumor and reveals the dynamic changes at individual locations with respect to interventions. We have previously evaluated the tumor oxygen response to varying interventions such as hyperoxic gas breathing (26, 27). We also had an anecdotal example of pO_2 response to a tumor-selective infarcting agent (28). We have now applied both DCE-MRI and FREDOM to evaluate tumor perfusion/permeability and oxygen dynamics in response to CA4P in conjunction with confirmatory histologic examination.

METHODS AND MATERIALS

Tumor model

Rat mammary carcinoma 13762NF was implanted syngeneically in a skin pedicle surgically created on the fore back of Fisher 344 adult female rats (n = 25, ~150 g, Harlan), as previously described in detail (29). Of the 25 rats, 9 were used for DCE-MRI, 10 for FREDOM, and 6 for histologic study. The Institutional Animal Care and Use Committee approved the investigations.

Drug preparation and dosing

CA4P was provided by OXiGENE (Waltham, MA). CA4P was dissolved in 0.9% saline at a concentration of 30 mg/mL before each experiment. A single dose of 30 mg/kg CA4P was chosen for this study, because it is considered a clinically relevant dose (18).

MRI experiments

When tumors reached ~1 cm diameter (~0.6 cm^3), MRI was performed using a 4.7 T horizontal bore magnet with a Varian Unity Inova system. Each rat was given intraperitoneal ketamine hydrochloride (120 μL; 100 mg/mL, Aveco, Fort Dodge, IA) as a relaxant and maintained under general anesthesia (air and 1% isoflurane, Baxter International, Deerfield, IL). A 27-gauge butterfly catheter (Abbott Laboratories, Abbott Park, IL) was placed intraperitoneally for infusion of CA4P or saline alone. For DCE-MRI, a tail vein was catheterized using a second 27-gauge butterfly catheter for contrast agent administration. For oximetry, hexafluorobenzene (50 μL, Lancaster, Gainesville, FL) was injected directly into the tumor along two or three tracks in a single central plane of the tumor, coronal to the rat's body using a Hamilton syringe (Reno, NV) with a custom-made, fine, sharp needle (32-gauge), as previously described in detail (25). A tunable ($^1H/^{19}F$) volume radiofrequency (RF) coil was placed around the tumor-bearing pedicle. Each animal was placed on its side in the magnet with no change in position during the whole study, so that individual regions could be tracked. A thermal blanket was used to maintain body temperature.

^1H DCE-MRI

Nine tumor-bearing rats were studied before CA4P injection (n = 6) or saline alone (n = 3) and 2 and 24 h after treatment. On each occasion, a series of T_1-weighted spin echo images (TR 160 ms, TE 16 ms, field of view 40 × 40 mm, matrix 128 × 128, voxel size 2.0 × 0.3 × 0.3 mm, total time for 3 slices 23 s) was acquired before and after a bolus injection of Gd-DTPA-BMA (injection within 1 s; 0.1 mmol/kg, Omniscan, Amersham Health, Princeton, NJ) on three 2-mm-thick cross-sections parallel to the animal. Data were processed on a voxel-by-voxel basis using software written by us using Interactive Data Language (IDL), version 5.3/5.4 (Research Systems, Boulder, CO). For each slice, the tumor was separated into central and peripheral regions. The tumor periphery was taken to be a 1–2-mm-thick rim aligned around the whole tumor. Signal intensity vs. time curves were plotted and relative signal intensity changes (ΔSI) of each tumor voxel were analyzed using the equation: $(\Delta SI) = (SI_E - SI_b)/SI_b$, where SI_E refers to the enhanced signal intensity in the voxel and SI_b is defined as the average of the baseline images. The area under the normalized signal intensity-time curve (IAUC) for the first 1.5 min after Gd-DTPA-BMA injection was integrated.

^{19}F tumor oximetry—FREDOM

A separate cohort of 10 tumors (7 treated and 3 controls) was used for pO_2 measurement. A single 4-mm slice parallel to the rat body containing the strongest fluorine signal was chosen for the ^{19}F MRI pO_2 studies. ^1H and ^{19}F MR images were acquired using a spin-echo sequence. Overlaying the ^{19}F MR image on the corresponding ^1H image revealed the distribution of HFB. After conventional MRI, tumor oxygenation was estimated on the basis of ^{19}F pulse burst saturation recovery echo planar imaging relaxometry of the HFB, as previously described (24). This approach provided pO_2 maps with 1.25 mm in plane resolution and 6-μL voxel size in 6.5 min. The spin-lattice relaxation rate [R1 (s^{-1}) = 1/T1] was estimated on a voxel-by-voxel basis using a three-parameter monoexponential function. pO_2 was estimated using the relationship pO_2 mm Hg = (R1 − 0.0835)/0.001876 (24). The data are presented in bins of 5 mm Hg, except for the highest and lowest bins, which were open ended. Before CA4P or saline injection, a series of pO_2 maps was acquired with respect to respiratory challenge with oxygen: typically, two baseline measurements, three with oxygen and four on return to air. Immediately after the last (fourth) air measurement, CA4P (30 mg/kg) or saline (0.15 mL) was injected intraperitoneally. An additional series of pO_2 maps was acquired after 10, 30, 60, 90, and 120 min, and finally another three maps while breathing oxygen. The 24 h follow-up study comprised two measurements with air and four with oxygen. The oxygen challenge was included to evaluate vascular function.

Markers of vascular perfusion and endothelium

Six animals were used to study the total blood vessels and perfused vessels before (n = 2), 2 h (n = 2), and 24 h (n = 2) after CA4P. The blue fluorescent dye Hoechst 33342 (Molecular Probes, Eugene, OR) was injected into the tail vein of the anesthetized rats at a concentration of 10 mg/kg in 0.9% saline (0.1 mL), and the tumors were excised 1 min later. Tumor specimens were immediately immersed in liquid nitrogen and then stored at −80°C. Immediately after cryostat sectioning (6 μm thick), the slices were imaged for Hoechst 33342 under ultraviolet wavelength (330–380 nm). Perfused vessels were determined by counting the total number of structures stained by Hoechst 33342 in four fields per section selected to show high perfusion and calculating

the mean number of vessels per millimeter squared. On the following day, the same slices, as well as their adjacent slices, were immunostained for the endothelial marker, CD31. A primary mouse anti-rat CD31 monoclonal antibody (1:20 dilution, Serotec, Raleigh, NC) was added and incubated for 2 h at 37°C in a humid box. The slides were incubated with Cy3-conjugated goat anti-mouse secondary antibody (1:100 dilution, Jackson Immunoresearch Laboratories, West Grove, PA) for 1 h at 37°C. After mounting with Vectorshield medium (Vector Laboratories, Burlingame, CA), the slides were observed under red fluorescence (530–550 nm excitation) to detect anti-CD31 and then the corresponding Hoechst 33342 again under ultraviolet light. Image analysis was performed using Metaview software (Universal Imaging, West Chester, PA).

Statistical analysis

Statistical significance was assessed using analysis of variance on the basis of Fisher's Protected Least Significant Difference (StatView, SAS Institute, Cary, NC) or Student's *t* tests.

RESULTS

DCE-MRI findings

Baseline ^{1}H MRI showed stable signal throughout the tumor (not shown). Immediately after a bolus injection of Gd-DTPA-BMA, the signal intensity increased significantly, reaching a peak after 23–69 s, and then gradually decreasing toward baseline. The maximal signal enhancement averaged over the whole tumor in all three slices ranged from ~52% to 85% for the nine tumors.

A single dose of CA4P 30 mg/kg caused a dramatic decrease in signal enhancement at the 2 h point, and a 24 h follow-up image showed signal recovery in a thin tumor rim, as shown for a representative tumor (Fig. 1). Distribution of the IAUC values showed a distinct shift to the left at both 2 and 24 h after treatment (Fig. 1b). The highly enhancing fraction (IAUC >1.5) at 24 h after CA4P reached the pretreatment level, indicating complete recovery in the tumor periphery (Fig. 1b). For all six tumors treated with

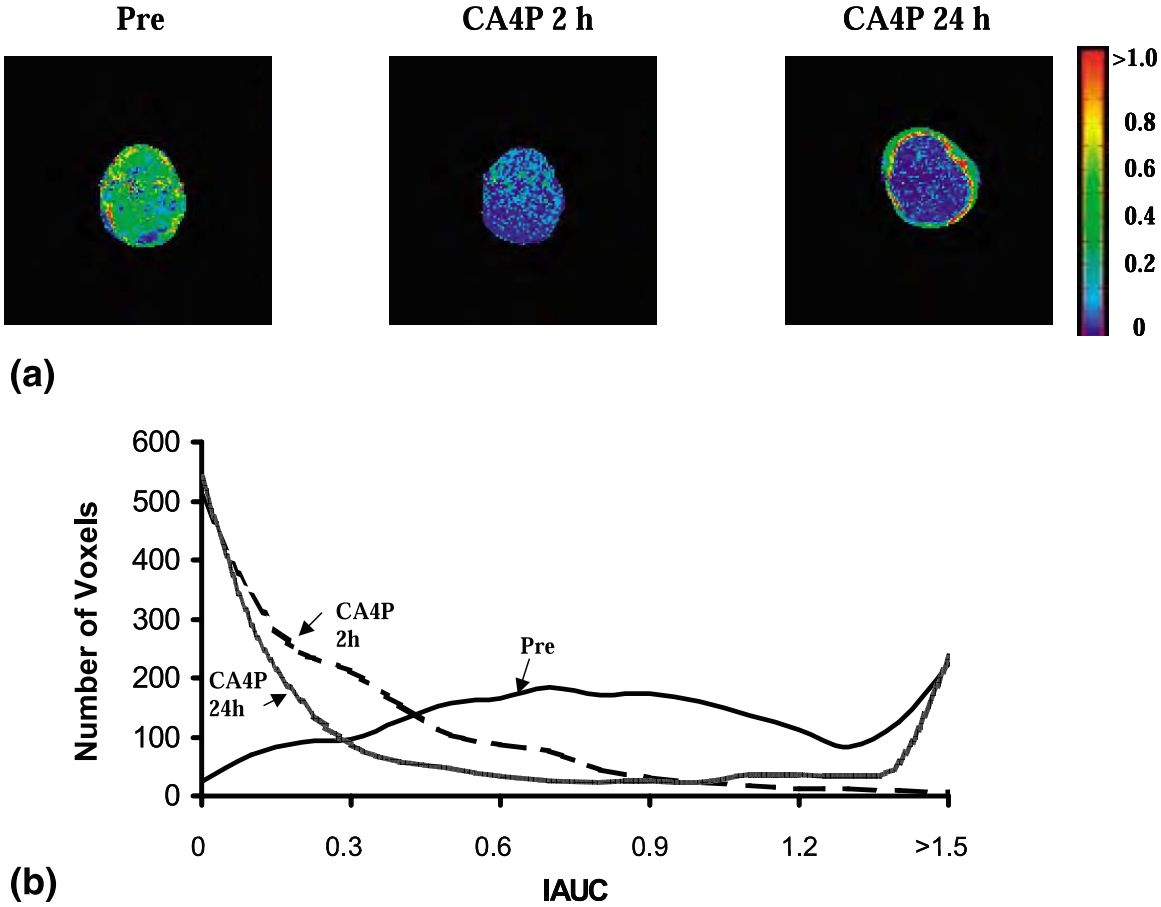

Fig. 1. Dynamic contrast-enhanced-magnetic resonance imaging (DCE-MRI) performed before, 2 h, and 24 h after treatment with CA4P (30 mg/kg). Series of T_1-weighted contrast-enhanced images acquired at these times with respect to infusion of bolus injection of contrast agent. (a) Normalized images of signal enhancement 23 s after contrast agent administration shown for representative tumor. Significantly less signal enhancement was observed for whole tumor region 2 h after treatment. Full recovery is apparent in tumor rim 24 h after treatment. (b) Based on serial images obtained with respect to contrast agent infusion, Initial area under signal-intensity curve (IAUC) was calculated on voxel-by-voxel basis. Frequency distribution of IAUC values is shown. Distributions at 2 and 24 h showed significant increases in number of voxels with no signal enhancement (IAUC <0.05). However, frequency of highly enhancing voxels (IAUC >1.5) at 24 h recovered to pretreatment level.

CA4P, a significant decrease in IAUC was observed for the whole tumor region at 2 h: the tumor peripheral and central region was reduced by 65% and 70%, respectively ($p < 0.05$; Table 1). A complete recovery in IAUC for the tumor periphery was seen 24 h after treatment, but the tumor center remained low (Table 1). IAUC frequency data from these six tumors also showed a significant increase in the number of nonenhancing voxels (IAUC <0.05), and the percentage of voxels with IAUC >0.5 decreased from 55% to 5% 2 h after administration of CA4P ($p < 0.05$, Table 2). In control tumors treated with saline, the IAUC was similar at all points (Tables 1 and 2).

Tumor oximetry—FREDOM

Overlay of ^{19}F on ^{1}H image (Fig. 2a) confirmed that HFB was distributed in both peripheral and central regions of a central plane of the tumor. In the series of echo planar imaging relaxation data sets, typically ~40–100 voxels provided an R1 fit, and potential pO_2 value. Because noise may give an apparent relaxation curve (R1) fit, data were selected by applying thresholds of T1 error <2.5 s and T1 error/T1 ratio <50%. Only those voxels, which provided consistently reliable data throughout the time course, were included for additional analysis. As an example (Fig. 2b), 25 voxels qualified for all these prerequisites and could be followed through the 17 measurements from baseline to 2 h after CA4P. At 24 h, 31 voxels were traceable through the six measurements with respiratory challenge. As expected, on the basis of the distribution of HFB (Fig. 2a), each pO_2 map (Fig. 2b) comprised two distinct groups of voxels, representing the peripheral and central location of HFB, respectively. Variations in the mean pO_2 with respect to intervention for these two groups of voxels are presented separately in Fig. 2c. Before CA4P administration, the mean pO_2 was 45 mm Hg in the tumor periphery and 36 mm Hg in the center during air breathing. Both regions responded significantly to oxygen breathing ($p < 0.05$), and this was reversed on return to air breathing. A significant decrease in pO_2 was detected as early as 30 min after CA4P administration in the tumor periphery and by 60 min in the center ($p < 0.05$). The decline continued with the lowest pO_2 values (13 mm Hg and 10 mm Hg) at the 2-h point. At this time, oxygen challenge no longer produced an increase in pO_2 for either region. At 24 h later, the peripheral pO_2 had increased significantly (24 mm Hg), but was still significantly lower than the pretreatment value ($p < 0.05$). After 24 h, pO_2 again responded significantly to breathing oxygen in the tumor periphery ($p < 0.01$). However, pO_2 in the central regions (4 mm Hg) was even lower at 24 h than at 2 h and did not respond to oxygen breathing. Histograms of pooled voxels assessed for the seven tumors showed significantly decreased pO_2 at 1, 2, and 24 h after treatment ($p < 0.01$). The hypoxic fraction <5 mm Hg (HF_5) increased significantly from a pretreatment value of 21% to 36% at 1 h and 68% at 2 h, but was only 34% at 24 h (Fig. 3). For the seven treated tumors, two tumors showed a significant decrease in pO_2 as early as 30 min after treatment ($p < 0.05$). A significant decrease in the mean pO_2 for the group was found at 90 min after CA4P (23 ± 5 vs. 9 ± 3 mm Hg; $p < 0.05$) and a further decrease at 2 h (2 ± 2 mm Hg; Table 3). The mean pO_2 increased significantly to 15 ± 4 mm Hg at 24 h compared with 2 h ($p < 0.05$). For the control tumors, no significant differences in pO_2 were found among any of the measurements (before and 2 or 24 h after).

Histologic examination and immunohistochemistry

On the basis of the perfusion assessed by distribution of Hoechst 33342, a significant decrease in the number of perfused vessels was evident at 2 h (21 ± 6/mm^2 vs. 145 ± 23/mm^2 pre-CA4P, $p < 0.01$), followed by recovered perfusion at 24 h (114 ± 19/mm^2). Comparisons of perfused vessels marked by Hoechst 33342 and with the total vessels labeled by anti-CD31 before and 2 and 24 h after CA4P are shown in Fig. 4.

DISCUSSION

In common with previous reports in the literature (15, 18), CA4P caused a significant reduction in tumor perfusion within 2 h. DCE-MRI showed that the IAUC in the tumor

Table 1. Normalized IAUC by DCE-MRI

Group	Mean IAUC		
	Baseline	2 h	24 h
CA4P (n = 6) (30 mg/kg)			
Periphery	0.88 ± 0.06	0.31 ± 0.08‡	0.86 ± 0.06
Center	0.44 ± 0.11†	0.13 ± 0.08‡	0.12 ± 0.05*†‡
Control (n = 3) (saline)			
Periphery	1.09 ± 0.04	0.93 ± 0.13	0.86 ± 0.05
Center	0.52 ± 0.19†	0.46 ± 0.05†	0.44 ± 0.03†

Abbreviations: IAUC = initial area under signal-intensity curve; DCE = dynamic contrast enhanced; CA4P = combretastatin A4 phosphate.

* $p < 0.05$ from baseline.

† $p < 0.05$ from periphery.

‡ $p < 0.05$ from control.

Table 2. Comparison of weakly (IAUC <0.05) and strongly (IAUC >0.05) responding voxels with respect to DCE-MRI and drug administration

Group	IAUC	Total voxels (%)		
		Baseline	2 h	24 h
CA4P (n = 6) (30 mg/kg)	<0.05	16	54*†	41*†
	>0.5	55	5*†	32*†
Control (n = 3) (saline)	<0.05	14	15	19
	>0.5	62	58	51

Individual voxels (total = 10,508 in CA4P vs. 5376 in control) categorized according to IAUC.

Abbreviations as in Table 1.

* p <0.01 from baseline.

† p <0.05 from control.

periphery was reduced 70% 2 h after a single dose of CA4P (30 mg/kg), followed by a full recovery by 24 h. However, the drop in the IAUC of the tumor center was not reversible (Table 1). The IAUC reflects tumor blood flow, vascular permeability, and a fraction of interstitial space. Histologic data using the perfusion marker, Hoechst 33342, confirmed a significant decrease in perfused vessels 2 h after CA4P, with recovery evident at 24 h (Fig. 4).

Vascular shutdown induced by VTA is expected to decrease tumor pO_2. Horsman *et al.* (23) recently reported that tumor pO_2, measured by Eppendorf electrode, was significantly decreased 3 h after ZD6126. In line with that study, ^{19}F MRI oximetry showed that CA4P caused a significant decrease in pO_2 within 90 min and a further reduction within 2 h. As for perfusion, pO_2 recovered toward pretreatment levels after 24 h in the tumor periphery (Fig. 2C).

Although VTAs cause vascular shutdown and lead to extensive hemorrhagic tumor necrosis, rapid tumor regrowth occurs from the surviving rim. Many preclinical studies have shown that a single dose of VTA is associated with very little tumor growth delay (4, 5, 23). Thus, a combination with other therapeutic modalities (e.g., radiotherapy and conventional chemotherapy) will be needed to achieve complete control. The rationale for such combinations is that VTAs target the poorly perfused and relatively hypoxic regions of the central tumor, and conventional therapy is applied to attack the relatively better oxygenated, highly proliferating rim. A critical issue regarding such combinations is the timing and sequencing of the agents. Thus, a primary goal of this study was to monitor longitudinal pO_2 changes after CA4P to facilitate and potentially optimize such combinations. Others have demonstrated enhanced therapeutic efficacy by combining CA4P, ZD6126, or 5,6-dimethylxanthenone-4-acetic acid (DMXAA) with radiotherapy (8–11), radioimmunotherapy (30), or chemotherapy (12). In the study of combined ZD6126 with radiotherapy, Siemann and Rojiani (8) reported increased tumor cell kill by administering drug immediately (30 min to 1 h) after a single radiation dose compared with administering the drug 24 h or 1 h before. This observation coincides with our present findings that tumor pO_2 declined 1 h after drug administration and had not recovered fully at 24 h (Figs. 2C and 3).

Oxygen challenge before and after treatment was used to compare vascular function in this study. In common with our previous observations (31, 32), oxygen breathing significantly increased tumor oxygenation in mammary carcinoma 13762NF under control conditions (Fig. 2 and Table 3). The pO_2 response to CA4P was equally effective in the peripheral and central regions through 2 h after administration (Fig. 2C). pO_2 decreased in both regions within 30 min and continued to decrease for 2 h. Differential behavior with respect to oxygen challenge between the peripheral and central tumor regions was observed only after 24 h. At 24 h, pO_2 in the tumor center was even lower than the pretreatment baseline or the 2-h level and showed no response to oxygen inhalation (Fig. 2). However, oxygen breathing produced a significant increase in pO_2 of the peripheral region, even though the pO_2 was significantly lower than before treatment (Fig. 2). These observations provide further evidence that CA4P at 30 mg/kg induces irreversible vascular damage in the tumor center, and peripheral vessels survived and were functional by 24 h. One would expect that hypoxia modifiers (e.g., oxygen breathing), if given 24 h after CA4P, might improve tumor radiosensitivity.

Hypoxia in solid tumors has been widely recognized as a potent factor that leads to resistance to radiotherapy and some anticancer drugs (33). Recently, increasing evidence has shown that tumor malignant progression may be associated with a hypoxic microenvironment (34, 35). Given the importance of oxygen, many techniques for monitoring pO_2 have been developed (25, 36). Although each method has specific attributes, many are highly invasive and impractical for longitudinal studies of specific regions of interest. The Eppendorf has been considered the gold standard for pO_2 measurement, but it is not suitable for a longitudinal study of the type reported here. *In vivo*, proton MRI (e.g., DCE-MRI and blood oxygen level-dependent MRI) provides a noninvasive approach to assess tumor vasculature, particularly useful in response to interventions, but neither DCE nor blood oxygen level-dependent MRI provides a straightforward correlation with pO_2 (37, 38). FREDOM not only provides pO_2 values simultaneously at multiple specific locations within a tumor, but also reveals dynamic changes at individual locations with respect to interventions.

Central necrosis develops in 13762NF tumors even at a small size and becomes substantial when tumors become bigger, which has been confirmed previously by histologic examination (32). In some of the tumors used in this study, a low-intensity central region was observed in T_1-weighted images, in which little enhancement was noted after infusion of the contrast agent. After treatment with CA4P, the area of these regions of low-signal intensity increased slightly (data not shown). A similar observation was reported by Beauregard *et al.* (39) in human colon carcinoma xenograft. In common with our previous study of 13762NF tumors (31, 32), we found considerable intratumoral heterogeneity in the distribution of pO_2 values, ranging from

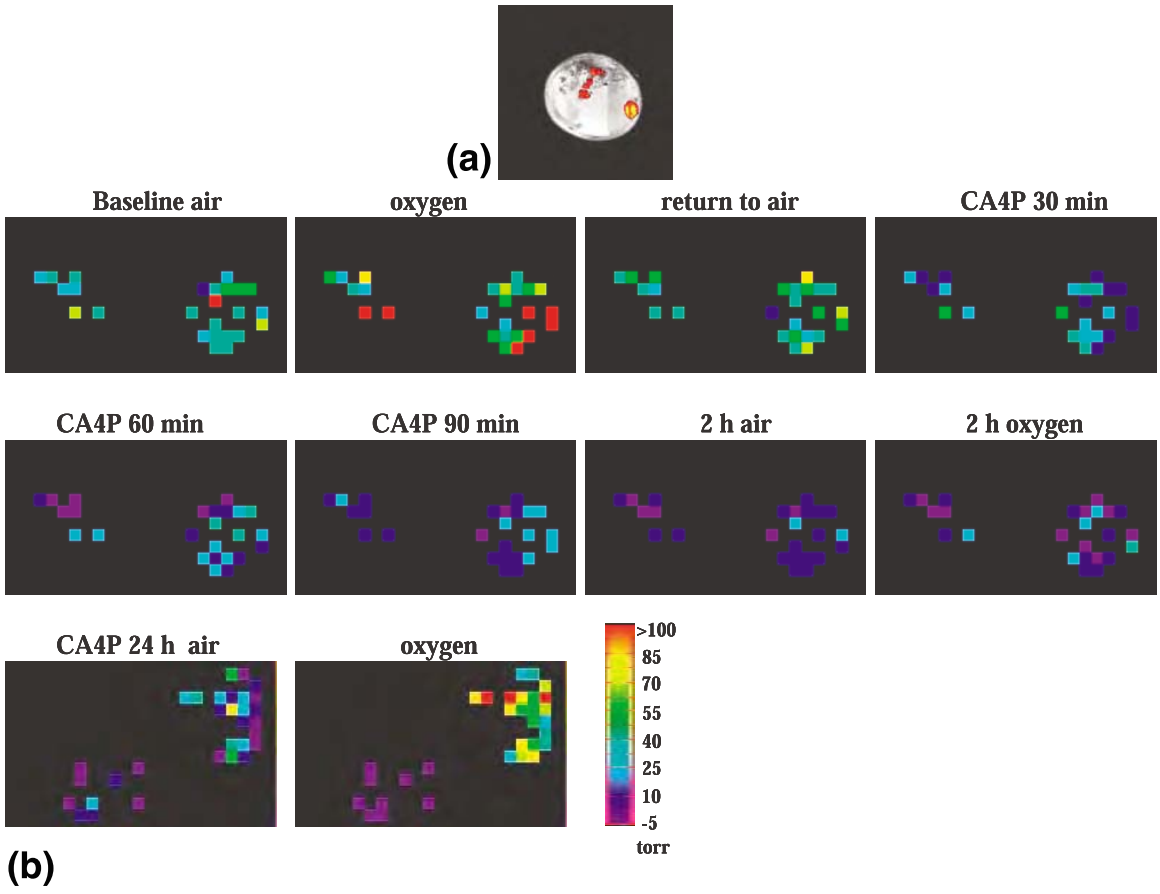

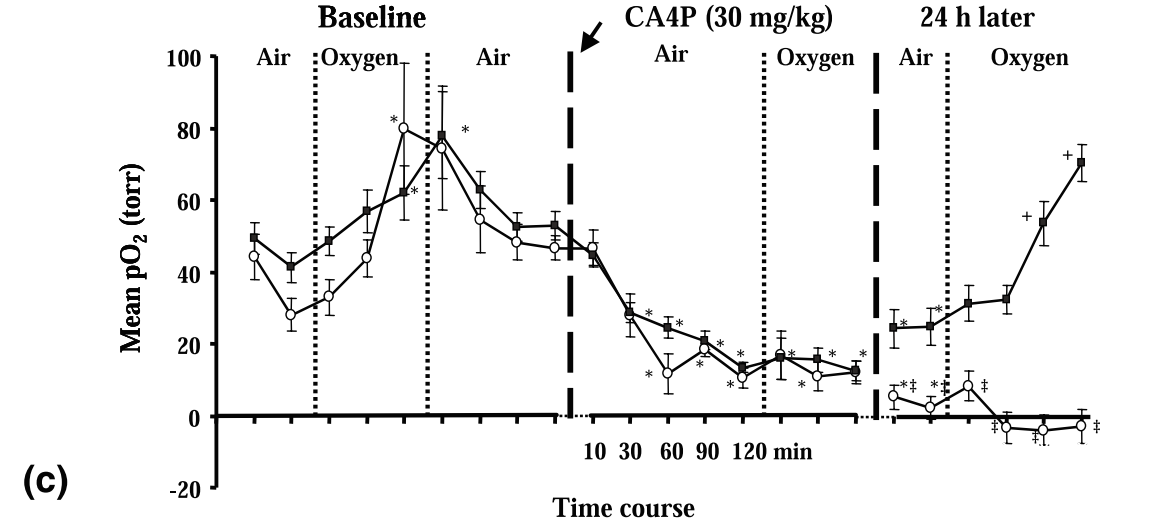

Fig. 2. (a) Distribution of hexafluorobenzene (HFB) in representative tumor (No. 4 in Table 3). Overlay of ^{19}F signal density on anatomic image indicates HFB in both peripheral and central regions. (b) pO_2 maps obtained from same tumor comprise two separated groups of voxels that correspond to locations of HFB on anatomic image; 25 individual voxels were traceable from pretreated baseline to 2 h after CA4P with oxygen breathing; and 31 voxels could be followed 24 h after treatment. Significant decrease in pO_2 was evident for all individual voxels after CA4P. pO_2 did not respond to oxygen inhalation after 2 h; 24-h maps showed improved pO_2 and significant response to oxygen breathing in peripheral region (right), but not in central region (left). (c) Mean pO_2 curves shown for peripheral (black squares) and central (white circles) voxels of tumor. $^{*}p < 0.05$ from baseline air, $^{+}p < 0.05$ from 24-h air, $^{\ddagger}p < 0.05$ from periphery.

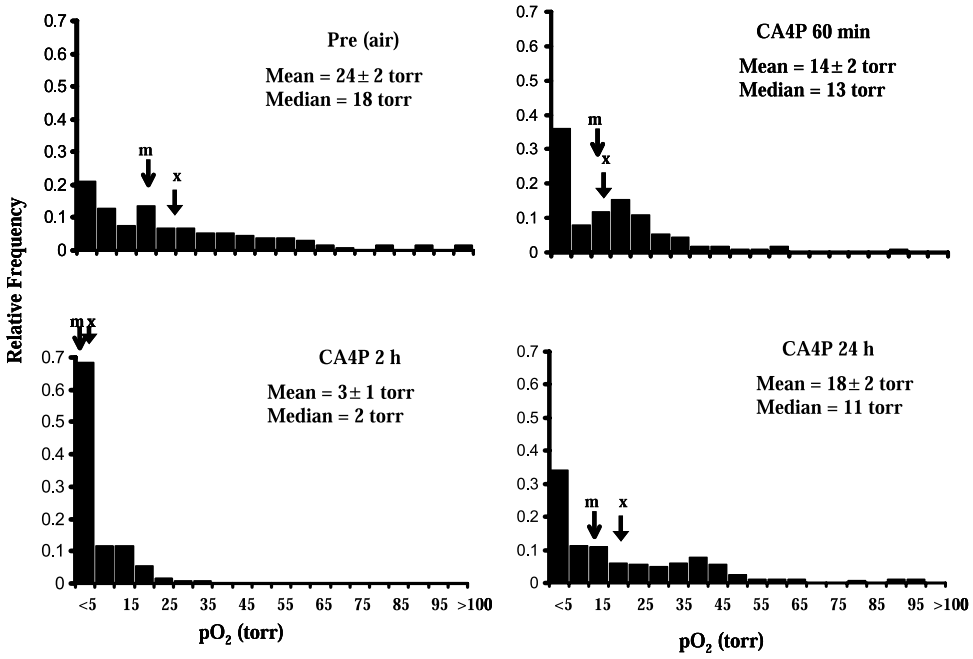

Fig. 3. pO_2 histograms based on relative numbers of voxels in seven tumors showing left shift after CA4P. Ordinate ranges (e.g., 15 refers to 10 mm Hg $\leq pO_2 <$ 15 mm Hg). x = mean; m = median.

hypoxic to well oxygenated. Compared with our previous data on 13762NF tumors, we found the average baseline pO_2 values were lower in the present study (mean 25 mm Hg vs. 63 mm Hg). This difference likely resulted from an altered anesthesia protocol, because we now use a baseline of air/isoflurane, instead of 33% oxygen in nitrous oxide with metafane (32). However, oxygen challenge produced a remarkably similar extent of increase in pO_2 values observed in both studies (72 mm Hg vs. 73 mm Hg).

Previous studies showed little macroscopic redistribution of HFB during a period of hours (40), but it did clear from the tumors with a typical half-life about 600 min (41). The clearance of HFB normally precludes chronic long-term studies of oxygenation, unless additional doses of HFB are administered. For all three control tumors in this study, additional HFB (50 μL) was required for the 24-h follow-up study. However, no additional HFB was required for studies 24 h after CA4P, presumably owing to vascular shutdown.

These results provide the first insight into regional tumor oxygen dynamics in response to CA4P in a syngeneic rat

Table 3. Tumor oxygen dynamics assessed by ^{19}F MRI with respect to CA4P treatment

			pO_2 (mm Hg)							
				Time course post CA4P						
Group	Case No.	Size (cm^3)	Baseline air	30 min	60 min	90 min	2 h	Oxygen	24 h base	Oxygen
CA4P (30 mg/kg)	1	2.0	36 ± 1	NA	NA	NA	2 ± 3*	5 ± 2*	NA	NA
(n = 7)	2	0.9	12 ± 2	NA	NA	NA	−3 ± 2*	−3 ± 2*	NA	NA
	3	1.2	13 ± 0	35 ± 11	11 ± 3	9 ± 4	1 ± 2*	2 ± 2*	5 ± 0*	30 ± 6†
	4	0.7	43 ± 5	29 ± 3*	21 ± 3*	20 ± 2*	13 ± 1*	16 ± 5*	20 ± 2*	48 ± 7†
	5	0.4	12 ± 2	5 ± 3*	9 ± 3	4 ± 2*	2 ± 1*	7 ± 3*	NA	NA
	6	0.7	15 ± 1	19 ± 3	9 ± 2*	4 ± 2*	1 ± 2*	0 ± 3*	12 ± 1	73 ± 12†
	7	0.3	28 ± 6	29 ± 2	16 ± 4	6 ± 2*	1 ± 1*	7 ± 2*	23 ± 2*	79 ± 6†
	Mean	0.9 ± 0.2	23 ± 5	23 ± 13	13 ± 5	9 ± 3*	2 ± 2*	5 ± 3*	15 ± 4	58 ± 11†
Saline (n = 3)	8	0.6	34 ± 2	47 ± 5	40 ± 5	36 ± 10	31 ± 8	88 ± 10*	37 ± 0	86 ± 5†
	9	0.2	47 ± 2	62 ± 8	65 ± 6	64 ± 5	61 ± 4	114 ± 8*	67 ± 1	159 ± 7†
	10	0.6	13 ± 1	16 ± 6	10 ± 4	9 ± 4	12 ± 6	35 ± 10*	14 ± 1	78 ± 15†
	Mean	0.5 ± 0.1	31 ± 10	42 ± 14	38 ± 16	36 ± 16	35 ± 14	79 ± 23*	39 ± 15	108 ± 26†

Abbreviations: NA = no measurement; other abbreviations as in Table 1.
Data presented as mean ± SE.
* $p < 0.05$ from baseline.
† $p < 0.05$ from 24 h air (24 h after injection of CA4P).

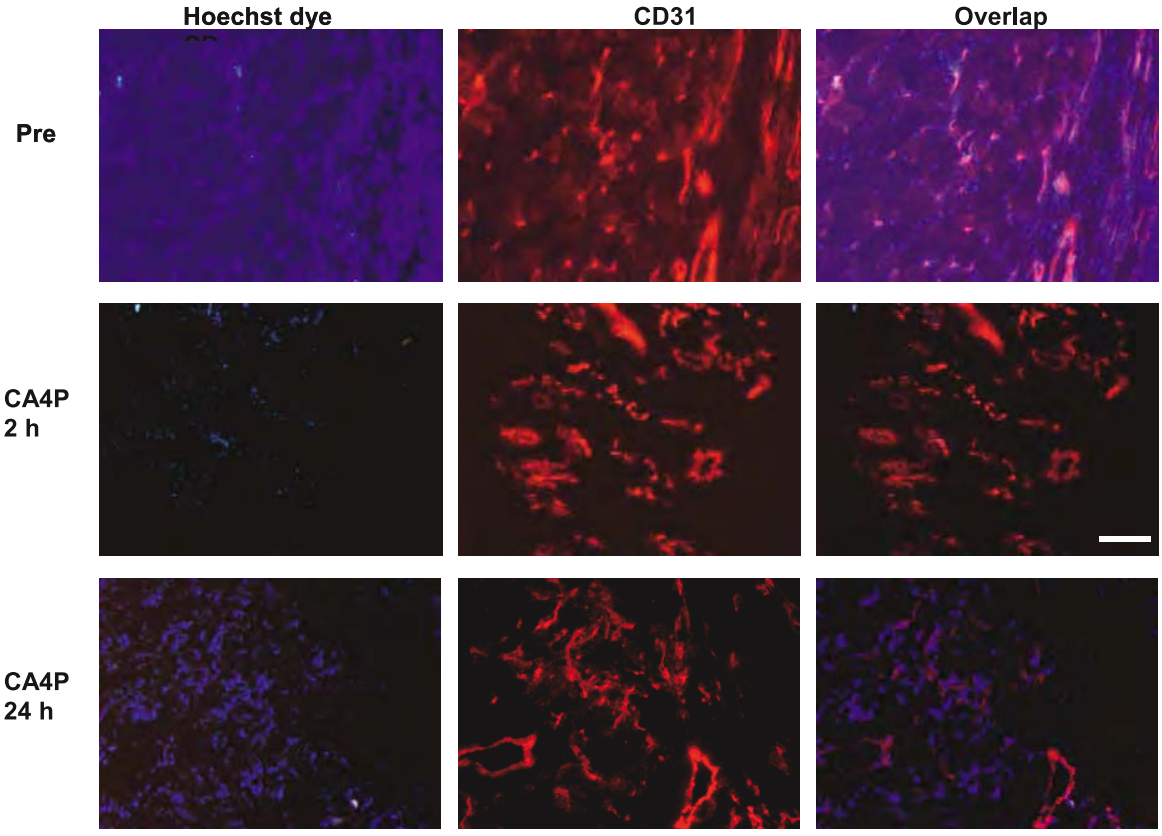

Fig. 4. Perfusion marker Hoechst staining before, 2 h, and 24 h after CA4P (left). Vascular endothelium of same field immunostained by anti-CD31 (red, middle). Good match (right) between Hoechst and anti-CD31–stained vascular endothelium found in pretreated tumor. Significant reduction in perfused vessels detected 2 h after treatment followed by a recovery at 24 h. Bar = 100 μm.

tumor. A distinct similarity was noted between the results of the pO_2 measurements and the more traditional DCE, but the quantitative pO_2 values provide the potential for exploiting synergy with other oxygen-dependent therapies. The observations also demonstrate the value of FREDOM in assessing dynamic changes in regional tumor pO_2 *in vivo* in response to intervention. We believe that dynamic measurements are particularly valuable for understanding the mode of action of therapeutic response to VTAs. Most significantly, these measurements lay a foundation to optimize the timing of combination therapy involving fractionated radiotherapy and multiple doses of VTAs.

REFERENCES

1. Folkman J. Anti-angiogenesis: New concept for therapy of solid tumors. *Ann Surg* 1972;175:409–416.
2. Denekamp J. Vascular attack as a therapeutic strategy for cancer. *Cancer Metastasis Rev* 1990;9:267–282.
3. Pettit GR, Temple C Jr, Narayanan VL, *et al.* Antineoplastic agents 322. synthesis of combretastatin A-4 prodrugs. *Anticancer Drug Des* 1995;10:299–309.
4. Davis PD, Dougherty GJ, Blakey DC, *et al.* ZD6126: A novel vascular-targeting agent that causes selective destruction of tumor vasculature. *Cancer Res* 2002;62:7247–7253.
5. Dark GG, Hill SA, Prise VE, *et al.* Combretastatin A-4, an agent that displays potent and selective toxicity toward tumor vasculature. *Cancer Res* 1997;57:1829–1834.
6. Siemann DW, Warrington KH, Horsman MR. Targeting tumor blood vessels: An adjuvant strategy for radiation therapy. *Radiother Oncol* 2000;57:5–12.
7. Thorpe PE, Chaplin DJ, Blakey DC. The first international conference on vascular targeting: Meeting overview. *Cancer Res* 2003;63:1144–1147.
8. Siemann DW, Rojiani AM. Enhancement of radiation therapy by the novel vascular targeting agent ZD6126. *Int J Radiat Oncol Biol Phys* 2002;53:164–171.
9. Murata R, Siemann DW, Overgaard J, *et al.* Interaction between combretastatin A-4 disodium phosphate and radiation in murine tumors. *Radiother Oncol* 2001;60:155–161.
10. Murata R, Siemann DW, Overgaard J, *et al.* Improved tumor response by combining radiation and the vascular-damaging drug 5,6-dimethylxanthenone-4-acetic acid. *Radiat Res* 2001; 156:503–509.
11. Li L, Rojiani AM, Siemann DW. Preclinical evaluations of therapies combining the vascular targeting agent combretastatin A-4 disodium phosphate and conventional anticancer therapies in the treatment of Kaposi's sarcoma. *Acta Oncol* 2002; 41:91–97.
12. Siemann DW, Rojiani AM. Antitumor efficacy of conventional anticancer drugs is enhanced by the vascular targeting agent ZD6126. *Int J Radiat Oncol Biol Phys* 2002;54:1512–1517.

13. Tozer GM, Prise VE, Wilson J, *et al.* Combretastatin A-4 phosphate as a tumor vascular-targeting agent: Early effects in tumors and normal tissues. *Cancer Res* 1999;59:1626–1634.
14. Kragh M, Quistorff B, Horsman MR, *et al.* Acute effects of vascular modifying agents in solid tumors assessed by noninvasive laser Doppler flowmetry and near infrared spectroscopy. *Neoplasia* 2002;4:263–267.
15. Goertz DE, Yu JL, Kerbel RS, *et al.* High-frequency Doppler ultrasound monitors the effects of antivascular therapy on tumor blood flow. *Cancer Res* 2002;62:6371–6375.
16. Rustin GJ, Galbraith SM, Anderson H, *et al.* Phase I clinical trial of weekly combretastatin A4 phosphate: Clinical and pharmacokinetic results. *J Clin Oncol* 2003;21:2815–2822.
17. Galbraith SM, Maxwell RJ, Lodge MA, *et al.* Combretastatin A4 phosphate has tumor antivascular activity in rat and man as demonstrated by dynamic magnetic resonance imaging. *J Clin Oncol* 2003;21:2831–2842.
18. Prise VE, Honess DJ, Stratford MR, *et al.* The vascular response of tumor and normal tissues in the rat to the vascular targeting agent, combretastatin A-4-phosphate, at clinically relevant doses. *Int J Oncol* 2002;21:717–726.
19. Robinson SP, McIntyre DJ, Checkley D, *et al.* Tumour dose response to the antivascular agent ZD6126 assessed by magnetic resonance imaging. *Br J Cancer* 2003;88:1592–1597.
20. McIntyre DJ, Robinson SP, Howe FA, *et al.* Single dose of the antivascular agent, ZD6126 (*N*-acetylcolchinol-O-phosphate), reduces perfusion for at least 96 hours in the GH3 prolactinoma rat tumor model. *Neoplasia* 2004;6:150–157.
21. Padhani AR. MRI for assessing antivascular cancer treatments. Br J Radiol 2003;76(Spec No 1):S60–S80.
22. Horsman MR, Ehrnrooth E, Ladekarl M, *et al.* The effect of combretastatin A-4 disodium phosphate in a C3H mouse mammary carcinoma and a variety of murine spontaneous tumors. *Int J Radiat Oncol Biol Phys* 1998;42:895–898.
23. Horsman MR, Murata R. Vascular targeting effects of ZD6126 in a C3H mouse mammary carcinoma and the enhancement of radiation response. *Int J Radiat Oncol Biol Phys* 2003;57:1047–1055.
24. Hunjan S, Zhao D, Constantinescu A, *et al.* Tumor oximetry: Demonstration of an enhanced dynamic mapping procedure using fluorine-19 echo planar magnetic resonance imaging in the Dunning prostate R3327-AT1 rat tumor. *Int J Radiat Oncol Biol Phys* 2001;49:1097–1108.
25. Zhao D, Jiang L, Mason RP. Measuring changes in tumor oxygenation. *Methods Enzymol* 2004;386:378–418.
26. Zhao D, Constantinescu A, Hahn EW, *et al.* Differential oxygen dynamics in two diverse Dunning prostate R3327 rat tumor sublines (MAT-Lu and HI) with respect to growth and respiratory challenge. *Int J Radiat Oncol Biol Phys* 2002; 53:744–756.
27. Zhao D, Constantinescu A, Hahn EW, *et al.* Tumor oxygen dynamics with respect to growth and respiratory challenge: Investigation of the Dunning prostate R3327-HI tumor. *Radiat Res* 2001;156:510–520.
28. Mason RP, Ran S, Thorpe PE. Quantitative assessment of tumor oxygen dynamics: Molecular imaging for prognostic radiology. *J Cell Biochem* 2002;87:45–53.
29. Hahn EW, Peschke P, Mason RP, *et al.* Isolated tumor growth in a surgically formed skin pedicle in the rat: A new tumor model for NMR studies. *Magn Reson Imaging* 1993;11:1007–1017.
30. Pedley RB, Hill SA, Boxer GM, *et al.* Eradication of colorectal xenografts by combined radioimmunotherapy and combretastatin a-4 3-O-phosphate. *Cancer Res* 2001;61:4716–4722.
31. Song Y, Worden KL, Jiang X, *et al.* Tumor oxygen dynamics: Comparison of ^{19}F MR EPI and frequency domain NIR spectroscopy. *Adv Exp Med Biol* 2003;530:225–236.
32. Song Y, Constantinescu A, Mason RP. Dynamic breast tumor oximetry: The development of prognostic radiology. *Technol Cancer Res Treat* 2002;1:1–8.
33. Brown JM. The hypoxic cell: A target for selective cancer therapy—Eighteenth Bruce F. Cain memorial award lecture. *Cancer Res* 1999;59:5863–5870.
34. Höckel M, Schlenger K, Aral B, *et al.* Association between tumor hypoxia and malignant progression in advanced cancer of the uterine cervix. *Cancer Res* 1996;56:4509–4515.
35. Brizel DM, Scully SP, Harrelson JM, *et al.* Tumor oxygenation predicts for the likelihood of distant metastases in human soft tissue sarcoma. *Cancer Res* 1996;56:941–943.
36. Höckel M, Vaupel P. Tumor hypoxia: Definitions and current clinical, biologic, and molecular aspects. *J Natl Cancer Inst* 2001;93:266–276.
37. Baudelet C, Gallez B. How does blood oxygen level-dependent (BOLD) contrast correlate with oxygen partial pressure (pO_2) inside tumors? *Magn Reson Med* 2002;48:980–986.
38. Zhao D, Jiang L, Constantinescu A, *et al.* Evaluation of breast tumor microcirculation and oxygenation using a combination of BOLD, DCE and ^{19}F MRI [Abstract]. *Proc Int Soc Magn Reson Med* 2004;1:222.
39. Beauregard DA, Pedley RB, Hill SA, *et al.* Differential sensitivity of two adenocarcinoma xenografts to the anti-vascular drugs combretastatin A4 phosphate and 5,6-dimethylxanthenone-4-acetic acid, assessed using MRI and MRS. *NMR Biomed* 2002;15:99–105.
40. Le D, Mason RP, Hunjan S, *et al.* Regional tumor oxygen dynamics: ^{19}F PBSR EPI of hexafluorobenzene. *Magn Reson Imaging* 1997;15:971–981.
41. Mason RP, Rodbumrung W, Antich PP. Hexafluorobenzene: A sensitive ^{19}F NMR indicator of tumor oxygenation. *NMR Biomed* 1996;9:125–134.

Antivascular effects of combretastatin A4 phosphate in breast cancer xenograft assessed using dynamic bioluminescence imaging and confirmed by MRI

Dawen Zhao, Edmond Richer, Peter P. Antich, and Ralph P. Mason[1]

Department of Radiology and Simmons Cancer Center, University of Texas Southwestern Medical Center, Dallas, Texas, USA

ABSTRACT **Bioluminescence imaging (BLI) has found significant use in evaluating long-term cancer therapy in small animals. We have now tested the feasibility of using BLI to assess acute effects of the vascular disrupting agent combretastatin A4 phosphate (CA4P) on luciferase-expressing MDA-MB-231 human breast tumor cells growing as xenografts in mice. Following administration of luciferin substrate, there is a rapid increase in light emission reaching a maximum after about 6 min, which gradually decreases over the following 20 min. The kinetics of light emission are highly reproducible; however, following i.p. administration of CA4P (120 mg/kg), the detected light emission was decreased between 50 and 90%, and time to maximum was significantly delayed. Twenty-four hours later, there was some recovery of light emission following further administration of luciferin substrate. Comparison with dynamic contrast-enhanced MRI based on the paramagnetic contrast agent Omniscan showed comparable changes in the tumors consistent with the previous literature. Histology also confirmed shutdown of tumor vascular perfusion. We believe this finding provides an important novel application for BLI that could have widespread application in screening novel therapeutics expected to cause acute vascular changes in tumors.—Zhao, D., Richer, E., Antich, P. P., Mason, R. P. Antivascular effects of combretastatin A4 phosphate in breast cancer xenograft assessed using dynamic bioluminescence imaging and confirmed by MRI. *FASEB J.* 22, 2445–2451 (2008)**

Key Words: breast tumor · vascular targeting agent · vascular disrupting agent · pharmacodynamics

Bioluminescence imaging (BLI) has found a major role in small animal research (1–3). For tumor cells transfected to constitutively express luciferase, there are numerous reports examining tumor growth and metastatic spread (4, 5). BLI has also found widespread use in examining changes in tumor growth over a period of many weeks with diverse therapies (6–10). BLI requires administration of luciferin substrate, which may be achieved by multiple routes, including intravenous (i.v.), intraperitoneal (i.p.), or subcutaneous (s.c.) (11, 12). Luciferin is then carried throughout the vasculature and has been shown to readily permeate every region of the body (9, 13, 14). Given the importance of vascular transport, it occurred to us that the measurement of the light-emitting dynamics would be related to vascular delivery of the substrate. Thus, any agent causing major acute affects on tumor vasculature could influence the light emission kinetics. In particular, it appeared that vascular targeting agents (VTAs; also referred to as vascular disrupting agents), such as combretastatin, could be assessed based on the dynamics of light emission detected by BLI.

Tumor growth, survival, and metastasis depend critically on the development of new blood vessels (15). Therefore, extensive research has focused on developing strategies to attack tumor vasculature (16–19). Tubulin-binding agents (*e.g.*, combretastatin A-4-phosphate (CA4P) and ZD6126) represent one kind of VTA (17). Promising preclinical studies have shown that such agents selectively cause tumor vascular shutdown and subsequently trigger a cascade of tumor cell death in experimental tumors (20). Although massive necrosis can be induced, tumors usually regrow from a thin viable rim. To better understand the mode of action and, hence, facilitate optimized therapeutic combinations, *in vivo* imaging approaches have been applied to monitor physiological changes resulting from VTA administration (21–23). Dynamic contrast-enhanced (DCE) MRI based on the transport properties of the small paramagnetic contrast agent gadolinium-DTPA (Gd-DTPA) is the most commonly used imaging approach to study tumor vascular perfusion and permeability. DCE MRI was included as part of the Phase I clinical trials of CA4P (24, 25). Results of preclinical and clinical DCE MRI studies have shown a reversible change in vascular perfusion in the tumor periphery following a single dose of VTA (26–29).

The VTA CA4P causes tumor vascular shutdown, inducing massive cell death. We recently showed acute hypoxiation within 90 min following CA4P administra-

[1] Correspondence: Department of Radiology, University of Texas Southwestern Medical Center, 5523 Harry Hines, Dallas, TX 75390-9058, USA. E-mail: ralph.mason@utsouthwestern.edu

doi: 10.1096/fj.07-103713

tion to rats bearing syngeneic breast 13762NF tumors using MRI (30). Rapid vascular shutdown in tumors after administration of CA4P to animals and patients has also been observed by many other imaging modalities, including positron emission tomography based on the distribution of ^{15}O water (31), DCE MRI (24, 32, 33), DCE computed tomography (CT) (34), ^{19}F MRI of tumor oxygenation (30), laser Doppler flowmetry (35), radiolabeled iodoantipyrine uptake (27), near infrared spectroscopy (36), interstitial fluid pressure (35), and intravital microscopy (37). By comparison, BLI is particularly inexpensive and easy to apply in animal models, and we believe it could be an effective screening tool for evaluation and comparison of vascular targeting agents as well as long-term tumor growth. BLI is exceedingly sensitive with the capability of detecting subpalpable tumor volumes.

We have now explored the ability of planar BLI, a widely available modality, to investigate the acute effects of CA4P on human breast MDA-MB-231 xenograft tumors and provide correlates with the more traditional MRI approach and histology.

MATERIALS AND METHODS

Tumor model

Human mammary MDA-MB-231 cells were infected with a lentivirus containing a firefly luciferase reporter, and highly expressing stable clones were isolated. Tumors were induced by injecting 10^6 cells subcutaneously in the flank of 13 athymic nude mice (BALB/c nu/nu; Harlan, Indianapolis, IN, USA). Tumors were allowed to grow to ~6 mm diameter (~100 mm^3) and then selected for BLI or MRI.

In vivo BLI

Tumor-bearing mice were anesthetized (isoflurane/O_2 in an induction chamber; isoflurane from Baxter International Inc., Deerfield, IL, USA) and a solution of D-luciferin (450 mg/kg in PBS in a total volume of 250 μl; Biosynthesis, Naperville, IL, USA) was administered s.c. in the neck region. Anesthesia was maintained with isoflurane (1%) in oxygen (1 dm^3/min) and a series of light images (60 s each) was acquired using a single reference camera of our multicamera Light Emission Tomography System over a period of 20–30 min and the light intensity-time curves evaluated.

The imaging system uses CCD (charge-coupled device) cameras selected for their high and nearly constant sensitivity over the full range of wavelengths commonly used in optical imaging, from blue to near infrared. The CCD is a noncolor, back-illuminated, full-frame image sensor with 512 × 512 pixels [(SITe) SI-032AB CCD; Scientific Imaging Technologies Inc., Tigard, OR, USA]. The quantum efficiency of the CCD is greater than 85% from 400–750 nm, and remains above 50% up to 900 nm. The CCD has a pixel size of 24 × 24 μm, providing a large well capacity of 350,000 e^-, with a sensitivity of 2.6 μV/e^-, low dark current (20 pA/cm^2 at 20°C), and low readout noise (5 e^- RMS), providing a dynamic range of 75,000. The CCD is cooled to −40°C, reducing the dark current signal to less than 0.1 e^-/pixel/s. The large dynamic range of the detector is coupled with a 16 bit analog to digital converter, allowing quantitative detection of both high and very low signals simultaneously. The CCD is incorporated in a self-contained, cooled camera equipped with electronic circuitry and fast optics (25 mm focal length, f/0.95). Each camera is calibrated using a low-intensity, diffuse, flat-field source that gives a known radiance (adjusted typically at 3.0×10^{-7} W/cm^2/sr). The light source is periodically checked for uniformity using a NIST-traceable research radiometer (model IL 1700; International Light, Inc. Newburyport, MA, USA). By imaging this source, the digital units provided by the camera digitizer can be converted directly into absolute physical units (W/cm^2/sr or photons/s/cm^2/sr).

Saline control or combretastatin A4P (CA4P; 120 mg/kg; OXiGENE, Inc. Waltham, MA, USA) in saline (120 μl) was injected i.p. immediately after baseline BLI and the mouse allowed to wake up. Two hours later, the BLI time course was repeated based on new injections of luciferin. In some cases, mice were examined again 24 h after CA4P administration.

In vivo MRI

A second cohort of nude mice (n=3) with size-matched tumors was studied by MRI using a 4.7 T horizontal bore magnet with a Varian INOVA Unity system (Palo Alto, CA, USA). Each mouse was maintained under general anesthesia (air and 1% isoflurane). A 27 G butterfly (Abbott Laboratories, Abbott Park, IL, USA) was placed in a tail vein for contrast agent administration. Pertinent image slice positions were based on fast scout images. T1-weighted (TR=200 ms; TE=15 ms; slice thickness=1.5 mm; FOV=50×50; in plane resolution 390 μm) and corresponding T2-weighted (TR=1500 ms; TE=80 ms) spin-echo multislice axial images were acquired. For DCE MRI, a series of 3 contiguous T1-weighted images (TR=70 ms; TE=12 ms; total acquisition time 10 s with same voxel dimensions as above) was acquired before and after i.v. bolus injection of the contrast agent Gd-DTPA-BMA (0.1 mmol/kg body weight; Omniscan™, Amersham Health Inc., Princeton, NJ, USA) through a tail vein catheter. DCE MRI was performed before and 2 h after CA4P infusion (120 mg/kg, i.p.).

Data were processed on a voxel-by-voxel basis using software written by us using IDL 5.3/5.4 (Research Systems, Boulder, CO, USA). For each slice, the tumor was separated into regions of center and periphery, respectively. The tumor periphery was taken to be a 1–2 mm thick rim aligned around the whole tumor. Signal intensity *vs.* time curves were plotted and relative signal intensity changes (ΔSI) of each tumor voxel were analyzed using the equation $\Delta SI = (SI_E - SI_b)/SI_b$, where SI_E is enhanced signal intensity in the voxel, and SI_b is the average of the baseline images. The area under the normalized signal intensity-time curve (IAUC) was integrated for the first 60 s after Gd-DTPA-BMA injection.

Immunohistochemistry

Two hours after saline or CA4P injection, the blue fluorescent dye Hoechst 33342 (10 mg/kg, Molecular Probes, Eugene, OR, USA) was injected into the tail vein of anesthetized mice, and the tumors were excised 1 min later. Tumor specimens were immediately immersed in liquid nitrogen and then stored at −80°C. A series of 6 μm frozen sections from several regions of each tumor was immunostained for luciferase (Serotec Inc., Raleigh, NC, USA). Slices were imaged for Hoechst 33342 under ultraviolet (UV) wavelengths (330–380 nm). Perfused vessels were determined by counting the total number of structures stained by Hoechst 33342 in 4 fields per section selected to show high perfusion and calculating the mean number of vessels per square millimeter. On the following day, the same slices, as well as the adjacent ones,

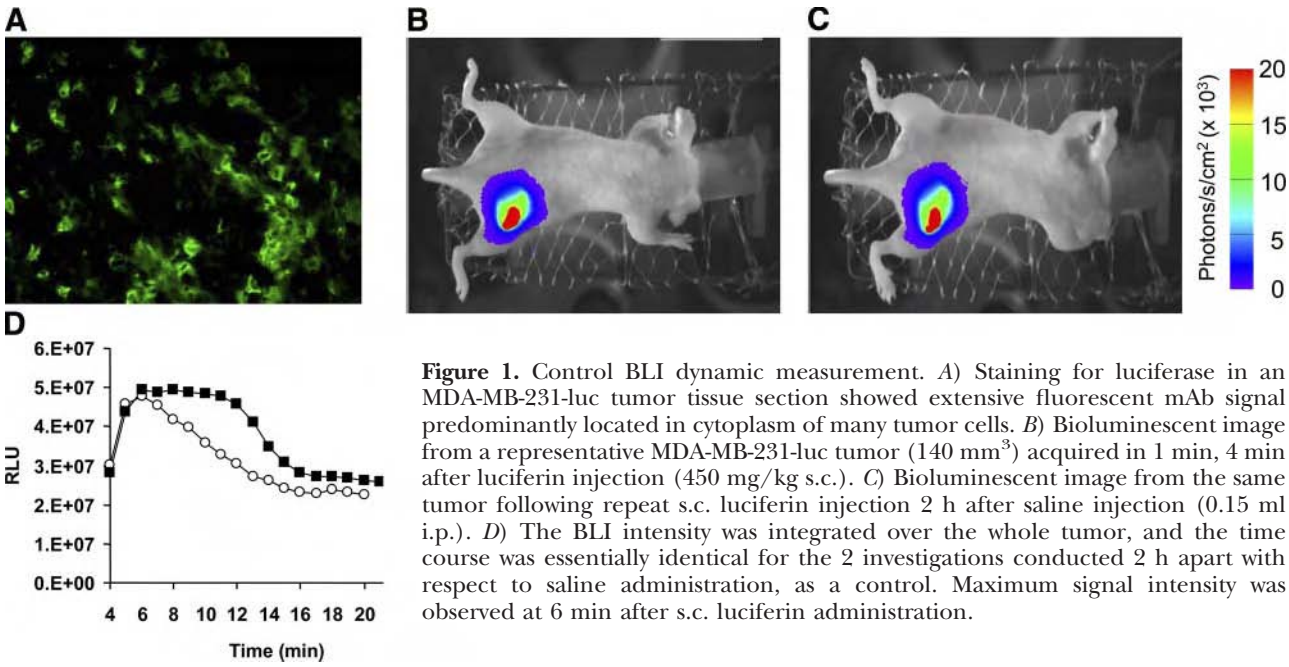

Figure 1. Control BLI dynamic measurement. *A*) Staining for luciferase in an MDA-MB-231-luc tumor tissue section showed extensive fluorescent mAb signal predominantly located in cytoplasm of many tumor cells. *B*) Bioluminescent image from a representative MDA-MB-231-luc tumor (140 mm^3) acquired in 1 min, 4 min after luciferin injection (450 mg/kg s.c.). *C*) Bioluminescent image from the same tumor following repeat s.c. luciferin injection 2 h after saline injection (0.15 ml i.p.). *D*) The BLI intensity was integrated over the whole tumor, and the time course was essentially identical for the 2 investigations conducted 2 h apart with respect to saline administration, as a control. Maximum signal intensity was observed at 6 min after s.c. luciferin administration.

were immunostained for the endothelial marker, CD31. A primary rat anti-mouse CD31 monoclonal antibody (1:20 dilution; Serotec) was added and incubated overnight at 4°C in a humid box. Slides were incubated with Cy3-conjugated goat anti-rat secondary antibody (1:100 dilution; Jackson Immunoresearch Laboratories, West Grove, PA, USA) for 1 h at 37°C. After mounting with Vectorshield® medium (Vector Laboratories, Burlingame, CA, USA), the slides were observed under red fluorescence (530–550 nm excitation) to detect anti-CD31 and then the corresponding Hoechst 33342 again under UV light. Image analysis was performed using Metaview software (Universal Imaging Corp., West Chester, PA, USA). For luciferase staining, monoclonal mouse antiluciferase mAb (1:150; Serotec) and fluorescein isothiocyanate-conjugated goat anti-mouse secondary antibody (Jackson) were used.

Statistical analysis

Statistical significance was assessed using an ANOVA on the basis of Fisher's protected least significant difference (PLSD; Statview; SAS Institute Inc., Cary, NC, USA) or Student's *t* tests.

RESULTS

Histology of MDA-MB-231-luc cells showed extensive expression of luciferase detected by antiluc mAb in all tumor cells (**Fig. 1**). BLI showed intense light emission from tumors following s.c. administration of luciferin reaching a maximum intensity ~6 min postadministration followed by a gradual decline over the next 20 min. Repeat measurements following administration of a second dose of luciferin 2 h after injecting saline i.p. showed highly reproducible results (Fig. 1, **Table 1**) in terms of light distribution, maximum light intensity, and time to maximum light emission. Five tumors were examined again after 24 h, and light emission remained highly consistent, with mean maximum intensity = 97 ± 6% (range 49–130%). By contrast, repeat BLI 2 h after treatment with CA4P showed a significantly lower light emission (peak intensity 2–10× lower) and delayed peak emission (**Fig. 2**; Table 1). Three mice were examined again 24 h post-CA4P, and signal was again significantly lower than baseline (mean 41±5, range 21–66%), though with some recovery compared with 2 h. Histology showed a well-developed, well-perfused vasculature in these tumors, but perfusion was essentially eliminated 2 h after administration of CA4P i.p. (**Fig. 3**).

Signal enhancement observed by DCE MRI was significantly less in all 3 tumors with a mean decrease of ~70% in perfusion/permeability 2 h after CA4P ($P<0.001$, **Table 2**, **Fig. 4**). Little change was observed in perfusion of the femoral artery (data not shown). Muscle in 1 mouse indicated a significant reduction in IAUC, but others showed no significant change (Table 2).

TABLE 1. *MDA-MB-231-luc mammary carcinoma response to CA4P observed by BLI*

Group	Max RLU change (%)	Time delay (min)	AUC change (%)	Signal change at 7 min (%)
Saline (n=6)	−16 ± 19 (−48 to 3)	0.1 ± 1.2 (0 to 2)	11 ± 20 (−20 to 31)	−18 ± 25 (−55 to 8)
CA4P (n=10)	−70 ± 15* (−53 to −92)	+7.1 ± 5.9* (0 to 11)	−72 ± 16** (−42 to −93)	−76 ± 17* (−97 to −53)

Comparison of light emission at baseline and 2 h after administering saline (control) or 120 mg/kg CA4P. Values are presented as mean ± SD (range). Changes are relative to baseline. AUC, area under curve for 20 min; RLU, relative luminescence unit. *$P < 0.05$; **$P < 0.01$.

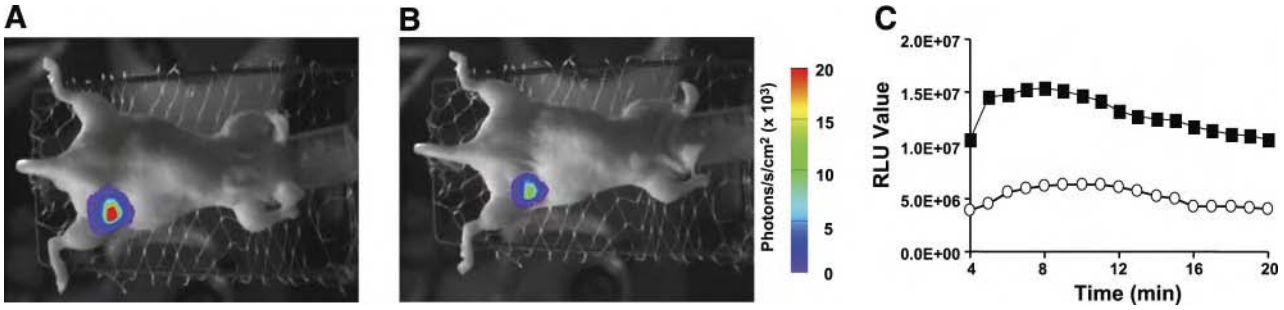

Figure 2. Tumor response to CA4P monitored by planar BLI. A second MDA-MB-231-luc tumor (130 mm^3) was monitored sequentially following saline or CA4P (120 mg/kg) i.p. infusion. Each image was acquired in 1 min, 4 min after s.c. luciferin injection. In contrast to saline, CA4P treatment caused a significant decrease in BLI signal intensity 2 h after treatment, which remained lower 24 h later. *A*) Baseline control, *B*) 2 h after CA4P, *C*) BLI intensity curves showing intense signal pretreatment (solid squares) with 99% less signal 2 h after CA4P (open circles).

DISCUSSION

Following administration of the vascular targeting agent CA4P, BLI showed significantly decreased and delayed signal in the human mammary MDA-MB-231 carcinoma. We interpret this finding as due to induced vascular shutdown. Dynamic contrast-enhanced MRI confirmed decreased tumor perfusion, which was further confirmed by histology. Both BLI and MRI are noninvasive and depict the same physiological effects, but BLI is much cheaper and offers a high throughput method for evaluating novel drugs and drug combinations and scheduling.

BLI is a very sensitive technique revealing transfected cells at even subpalpable volumes. Signal is attenuated at depth, but the technique can be applied routinely in both s.c. models and for monitoring orthotopic tumor development (3–8, 12). Several groups have shown robust correlations between detected light and tumor volume assessed by calipers or MRI (5, 12, 38, 39). In our early work (12), we found strong correlations ($r>0.8$) between peak light signal, initial area under the curve, or signal intensity at 10 min after luciferin infusion and tumor volume following i.p. administration of 150 mg/kg D-luciferin. However, individual measurements showed discrepancies, and consecutive observations could vary by as much as 60%. Overall estimates at 95% confidence intervals suggested error $< 20\%$. We later established better reproducibility based on 450 mg/kg luciferin administered s.c. It is important to note that light-emission kinetics depend on tumor location. Thus, for HeLa-luc cells growing subcutaneously, we found maximum light-emission around 10 (median) and 12.7 (mean) min following i.p. administration, whereas in the current study, using s.c. mammary tumors and s.c. administration of lucife-

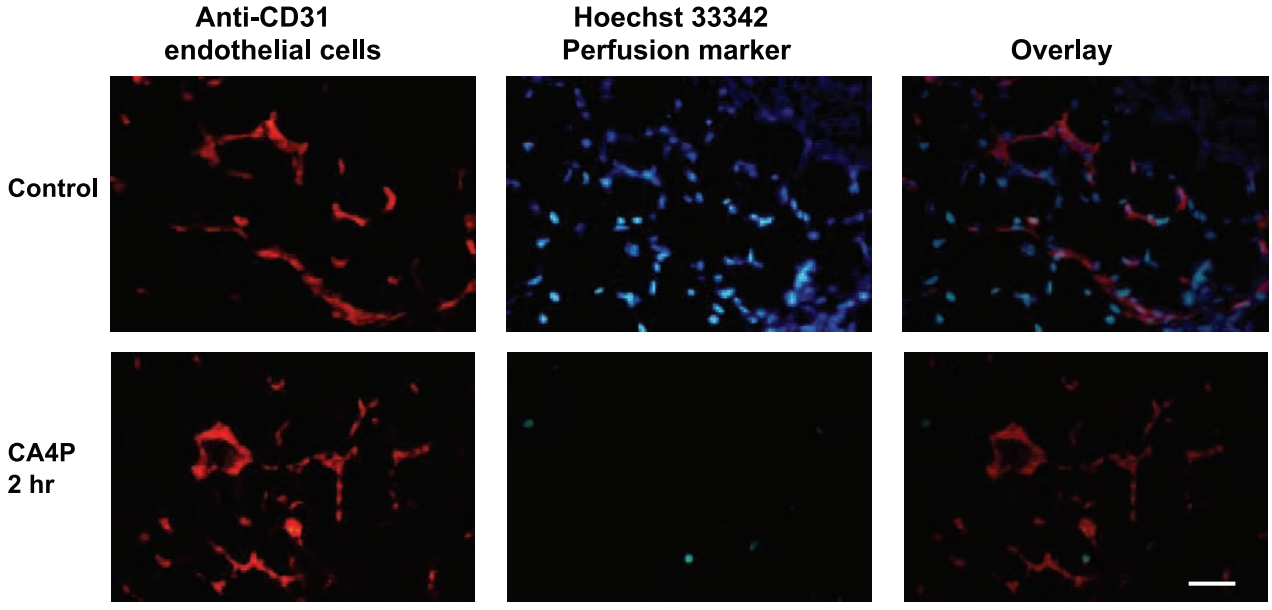

Figure 3. Immunohistochemical study of tumor vascular response to CA4P. Perfusion marker Hoechst 33342 staining pre- and 2 h post-CA4P (120 mg/kg). Vascular endothelium of the same field was immunostained by anti-CD31 (red). A good match between Hoechst and anti-CD31 stained vascular endothelium was found in the pretreated tumor (overlay). Two hours after treatment, significant reduction in perfused vessels was detected. Scale bar = 100 μm.

TABLE 2. *DCE MRI data*

	Tumor tissue			Normal muscle		
Tumor ID	Pretreatment	CA4P 2 h	Reduction (%)	Pretreatment	CA4P 2 h	Reduction (%)
1	0.74 ± 0.06	0.49 ± 0.08*	34	0.76 ± 0.04	0.67 ± 0.03	12
2	1.65 ± 0.09	0.48 ± 0.09*	71	1.17 ± 0.04	0.73 ± 0.04*	41
3	1.42 ± 0.08	0.30 ± 0.07*	79	1.07 ± 0.03	0.79 ± 0.02	28
Mean	1.27 ± 0.27	0.42 ± 0.06**	67 ± 14	1.00 ± 0.12	0.73 ± 0.03	27 ± 8

$IAUC_{60}$ (initial area under signal-time curve of first 60 s) assessed across regions of interest corresponding to tumor and contralateral thigh muscle over 3 contiguous MR image slices. Values are means ± SE. *$P < 0.05$, **$P < 0.001$ *vs.* pretreatment.

rin, maximum light-emission occurred after ~7.5 min. In the current study, BLI repeated 2 h after saline injection showed light-emission kinetics highly consistent with baseline in terms of maximum light emission, time to maximum light emission, integrated light, and signal observed at 7 min (Table 1; Fig. 1). In 5 mice, BLI measurements were again repeated 24 h later, and light emission remained highly consistent (not significantly different from baseline or 2-h time points). Two hours after CA4P administration, light-emission kinetics were significantly altered with both delayed emission and reduced light intensity (Table 1). Light-emission kinetics remained low 24 h later, when luciferin was readministered to a subgroup of mice.

Changes in vascular perfusion were confirmed by histology. These tumors show extensive vasculature as revealed by anti-CD31 staining, which is also extensively perfused (Fig. 3). Two hours after CA4P administration, vasculature was detectable, but now there was no evidence of perfusion.

Dynamic contrast-enhanced MRI has been applied previously both in animal models and the clinic to many tumor types with respect to combretastatin administration (24, 30, 32). The changes observed here (Fig. 4; Table 2) are consistent with previous observations (23, 30). Initial area under the curve reflects tumor blood flow, vascular permeability, and the involved fraction of interstitial space. For the initial control study, the signal enhancement was generally considerably greater in tumor than contralateral thigh muscle (Table 2; Fig. 4*F*). Following combretastatin administration, the IAUC decreased significantly in each tumor with a mean of ~70% in tumors (Table 2) but was not significantly changed in 2 of 3 muscles. One mouse did show decreased perfusion of normal muscle after combretastatin, as also reported previously by Tozer *et al.* (23) in rats.

BLI is more traditionally used to assess tumor growth and metastatic spread rather than physiological effects. BLI enables detection of subpalpable volumes and deep-seated tumors in mice although this capability has not been exploited in the current study. BLI is noninvasive but does require administration of luciferin substrate. Thus, sampling tumor vasculature is only achieved at discrete time points following administration of the substrate. The requirement for a reporter substrate is common to other methods of interrogation also, such as DCE MRI or DCE CT, which require administration of paramagnetic or radio opaque contrast agents (24, 30, 32, 34). Radionuclide approaches can be applied similarly (31), although they are more often used with autoradiography postmortem. Measurements based on Laser Doppler flowmetry (35), pressure probes (35), and NIR (36) may allow continuous sampling. Oximetry based on ^{19}F MRI of hexafluorobenzene allowed essentially continuous mapping of pO_2 changes with a 6.5 minute time resolution (30).

One disadvantage of the BLI approach to assessing tumor vasculature is the need for luciferase-expressing cells. However, numerous cell lines are now widely available and effective stable transfection is readily achievable though clonal selection could lead to differences between luciferase-expressing and parental tumor lines.

While combretastatin (or Zybrestat) is now in Phase II/III clinical trials for anaplastic thyroid cancer, studies will continue to be required in preclinical settings to optimize combinations with other chemotherapeutic drugs or radiation in diverse tumor types. We believe BLI provides an optimal approach for examining acute pharmacodynamics together with the potential for long-term chronic assessment of tumor control or growth. This approach could be equally applicable to other VTAs, which cause significant acute changes in blood flow, such as ZD6126 or 5,6-dimethylxanthenone-4-acetic acid (19).

There is increasing realization that drugs may behave differently with various tumor types and sites of implantation. The observations here are consistent with a previous report on the same tumor type, which showed extensive central necrosis 24 h after combretastatin administration while leaving a viable peripheral rim (20). BLI will facilitate effective screening of many tumor types implanted subcutaneously or orthotopically and with respect to monotherapy or combinations. We believe this is the first report of the use of BLI to monitor acute effects of a drug on tumor vasculature and represents an additional application of this new technology. FJ

This work was supported in part by the U.S. Department of Defense Breast Cancer Initiative Idea Awards to D.Z. (DAMD-170310363) and to P.P.A. (W81XWH-04–1-0551), the National Cancer Institute Cancer Imaging Program (pre-ICMIC CA86354 and U24 CA126608), and Simmons Cancer Center. NMR experiments were performed at the Advanced Imaging

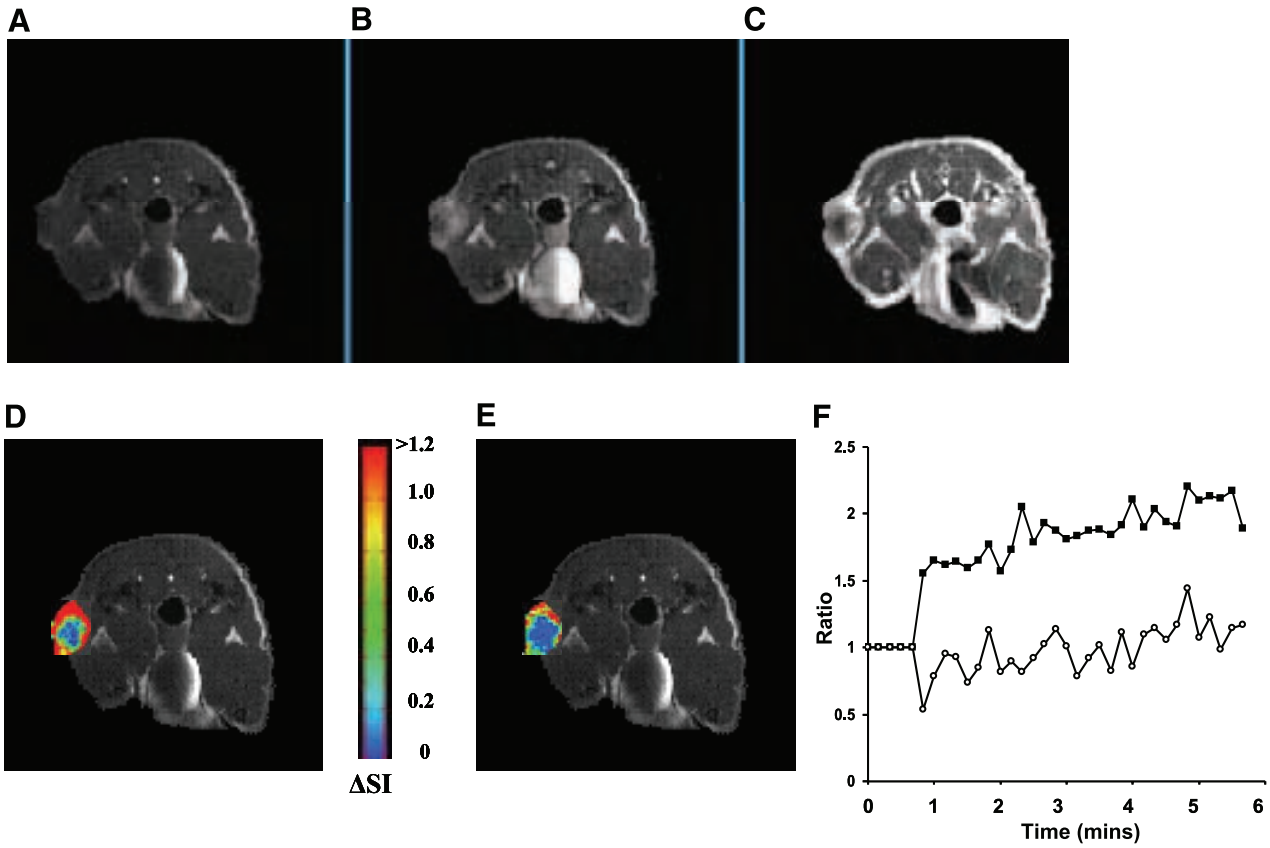

Figure 4. DCE MRI monitoring of tumor response to CA4P. *A–C*) Conventional MR images of a nude mouse with an MDA-MB-231-luc mammary tumor (Tumor 2 in Table 2): T1-weighted (*A*), T2-weighted (*B*), and T1-weighted (*C*) contrast-enhanced (Gd-DTPA-BMA). *D*, *E*) Dynamic contrast-enhanced MRI was performed in the mouse before (*D*) and 2 h after (*E*) CA4P i.p. injection. Color scale map = normalized contrast enhancement 30 s after a bolus injection of Gd-DTPA-BMA is overlaid on the T1-weighted images. Significantly decreased signal enhancement, compared with pretreatment, was observed 2 h after i.p. injection of CA4P. *F*) Ratio of tumor:muscle signal enhancement following infusion of Gd-DTPA-BMA in the single image slice shown in *D* and *E*. Solid symbols = baseline; open symbols = 2 h after CA4P.

Research Center, a National Institutes of Health Biological Threat Reduction Program facility (P41-RR02584). Combretastatin A4 phosphate was a gift of OxiGene. We are grateful to Dr. Jerry Shay (Department of Cell Biology, University of Texas Southwestern Medical Center, Dallas, TX, USA) for providing luciferase-expressing tumor cells, and to Drs. L. Liu and Y. Ren for generating the tumors. A. Harper and A. Contero performed the bioluminescent imaging.

REFERENCES

1. Li, J. Z., Holman, D., Li, H. W., Liu, A. H., Beres, B., Hankins, G. R., and Helm, G. A. (2005) Long-term tracing of adenoviral expression in rat and rabbit using luciferase imaging. *J. Gene Med.* **7,** 792–802
2. Rice, B. W., Cable, M. D., and Nelson, M. B. (2001) In vivo imaging of light-emitting probes. *J. Biomed. Optics* **6,** 432–440
3. Thorne, S. H., and Contag, C. H. (2005) Using in vivo bioluminescence imaging to shed light on cancer biology. *Proc. IEEE* **93,** 750–762
4. Jenkins, D. E., Yu, S. F., Hornig, Y. S., Purchio, T., and Contag, P. R. (2003) In vivo monitoring of tumor relapse and metastasis using bioluminescent PC-3M-luc-C6 cells in murine models of human prostate cancer. *Clin. Exp. Metastasis* **20,** 745–756
5. Szentirmai, O., Baker, C. H., Lin, N., Szucs, S., Takahashi, M., Kiryu, S., Kung, A. L., Mulligan, R. C., and Carter, B. S. (2006) Noninvasive bioluminescence imaging of luciferase expressing intracranial U87 xenografts: correlation with magnetic resonance imaging determined tumor volume and longitudinal use in assessing tumor growth and antiangiogenic treatment effect. *Neurosurg.* **58,** 365–372
6. Dikmen, Z. G., Gellert, G. C., Jackson, S., Gryaznov, S., Tressler, R., Dogan, P., Wright, W. E., and Shay, J. W. (2005) In vivo inhibition of lung cancer by GRN163l: a novel human telomerase inhibitor. *Cancer Res.* **65,** 7866–7873
7. Hsu, A. R., Cai, W. B., Veeravagu, A., Mohamedali, K. A., Chen, K., Kim, S., Vogel, H., Hou, L. C., Tse, V., Rosenblum, M. G., and Chen, X. Y. (2007) Multimodality molecular imaging of glioblastoma growth inhibition with vasculature-targeting fusion toxin VEGF(121)/rGel. *J. Nucl. Med.* **48,** 445–454
8. Mi, J., Sarraf-Yazdi, S., Zhang, X., Cao, Y., Dewhirst, M. W., Kontos, C. D., Li, C.-Y., and Clary, B. M. (2006) A comparison of antiangiogenic therapies for the prevention of liver metastases. *J. Surg. Res.* **131,** 97–104
9. Rehemtulla, A., Stegman, L. D., Cardozo, S. J., Gupta, S., Hall, D. E., Contag, C. H., and Ross, B. D. (2000) Rapid and quantitative assessment of cancer treatment response using in vivo bioluminescence imaging. *Neoplasia* **2,** 491–495
10. Verneris, M. R., Arshi, A., Edinger, M., Kornacker, M., Natkunam, Y., Karami, M., Cao, Y. A., Marina, N., Contag, C. H., and Negrin, R. S. (2005) Low levels of Her2/neu expressed by Ewing's family tumor cell lines can redirect cytokine-induced killer cells. *Clin. Cancer Res.* **11,** 4561–4570
11. Bollinger, R. A. (2006) *Evaluation of the light emission kinetics in luciferin/luciferase-based in vivo bioluminescence imaging for guidance in the development of small animal imaging study design.* Ph.D. dissertation, University of Texas Southwestern

12. Paroo, Z., Bollinger, R. A., Braasch, D. A., Richer, E., Corey, D. R., Antich, P. P., and Mason, R. P. (2004) Validating bioluminescence imaging as a high-throughput, quantitative modality for assessing tumor burden. *Mol. Imag.* **3,** 117–124
13. Contag, C. H., and Ross, B. D. (2002) It's not just about anatomy: in vivo bioluminescence imaging as an eyepiece into biology. *JMRI* **16,** 378–387
14. Lipshutz, G. S., Gruber, C. A., Cao, Y., Hardy, J., Contag, C. H., and Gaensler, K. M. (2001) In utero delivery of adeno-associated viral vectors: intraperitoneal gene transfer produces long-term expression. *Mol. Ther.* **3,** 284–292
15. Folkman, J. (2003) Angiogenesis and apoptosis. *Semin. Cancer Biol.* **13,** 159–167
16. Denekamp, J. (1990) Vascular attack as a therapeutic strategy for cancer. *Cancer Metastasis Rev.* **9,** 267–282
17. Horsman, M. R., and Siemann, D. W. (2006) Pathophysiologic effects of vascular-targeting agents and the implications for combination with conventional therapies. *Cancer Res.* **66,** 11520–11539
18. Siemann, D. W., Bibby, M. C., Dark, G. G., Dicker, A. P., Eskens, F. A., Horsman, M. R., Marme, D., and Lorusso, P. M. (2005) Differentiation and definition of vascular-targeted therapies. *Clin. Cancer Res.* **11,** 416–420
19. Thorpe, P. E. (2004) Vascular targeting agents as cancer therapeutics. *Clin. Cancer Res.* **10,** 415–427
20. Dark, G. G., Hill, S. A., Prise, V. E., Tozer, G. M., Pettit, G. R., and Chaplin, D. J. (1997) Combretastatin A-4, an agent that displays potent and selective toxicity toward tumor vasculature. *Cancer Res.* **57,** 1829–1834
21. Kragh, M., Quistorff, B., Horsman, M. R., and Kristjansen, P. E. (2002) Acute effects of vascular modifying agents in solid tumors assessed by noninvasive laser Doppler flowmetry and near infrared spectroscopy. *Neoplasia* **4,** 263–267
22. Goertz, D. E., Yu, J. L., Kerbel, R. S., Burns, P. N., and Foster, F. S. (2002) High-frequency Doppler ultrasound monitors the effects of antivascular therapy on tumor blood flow. *Cancer Res.* **62,** 6371–6375
23. Tozer, G. M., Prise, V. E., Wilson, J., Locke, R. J., Vojnovic, B., Stratford, M. R., Dennis, M. F., and Chaplin, D. J. (1999) Combretastatin A-4 phosphate as a tumor vascular-targeting agent: early effects in tumors and normal tissues *Cancer Res.* **59,** 1626–1163
24. Galbraith, S. M., Maxwell, R. J., Lodge, M. A., Tozer, G. M., Wilson, J., Taylor, N. J., Stirling, J. J., Sena, L., Padhani, A. R., and Rustin, G. J. S. (2003) Combretastatin A4 phosphate has tumor antivascular activity in rat and man as demonstrated by dynamic magnetic resonance imaging. *J. Clin. Oncol.* **21,** 2831–2842
25. Rustin, G. J., Galbraith, S. M., Anderson, H., Stratford, M., Folkes, L. K., Sena, L., Gumbrell, L., and Price, P. M. (2003) Phase I clinical trial of weekly combretastatin A4 phosphate: clinical and pharmacokinetic results. *J. Clin. Oncol.* **21,** 2815–2822
26. Robinson, S. P., McIntyre, D. J., Checkley, D., Tessier, J. J., Howe, F. A., Griffiths, J. R., Ashton, S. E., Ryan, A. J., Blakey, D. C., and Waterton, J. C. (2003) Tumour dose response to the antivascular agent ZD6126 assessed by magnetic resonance imaging. *Br. J. Cancer* **88,** 1592–1597
27. Prise, V. E., Honess, D. J., Stratford, M. R. L., Wilson, J., and Tozer, G. M. (2002) The vascular response of tumor and normal tissues in the rat to the vascular targeting agent, combretastatin A-4-phosphate, at clinically relevant doses. *Int. J. Oncol.* **21,** 717–726
28. Padhani, A. R. (2003) MRI for assessing antivascular cancer treatments. *Br. J. Radiol.* **76,** S60–S80
29. McIntyre, D. J. O., Robinson, S. P., Howe, F. A., Griffiths, J. R., Ryan, A. J., Blakey, D. C., Peers, I. S., and Waterton, J. C. (2004) Single dose of the antivascular agent, ZD6126 (N-acetylcoichinol-O-phosphate), reduces perfusion for at least 96 hours in the GH3 prolactinoma rat tumor model. *Neoplasia* **6,** 150–157
30. Zhao, D., Jiang, L., Hahn, E. W., and Mason, R. P. (2005) Tumor physiological response to combretastatin A4 phosphate assessed by MRI. *Int. J. Radiat. Oncol. Biol. Phys.* **62,** 872–880
31. Anderson, H. L., Yap, J. T., Miller, M. P., Robbins, A., Jones, T., and Price, P. M. (2003) Assessment of pharmacodynamic vascular response in a phase I trial of combretastatin A4 phosphate. *J. Clin. Oncol.* **21,** 2823–2830
32. Maxwell, R. J., Wilson, J., Prise, V. E., Vojnovic, B., Rustin, G. J., Lodge, M. A., and Tozer, G. M. (2002) Evaluation of the anti-vascular effects of combretastatin in rodent tumours by dynamic contrast enhanced MRI. *NMR Biomed.* **15,** 89–98
33. Beauregard, D. A., Pedley, R. B., Hill, S. A., and Brindle, K. M. (2002) Differential sensitivity of two adenocarcinoma xenografts to the anti-vascular drugs combretastatin A4 phosphate and 5,6-dimethylxanthenone-4-acetic acid, assessed using MRI and MRS. *NMR Biomed.* **15,** 99–105
34. Ng, Q.-S., Goh, V., Carnell, D., Meer, K., Padhani, A. R., Saunders, M. I., and Hoskin, P. J. (2007) Tumor antivascular effects of radiotherapy combined with combretastatin a4 phosphate in human non-small-cell lung cancer. *Int. J. Radiat. Oncol. Biol. Phys.* **67,** 1375–1380
35. Ley, C. D., Horsman, M. R., and Kristjansen, P. E. G. (2007) Early effects of combretastatin-A4 disodium phosphate on tumor perfusion and interstitial fluid pressure. *Neoplasia* **9,** 108–112
36. Kim, J. G., Liu, H., Zhao, D., and Mason, R. P. (2006) Acute effects of combretastatin A4 phosphate on breast tumor hemodynamics monitored by near infrared spectroscopy. *Biomed. Opt. Topical Meeting (Fort Lauderdale)* 19–23
37. Tozer, G. M., Prise, V. E., Wilson, J., Cemazar, M., Shan, S. Q., Dewhirst, M. W., Barber, P. R., Vojnovic, B., and Chaplin, D. J. (2001) Mechanisms associated with tumor vascular shut-down induced by combretastatin A-4 phosphate: intravital microscopy and measurement of vascular permeability. *Cancer Res.* **61,** 6413–6422
38. Wang, Y., Sun, Z. D., Peng, J. C., and Zhan, L. S. (2007) Bioluminescent imaging of hepatocellular carcinoma in live mice. *Biotechnol. Lett.* **29,** 1665–1670
39. Chen, C.-C., Hwang, J.-J., Ting, G., Tseng, Y.-L., Wang, S.-J., and Whang-Peng, J. (2007) Monitoring and quantitative assessment of tumor burden using in vivo bioluminescence imaging. *Nucl. Instruments Methods Phys. Res. A Accelerators Spectrometers Detectors Assoc. Equip.* **571,** 437–441

Received for publication November 30, 2007.
Accepted for publication January 10, 2008.